

Final Report

PERFORMANCE SPECIFICATIONS FOR A METEOROLOGICAL SATELLITE LIDAR

By: W. E. EVANS E. J. WEGMAN W. VIEZEE W. G. H. LIGDA

Prepared for:

NATIONAL AERONAUTICS AND SPACE ADMINISTRATION
WASHINGTON, D.C.
ATTN: OFFICE OF RESEARCH GRANTS AND CONTRACTS
CODE SC

CONTRACT NASr-49(22)

STANFORD RESEARCH INSTITUTE

MENLO PARK, CALIFORNIA

***SRI**

GPO PRICE \$ _____

CFSTI PRICE(S) \$ _____

Hard copy (HC) 57.00

Microfiche (MF) 1.25

MF 653 July 65

N66 29977

(ACCESSION NUMBER)

196

(PAGES)

CR-76087

(NASA OR CR TMA OR AD NUMBER)

(T/FAC)

1

(CORE)

(CATEGORY)



June 1966

Final Report

PERFORMANCE SPECIFICATIONS FOR A METEOROLOGICAL SATELLITE LIDAR

Prepared for:

NATIONAL AERONAUTICS AND SPACE ADMINISTRATION
WASHINGTON, D.C.
ATTN: OFFICE OF RESEARCH GRANTS AND CONTRACTS
CODE SC

CONTRACT NASr-49(22)

By: W. E. EVANS E. J. WIEGMAN W. VIEZEE M. G. H. LIGDA

SRI Project 5373

Approved: M. G. H. LIGDA, MANAGER
AEROPHYSICS LABORATORY

D. R. SCHEUCH, EXECUTIVE DIRECTOR
ELECTRONICS AND RADIO SCIENCES

Copy No. **22**

ABSTRACT

Numerous suggestions have been made regarding measurements of meteorological significance which might be made with a laser radar (lidar) carried in a satellite. In this study a wide variety of possibilities is examined, and it is concluded that the most important thing that can be done with reasonable amounts of power is to provide routine height and density data on cirrus cloud. Cloud-top elevations of lower cloud would also be determined.

A review of the literature emphasizes the widespread acceptance of cirrus as an important diagnostic tool of meteorology in spite of the traditional difficulty of observing it reliably from the ground, from aircraft, or even via satellite television.

In addition to its role as an indicator of large scale circulation features, such as cyclones and jetstreams, cirrus cover is currently of considerable interest in connection with infrared radiation studies of the earth. It is shown that even extremely low-density cirrus shields are capable of introducing several degrees of error into radiometric determinations of temperature made from space.

Calculations, supported by experimental backscatter measurements made at SRI with a ground-based pulsed ruby lidar, show that it should be barely possible to measure low-density cirrus cloud at night from a 1000 to 1500 km satellite using a radiated energy of one joule per sounding and a receiving aperture of one square meter.

This is roughly equivalent to proposing that within the next decade we duplicate in space equipment performance which is currently being achieved on the ground under controlled laboratory conditions.

Soundings frequent enough to provide complete map-like coverage are not presently feasible, but the unique ranging capability of the lidar, properly used in conjunction with television or HRIR, could provide very important supplementary information with a relatively small number of samples. A sounding rate of 1.8 per second is suggested as a goal, but lower rates might be considered.

The equipment requirements for all methods currently envisioned for measuring gaseous temperature, density, and composition by lidar from satellite elevations are shown to call for several orders of magnitude more power, and thus must be considered to be only extremely remote possibilities from the standpoint of the present state of laser technology.

It is recommended that planning toward a meteorological lidar satellite be continued with heavy emphasis on more precise definition of the optical and meteorological characteristics of potential atmospheric targets and improvement of lidar system efficiency.

CONTENTS

ABSTRACT	iii
LIST OF ILLUSTRATIONS	vii
LIST OF TABLES	ix
LIST OF SYMBOLS	xi
I INTRODUCTION	1
II POSSIBLE METEOROLOGICAL USES FOR SATELLITE-BORNE LIDAR	5
A. General	5
B. Observations of Unknown Practicality	8
C. Importance of Possible Observations	11
III RATIONALE FOR SELECTING CIRRUS AS THE MAJOR TOPIC OF THIS STUDY	15
IV CIRRUS-CLOUD FORMS	17
A. General	17
B. Data Coverage Recommended for Mapping Cirriiform Cloudiness	18
V EQUIPMENT DESIGN FACTORS	23
A. General	23
B. Power Levels Required for Detection	26
C. Choice of Reporting-Area and Sampling-Spot Sizes	47
D. Orbital Considerations	55
E. Data Handling and Display	65
F. Miscellaneous Equipment-Design Considerations	74
VI BACKSCATTER COEFFICIENTS	77
A. Predicted Values	77
B. Experimentally Determined Volume Backscatter Coefficients for Cirrus Clouds	85
C. Three-Day Lidar Test Run to Monitor Visible and Subvisible Cirrus	91

CONTENTS (Concluded)

VII	AN APPLICATION OF SATELLITE-LIDAR DATA TO INFRARED RADIATION STUDIES	95
	A. Introduction	95
	B. Computed Effect of Ice-Crystal Clouds on Infrared Radiation Measurements from Satellites	96
	C. Detection of Cirrus-Cloud Model I by Satellite Lidar . .	103
	D. Conclusions	109
VIII	CURRENT LASER TECHNOLOGY	113
IX	NONRUBY LASERS	117
	A. General	117
	B. Internal Noise	117
	C. CO ₂ Laser	120
X	USE OF SATELLITE-BORNE LASERS FOR PURPOSES OTHER THAN MEASURING NONRESONANT BACKSCATTER AS A FUNCTION OF RANGE . .	121
	A. General	121
	B. Multiple-Frequency Systems	121
	C. Raman-Scattering Measurements	124
	D. Polarization Measurements	128
XI	COMPETING METHODS OF MEASURING CLOUD-TOP ALTITUDES	131
XII	CONCLUSIONS AND RECOMMENDATIONS	133
	A. Conclusions	133
	B. Recommendations	135
	Appendix--NATURE AND DISTRIBUTION OF CIRRUS CLOUD	137
	CONTRIBUTORS	161
	GLOSSARY	163
	BIBLIOGRAPHY	169
	DD FORM 1473	

ILLUSTRATIONS

Fig. IV-1	Estimate of Dimensions of Spacing Between Jet-Stream Cirrus Bands	20
Fig. V-1	Lidar System Geometry	28
Fig. V-2	Predicted Lidar Return: Backscatter Distribution for Model A	33
Fig. V-3	Predicted Lidar Return: Backscatter Distribution for Model B	34
Fig. V-4	Predicted Lidar Return: Backscatter Distribution for Model C	35
Fig. V-5	Predicted Lidar Return: Backscatter Distribution for Model D	36
Fig. V-6	Background Light Levels Seen from Satellite	43
Fig. V-7	Detection and False-Alarm Probabilities	46
Fig. V-8	Detection and False-Alarm Statistics as Functions of Threshold Level	48
Fig. V-9	Signal Levels Required to Achieve Detection-- $P_f = 0.01$	49
Fig. V-10	Signal Levels Required to Achieve Detection-- $P_f = 0.0001$	51
Fig. V-11	Height-Dependent Orbital Parameters	58
Fig. V-12	Viewing Geometry for Satellite at 1000 km	60
Fig. V-13	Beam Geometry at Edge of Swath	61
Fig. V-14	Echo Power Level as a Function of Satellite Altitude	63
Fig. V-15	Satellite Period as a Function of Height	64
Fig. V-16	Block Diagram of Data-Handling Components	69
Fig. V-17	Simulated Lidar Data Added to TIROS Cloud Photograph	73
Fig. VI-1	Volume Backscatter Coefficients for a Clear Standard Atmosphere	82
Fig. VI-2	Backscatter and Attenuation Coefficients for Various Clouds and Hazes	84

ILLUSTRATIONS (Concluded)

Fig. VI-3	Lidar Returns from Medium and Weak Cirrus Systems . . .	89
Fig. VI-4	Mk II Lidar and Cirrus-Cloud Situation of 17 March 1966	90
Fig. VI-5	TIROS IX Pictures, Lidar Returns, Synoptic Conditions for 20-22 July 1965	93
Fig. VII-1	Infrared Attenuation and Absorption for Cloud Models I and II	99
Fig. VII-2	Errors in Determination of Black-Body Temperature due to Interference by Tenuous Cirrus Cloud	101
Fig. VII-3	Angular Scattering Efficiency in Region of the Glory	104
Fig. VII-4	Backscatter Efficiency as a Function of Particle Radius	106
Fig. VII-5	Average Backscatter Efficiency for Three Ranges of Particle Size	107
Fig. IX-1	Lidar System Design Factors as Functions of Wavelength	118
Fig. A-1	Average Altitudes of Base and Summit	141
Fig. A-2	Graphs of Cirrus Thickness	142
Fig. A-3	Size Estimate of Areas of Upper Cloudiness	143
Fig. A-4	Estimate of Frequency of Days with Major Cirrus-Producing Systems	147
Fig. A-5	Estimate of Frequency of Days when Major Cirrus Cloudiness Can Be Anticipated	149
Fig. A-6	Distribution of Percentage Frequency of Large-Scale Cirrus	150
Fig. A-7	Extratropical Cyclone Cloud System	153
Fig. A-8	Polar Front Jet-Stream Cloud System	154
Fig. A-9	Subtropical Jet-Stream Cloud System	156
Fig. A-10	Tropical Cyclone Cloud Systems	157
Fig. A-11	Air Mass Cloud System	158

TABLES

Table	V-1	Ambient Light Levels at the Planet Earth	41
Table	V-2	Effective Diffuse Reflection Coefficients	42
Table	V-3	Suggested Data-Storage/Transmission Capability	67
Table	VI-1	Volume Backscatter Coefficients β_{180}' for Rayleigh Component of Atmospheric Scattering	80
Table	VI-2	Predicted Volume Backscatter Coefficients for Water Clouds and Hazes	83
Table	VII-1	Cloud Models Used in Computations	97
Table	VII-2	Estimation of Errors in Determination of "Target" Black-Body Temperature from Satellite Altitude Due to Interference of Tenuous Cirrus Cloud	102
Table	A-1	Cirrus-Cloud Altitudes at Certain Geographical Locations	141
Table	A-2	Percent Frequency of Different Horizontal Spreads of Masses of Frontal Ci-Cs	141
Table	A-3	Percent Frequency of Ci-Cs as a Function of Synoptic Situation	145
Table	A-4	Percent Frequency of Jet-Stream and Cyclone Days for any 10° Increment of Longitude in the Northern Hemisphere	148

LIST OF SYMBOLS

A_r	Area of receiving aperture (meters ²)
$\overset{o}{A}$	Angstrom unit of length: $1\overset{o}{A} = 10^{-4}$ micron = 10^{-10} meter
B	Radiance (watts/m ² -sr- $\overset{o}{A}$)
B_E	Radiance of illuminated earth (watts/m ² -sr- $\overset{o}{A}$)
C	Effective attenuation cross section of an individual particle (meters ²)
D	Aperture diameter (meters)
I	Intensity of an electromagnetic wave (watts/steradian)
K	Kelvin (absolute) units of temperature
N	Concentration of particles (number/unit volume)
N_r	Concentration of Rayleigh scattering particles (number/unit volume)
P	Probability of occurrence
P_d	Probability of detection
P_f	Probability of a false alarm
P_s	Probability of occurrence due to presence of a signal
P_{s+b}	Probability of occurrence due to presence of a signal plus background
P_i	Incident power (watts)
P_r	Received power (watts)
P'_r	Received power (photons/second)
P_t	Transmitted power (watts)
Q	Efficiency factor for scattering: $Q = \frac{\text{Effective cross section}}{\text{Geometric cross section}}$

R	Radial distance, range (meters)
T	Temperature (degrees Kelvin)
T	Threshold level
T	Transmittance, $T = \exp(-\sigma R)$
U	Energy (joules)
U_t	Transmitted energy (joules)
V	Volume (meters ³)
a	Radius of a particle or droplet
c	Velocity of light (3×10^8 meters/second)
e	Electronic charge ($e = 1.602 \times 10^{-19}$ coulomb)
h	Elevation above sea level (meters)
i	rms current (amperes)
\bar{i}	Average current (amperes)
i_{180°	Individual particle backscatter efficiency: $i_{180^\circ} = \text{backscattering cross section}/\pi a^2$
m	meters
n	Index of refraction
n_b	Number of events due to background radiation per integration period
\bar{n}_b	Average or expected number of events due to background radiation per integration period
n_s	Number of events due to signal per integration period
\bar{n}_s	Average or expected number of events due to signal per integration period
q	Quantum efficiency of a photocathode
r_o	Equivalent radius of an electron (meters)
t	Time (seconds)

β'_{180}	Volume backscattering coefficient (meters ⁻¹)
θ_r	Receiver beamwidth (radians)
θ_t	Transmitter beamwidth (radians)
λ	Wavelength (meters)
σ	Attenuation coefficient (meters ⁻¹)
σ_a	Attenuation coefficient due to absorption (meters ⁻¹)
σ_s	Attenuation coefficient due to scattering (meters ⁻¹)
ν	Frequency of electromagnetic oscillation (Hz)
φ	Scattering angle (degrees)
ω_r	Receiver field of view (steradians)
ω_f	Transmitter beam size (steradians)
pps	Pulses per second
Hz	Hertz (cycles per second)
sr	Steradians

I INTRODUCTION

The virtually unique capabilities of lidar (laser or optical radar) equipment for observing cloud, clear-air aerosol, and even molecular gases suggest its possible utilization in meteorological satellites for atmospheric probing. This is the final report of an exploratory investigation of the meteorological utility of such a system, the general characteristics it should have, the possible system configuration, and other factors which should be taken into consideration in arriving at a decision whether or not to undertake further studies and experiments directed toward possible ultimate development of such a system. In this investigation a conscious effort was made to at least make reference or mention, however brief, of all the factors involved. These turned out to be so numerous that time and funds did not permit as thorough an investigation of some as their importance certainly deserves. Accordingly, this report should be regarded as a preliminary examination of the problem.

Optical wavelengths are well suited for meteorological probing since they are sufficiently small relative to the common atmospheric aerosols that the latter exhibit radar backscattering cross sections large enough to be useful. While prelaser optical radars using spark sources have been built and even proposed for use in meteorological satellites, currently available lasers now provide optical energy sources which are much more suitable in nearly all respects.

Major attention is focused on the giant-pulse, crystal or solid-state type of lidar system.* While the high efficiency, stability, ruggedness and relative simplicity of gas and diode-junction types of lasers would otherwise make them important contenders for a place

* A glossary of the more specialized laser and meteorological terms is included herein for the benefit of the reader not well versed in one or the other of these fields.

in the system, the peak power of their emissions is at present many orders of magnitude less than that of solid-state lasers, and thus their ability to provide the all-important range discrimination from satellite altitudes is limited, at least without the use of very elaborate signal-processing techniques.

Impressive progress has been made in the development of these types of lasers during the course of this 15-month study. Since average power levels from CW and high-PRF lasers are now comparable to those discussed herein for the giant-pulse mode, methods of employing CW, Doppler and pulse-Doppler radar techniques will need to be reviewed constantly for applicability to the meteorological problem. At present, however, the pulsed ruby lidar provides a performance standard against which any new contenders must compete.

Although, as will be discussed later, observations of a more sophisticated nature have been proposed, the decision was reached early in the course of this investigation to concentrate primary attention on the relatively straightforward capability of the giant-pulse lidar to obtain simple range information, principally on atmospheric aerosols. This decision was made on the basis of several years of firsthand experience in the adjustment and operation of lidar equipment which, except in its simplest and ruggedest form, is clearly still more of a laboratory than a practical instrument for field use (much less an instrument that could sustain its delicate adjustments during the shock and vibration of a satellite launching and operate unattended for weeks or months in the hostile environment of space). It is our considered opinion it is clearly beyond the state of the art to construct a lidar which requires very precise temperature control (on the order of a degree or so Kelvin) and optical alignment and adjustment even more precise, and the use of substantially greater powers than those required in ordinary ranging lidar systems. Such characteristics would be required to accomplish some of the more sophisticated spectroscopic observations that have been suggested and are mentioned below. It has been our approach that until the theoretical possibility of any observation has at least been confirmed by demonstration in the

free atmosphere we should not give it detailed consideration as a possible lidar satellite observation or experiment. While time and the rapid advances of laser and detector technology may very well solve many (if not all) of the practical objections that can be raised against more complex systems, this investigation is concerned with what could conceivably be accomplished within perhaps five to eight years, based upon what is already being done with laboratory-type ground-based equipment.

II POSSIBLE METEOROLOGICAL USES FOR SATELLITE-BORNE LIDAR

A. General

The list of known atmospheric constituents potentially detectable by a lidar-equipped meteorological satellite is impressive enough. In this section we enumerate the wide range of possible observations, with a minimum of attention to technical feasibility. Many of the phenomena mentioned below could not be detected with the lidar system we propose, which has as the upper limit of its capability the bare detection of the Rayleigh backscatter from the atmosphere at an altitude of 10 km. Until surface-based lidar observations have provided more information about the occurrence and optical properties of some of these phenomena, their measurement from satellite altitudes must necessarily be highly speculative.

Starting at the top of the atmosphere, the first major particulate constituents to be encountered are the meteoric dust layers or trails. Micron and submicron sized particles drifting in from outer space or left behind as debris from the downward plunge of larger bodies are plentiful, especially on the forward hemisphere of the earth as it moves in orbit around the sun. The ability of lidar to detect meteoric dust seems possible if Fiocco's observations (1963)* are a reliable criterion. The global observation of meteoric dust on a systematic basis may allow more detailed examination of possible relationships between precipitation and the earth's encounter with or attraction of extra-terrestrial matter (Roberts, 1965; Twitchell, 1965).

In this same region of the upper atmosphere the lidar may detect the elusive "leuchtstreifen" (Götz, 1942; Hoffmeister, 1946). Again, Fiocco has reported observation of particulate matter concentration in

* All references mentioned in the text are included in the Bibliography at the end of this report.

in this region (90 to 180 km). Observation of these "clouds" is evidently so rare that their very existence is somewhat problematical, but surface-based lidar observations may clear up this question in a few years.

Of course at this level and below lidar might fortuitously detect the exhaust plumes of rocket engines and the trails of re-entering artificial satellites.

At somewhat lower levels (80 to 90 km) the noctilucent clouds present themselves as very interesting targets. If these can be detected by satellite-borne lidar, many questions concerning their global distribution, diurnal variation, and vertical structure and possibly their nature and origin may conceivably be resolved. Efforts to detect these clouds with surface-based lidar have not yet (so far as we have been able to determine) been successful; but it seems not unreasonable to expect that their observation only awaits the assembly of suitable equipment and its operation while the clouds are within range.

In a similar category with noctilucent clouds but in the 20 to 30 km layer are the rare nacreous, or mother-of-pearl clouds. Much the same type of information concerning these clouds may be obtained from their observation by lidar as in the case of the noctilucent clouds. SRI scientists have reported the observation of what definitely appear to be particulate layers in this region (Collis, 1966).

In this region of the upper atmosphere are also to be found the maximum ozone concentration and Junge's 22 km ammonium sulfate layer (Mossop, 1963). The latter has been tentatively detected by surface-based lidar (Collis, 1966), and the former may be detectable by its attenuating effects on high-powered infrared or ultraviolet lidar systems (Schotland, 1965). Also in this region are the cirrus blowoffs from especially violent thunderstorms and dust from major volcanic and H-bomb surface explosions, all of which are promising phenomena for observation. Considerable interest is currently centered on the circulation of the atmosphere in this region, such as the vertical-transport rates and processes affecting the transport of aerosols and ozone from above to below the critical "Junge layer" near 22 km.

The highly reflective properties of most of the usual cloud types of the lower, middle, and upper troposphere make them excellent lidar targets about which more will be said later. Precipitation, although quite reflective to laser beams (Ligda, 1964) will normally occur beneath rather thick and opaque cloud formations and so should only rarely present a detectable target. An exception to this may be snow generated from thin cirrus. Contrails should be readily detectable, but whether observations can be made at short enough intervals to distinguish them from thin cirrus layers and trails is open to question, at least in early-generation systems.

While requiring laser power levels which present the possibility of causing eye damage to persons on the surface who might accidentally look straight up the beam toward the lidar satellite, interesting possibilities exist for making worthwhile observations of atmospheric conditions in the cloud-free regions of the troposphere by means of backscattering from the relatively low-density but all-pervasive particulate matter. Such phenomena as dust storms which were apparent in the TIROS VII observations over the Persian Gulf on 11 April 1964, haze and smoke layers, volcanic dust, and regions of blowing snow all appear to be observable with a suitably designed lidar satellite system. It has been suggested that air masses and the boundaries between them may be distinguished by lidar since a "sea breeze" front has at least once apparently been observed with a surface-based lidar by the aerosol discontinuity across it (Collis, 1964). Those temperature inversions accompanied by smoke, haze, and dust variations are also within the realm of possibility of detection. Inasmuch as the tropopause is not infrequently coincident with the boundary between aerosol-laden tropospheric air and the less turbid air of the stratosphere, the height of this important region of the atmosphere may also occasionally be subject to satellite lidar observation.

The above summarizes those phenomena for which there seems to be at least a slight hope of observation with a satellite-borne pulse lidar system of adequate power and receiver sensitivity. It has been suggested that additional atmospheric phenomena might also be detectable by various

optical systems incorporating lasers and more sophisticated signal-analysis techniques. It is instructive to briefly discuss those which have come to our attention and note the special technological and practical problems each evidently presents.

B. Observations of Unknown Practicality

1. Clear-Air Turbulence

There are two suggested ways in which lidar systems might possibly be able to detect turbulent regions in cloud-free air (Zirkle, 1966). The first is based upon the use of the Doppler shift of the backscattered return somewhat along the approach used with Doppler radar to determine the component of raindrop velocity along the beam. The other is based upon the way that radar detects turbulent regions in thunderstorms, namely by distinctive patterns or characteristics of the precipitation echoes. There has been hope that lidar might operate in a similar fashion from the aerosol return always present to some degree even in very clean air.

Even at very short range, no positive observational evidence with lidars has yet been obtained that either of these hypotheses is correct despite the considerable experimental effort expended so far in their evaluation (Franken, Jenney, and Rank, 1965; Breece et al, 1966). Also, there is as yet no proof from other types of observations that significant aerosol or density gradients are present in turbulent regions of the upper or lower atmosphere. A satellite lidar system for CAT detection would evidently need to observe over large areas with exceedingly good horizontal and vertical resolution to provide useful information.

2. Atmospheric Density

Following the approach of scientists who have employed searchlight beams to measure upper-atmosphere density by Rayleigh molecular backscatter, experiments have been performed with lidars toward the same goal. To date, these have not been highly successful because of the difficulty of measuring the intensity of the very weak returns obtained, although the potentialities are interesting. The need is for much more

power and a shorter interval between observations to exploit the benefits obtainable from signal integration. Because the presence of even a very few ice crystals or water droplets can result in erroneous determination of molecular backscatter, complications exist in the selection of optimum beam cross sections. Further studies of the short-term density variations of the upper atmosphere are needed to assess how well widely spaced satellite lidar observations can represent general conditions.

3. Vertical Atmospheric Gas-Density Profile by Selective Attenuation

Experiments have been made and are currently in progress (Schotland, 1965) to determine whether lidar systems can be made to function reliably at two wavelengths, one at some atmospheric-absorption band or line such as water vapor and the other at a nearby absorption-free wavelength of the spectrum. Theoretically it should be possible by this means to determine the density profile of the particular gas along the beam with such a system by comparison of the relative intensity of the returns at the two wavelengths until backscatter in the attenuated wavelength is reduced below measurable levels.

At the time of this writing (April 1966) no reports indicating that this observation had been successfully accomplished have yet come to the attention of the writers. Brief experiments at SRI to temperature-tune an air-cooled ruby laser to the water-vapor absorption band at $6943.8\overset{\circ}{\text{A}}$ emphasized the difficulty of maintaining adequate temperature control (the absorption line is only a few angstroms wide). Difficulties are introduced by the variation of the laser-rod temperature during its pumping cycle, but these may be overcome by more efficient cooling.

With no observational experience yet available on which to base estimates of the accuracy with which density profiles could be measured or the depths to which the atmosphere could conceivably be probed from a satellite, the possibility of making this observation with a satellite lidar is indeterminable except on a theoretical and speculative basis at this time. It is not at all improbable that the technical problems can and will be solved, perhaps quite soon, and this highly worthwhile

experiment can be accorded a place in the list of potential lidar satellite observations.

4. Molecular Structure Observation by Raman-Line Observation

The idea behind this suggested observation is to exploit the Raman effect (shifts in molecular vibrational levels in gases and liquids when excited by electromagnetic radiation) which results in rotational emission lines at different wavelengths from the excitation wavelength. Given sufficient spectral frequency resolution and accuracy of determination of line intensity, information about the temperature and species content of a gas mixture can be obtained. Again, demonstrations that this is a practical observation in the free atmosphere using lasers have apparently not yet been made even at short range, so reliable data are lacking on which to base estimates of system power, sensitivity, and stability. Other aspects of this suggested observation must also be tested in the real atmosphere before its practicability can be ascertained with any degree of confidence.

5. Gaseous Species Observation by Resonant Backscatter

By radiational excitation of a gas at an appropriate wavelength its molecules may absorb and reradiate very strongly. A lidar based on this principle might radiate at such wavelengths. The lidar must necessarily function in an absorption band or line of the spectrum, which of course attenuates the energy available for working at greater ranges than would be the case otherwise because much of the energy incident is absorbed and re-emitted. This experiment, like those suggested above, is theoretically possible; however no actual observational evidence that it can be accomplished at available laser wavelengths is known.

6. Differentiation Between Water-Droplet and Ice-Crystal Clouds

Because of the high degree of polarization of some types of laser-system beams, some investigators have wondered about the possibility of distinguishing between the backscattering produced by spherical cloud droplets of middle and lower cloud types and the

asymmetrical, sometimes specularly reflecting ice crystals of cirrus clouds. Polarization techniques are exploited in microwave radar to eliminate the return from spherical rain drops.

The practicality of this suggestion has not yet been carefully examined; some degree of difficulty is expected because of depolarization of the beam along the path to and from the target. The extent to which this takes place is also uncertain at this time.

While advances in electro-optical technology may shift these several suggested experiments from the "theoretically possible" to the "actually possible" and even "highly desirable" categories, it seems more worthwhile to concentrate our attention on the possibilities which have--at least at present--a more reasonable expectation of fulfillment in the foreseeable future. Considering those observations which appear to be possible given a lidar satellite with the capability of detecting Rayleigh backscatter at 10 km above the surface, the extent to which these will be of interest to meteorologists, physicists, and operational users may now be broadly considered.

C. Importance of Possible Observations

1. Scientific

Putting a lidar aboard an experimental meteorological satellite may be considered worthwhile and interesting from a research or experimental point of view, just as was the first series of TIROS satellites. As has been learned, prior to the advent of the weather satellites even the best high-altitude aerial and rocket photographs of cloud cover hardly hinted at the wealth of information which is now routinely obtained on a global basis from the satellites. Similarly, it is reasonable to expect that since practically nothing is known about the global occurrence and distribution of thin high-level cloud layers, a great deal of entirely new and fresh information about these difficult-to-observe clouds will become available with the advent of the lidar satellite. To the physical meteorologist the data should be of considerable interest because of the influence of these cloud systems upon incoming and

outgoing radiation. The cloud physicist should gain new insight into the formation and dissipation of high cloud systems, the possible cosmic influences upon them, and the nature and extent of their influence upon precipitation formation at lower levels.* The synoptic meteorologist will examine the data to learn more about the source and sink regions of high-level clouds and their relationship to upper-level air movement.

It is a virtual certainty that, because of the limited number of lidar and searchlight observations of the upper atmosphere so far obtained, new and possibly significant optical-wavelength scattering layers may be found in the stratosphere and mesosphere. Gegenschein and zodiacal light both provide evidence of substantial particulate concentrations at very high levels and it may be supposed that other concentrations may exist in such low density or position with respect to the sun that they have heretofore completely eluded detection. While on this subject, it might be noted that the enormous sensitivity of lidar to particulate scattering offers opportunities for experiments involving the deliberate injection of highly reflective particles into the upper atmosphere for the observation of their subsequent motion (Langer and Stockham, 1960). Ground-based lidar can readily detect very thin contrails of jet aircraft and even their exhaust trails at a range of several miles.

To summarize, experimental or developmental lidar satellites could reasonably be expected to provide new data for study of the interrelationships between the mesosphere and stratosphere and possibly even the exosphere.

2. Operational

The operational value of lidar satellite observations will necessarily depend greatly upon the results of research using data obtained by

* Specific reference may be made to W. O. Roberts' suggestion (1965) that a cirrus-cloud sheet may develop over a region subject to an influx of solar particles. According to Twitchell (1965) plans are being formulated for a special study on the occurrence of cirrus clouds over auroral regions to check some of the aspects of Roberts' hypothesis.

developmental systems, i.e., the correlations found between lidar satellite observations and important weather conditions which precede, attend, or follow them. Because of the numerous uncertainties involved, any suggested operational applications are exceedingly speculative and those set forth below are only offered with this understanding clearly in view.

- (1) Jet-stream location by distinctive cirrus-cloud distribution
- (2) Minimum and maximum temperature and frost forecasting as influenced by subvisible middle and high cloud layers
- (3) Cloud-top determination and vertical structure of upper cloud systems for various aeronautical operations
- (4) Height and structure of tropopause for meteorological analysis
- (5) Horizontal and vertical water-vapor distribution (if such laser observations become possible)
- (6) Differentiation between overcast and clear snow-covered areas
- (7) Temperature and density determination from molecular scattering in the upper atmosphere.

Of course many of the above operational uses would require consideration of additional observational information such as TIROS-type cloud observations or Nimbus-type HRIR observations.

Users other than meteorologists may find operational applications for real-time lidar satellite observations. Photo and visual reconnaissance activities may be assisted in planning missions by more precise knowledge of the turbidity of the lower atmosphere or precise information on the height and thickness of cloud layers known to be present from TIROS cloud observations. By analysis of the polarization and intensity of the specular return from the sea surface, some information concerning waves and the low-level wind velocity creating them may be obtained.

III RATIONALE FOR SELECTING CIRRUS AS THE MAJOR TOPIC OF THIS STUDY

During the initial phase of this project, a number of meteorologists both outside and within the Institute and with interests in both research and operations were polled for ideas on what a lidar satellite could and should do to justify its existence. While the responses were of course quite varied and provided the basis for many of the listings in Sec. II, the application which appeared on virtually every list was the mapping of cirrus cloud.

From an equipment point of view, the use of cirrus as the target for an initial satellite lidar effort offers several obvious advantages. It is the first visible feature of undisputed meteorological significance to be encountered when looking down from satellite altitudes; it occurs in systems of large (often global) extent; it is difficult to observe by any presently known technique since low cloud frequently masks it from view either from the ground or from satellite television. Finally, the scattering cross sections of typical cirrus clouds, while small compared to those of other clouds or even the normal aerosol content of clear air at sea level, are large compared to those of molecular constituents at any altitude.

In short, monitoring of cirrus is about the easiest job that can be envisioned for a satellite lidar. As will be shown, even this is considered to be a very marginal proposition with present technology. Until it is shown that cirrus can be successfully monitored, there seems to be little point to considering appreciably more elaborate systems without more justification than is evident so far.

Accordingly, it was decided early in the project to devote a major effort to defining the meteorological significance of cirrus cloud and to accumulate the data on physical and optical characteristics and global distribution required to evaluate the technical feasibility of monitoring it from satellite altitude with lidar.

During the ensuing year, this decision was justified by an increased appreciation of the value of cirrus-cloud observations; both to operational meteorology and to radiation studies; of the need for more quantitative data on cirrus; and of the technical problems that need to be overcome in order to achieve even this initial goal.

IV CIRRUS-CLOUD FORMS

A. General

Cirrus clouds are generated by meteorological disturbances that range from small-scale thunderstorms to large-scale tropical and extra-tropical cyclones. With thunderstorms, the cirrus appears as broad streamers of cloud flowing with the prevailing wind at high altitudes. With cyclones the cirrus appears as a gigantic sheet of cloud (as much as 1200 x 1200 nautical miles in area) over and in advance of the system. The upper tropospheric wind field with these systems may transport such cirrus thousands of miles downwind from its parent system. There is evidence that jet streams which are associated with major circulation systems not only transport cirrus but in many instances also contribute to its generation. Here the typical pattern is one of a cirrus band or series of bands some 50 to 500 miles wide, located on the anticyclonic or warm side of the jet stream (in the northern hemisphere, the right side looking downwind) and extending some 1000 to 2000 nautical miles in length.

Naturally, the hope arises that through a better identification and description, observations of cirrus can provide useful information on the nature and location of its parent system or on the nature of the upper-level wind field in which it becomes imbedded. If it can, then a device capable of providing detailed cirrus observations will become an important tool in analysis and prediction.

Of particular value would be knowledge of the intensity and structure of tropical or extratropical cyclones and jet streams since these systems determine the current and future states of weather. Also, a description of the presence and/or characteristics of cirriform clouds would be valuable to radiation studies. It has obvious value to aviation since cirriform clouds can be troublesome to such activities as jet aircraft refueling or rendezvous, celestial navigation, optical tracking, or photoreconnaissance.

To evaluate the range-finding capability of the lidar satellite in the detection of cirrus clouds, it has been considered of fundamental interest to examine (on the basis of presently available data) (a) where and when cirrus clouds most frequently occur, (b) the associated configurations and dimensions of cirrus as seen from satellite altitude, and (c) what scanning patterns and spatial "sounding" coverage will be desired by an analyst and can be obtained from a satellite.

Complete data on the foregoing points have not yet been accumulated on a global or hemispheric basis for the following reasons: (a) cirrus often cannot be observed from the ground when it is believed to be most abundant (during bad weather conditions), (b) aircraft observations are only available for some specific situations and localities and therefore should not be generalized, and (c) cirrus, as it can be observed with presently available TIROS vidicon data, is difficult to map on a global or hemispheric scale because of inadequate satellite data coverage in space and time, not to mention interpretational problems.

The data on cirrus collected during the course of this project was first organized into an internal SRI Technical Memorandum, as yet unpublished, which was used as basic reference material by all project personnel. A condensation of this memorandum is included herein as Appendix A which, it is believed, will be of particular use to readers with little meteorological background but who have an interest in meteorological satellites. The material in the following section consists principally of conclusions drawn from Appendix A.

B. Data Coverage Recommended for Mapping Cirriform Cloudiness

Assuming that detection and mapping of cirrus clouds is desirable, a question then follows as to the form and density of the observation. This question ultimately must be answered with due regard for the engineering considerations discussed in other sections of this report. However, for the present we will assume only that for the lidar (as for any active system) the cost and complexity of the required equipment will increase with the number of soundings required and that from

satellite altitudes the absolute magnitude of the problem is such that continuous coverage with data density comparable to television or HRIR is out of the question. Thus it is important at this point to examine from a meteorological viewpoint what is the minimum sampling density which could be useful.

In very basic terms, the operational meteorologist is interested first in the simple presence of cirrus cloud, and secondly in how much is present in what general area. Then he may become interested in the small-scale conformation. The latter is of much concern to the cloud physicist.

If large quantities of cirrus observations by satellite-borne lidar are to be made to evaluate the significance of cirrus in analysis and forecasting of tropical and extra-tropical cyclones, the density of data coverage should preferably be such that cirrus features on the mesoscale of the thunderstorm cell (3 to 10 nmi) can be detected and identified. This should be especially applicable to tropical and subtropical areas where the importance of convective cells and the cirrus generated therefrom in the intensification and development of tropical cyclones is recognized. On the other hand, as previously stated, cirriform coverage generated from a single tropical or extra-tropical cyclone of interest may extend over an area in excess of 1200×1200 nmi; with respect to jet streams, the cirrus often appears in bands of extended length (2000 miles or more). Coordinated data coverage should be extensive enough that complete systems of this size can be examined.

While one data point every 3 to 10 nmi (in both the north-south and east-west directions) can be accepted as an upper limit of data-point density required in cyclone analysis, the lower limit should probably not be less than one data point per 50 to 60 nmi square. The minimum scale features that can be analyzed from a data coverage of one point per 50 to 60 nmi square are compatible with the scale of the convergence zones and frontal zones of a cyclone system. These zones constitute an essential part of the tropospheric models that are used

to describe the weather and that are currently being analyzed with the standard meteorological observations (e.g., frontal cyclone model). The required data density on jet streams can be evaluated from data on typical spacing of cirrus bands (Conover, 1960) (see Fig. IV-1).

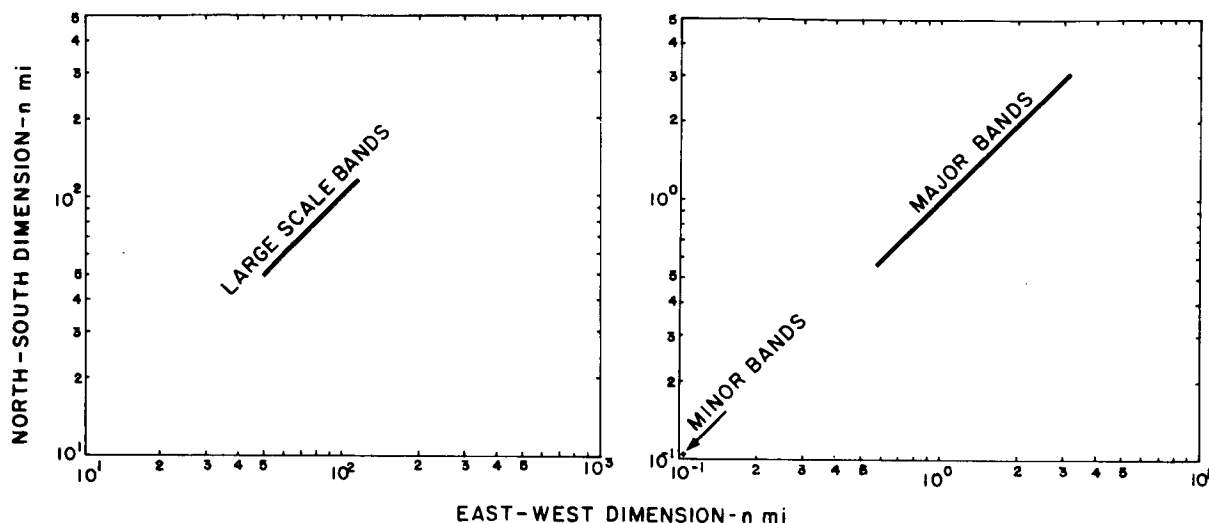


FIG. IV-1 ESTIMATE OF DIMENSIONS OF SPACING BETWEEN JET-STREAM CIRRUS BANDS

The optimum method will be dependent not only upon the purpose for which the data will be used and upon an agreement as to what is "significant" in cirriform cloudiness, but on engineering factors as well. However, from the standpoint of meteorology, it seems likely that the operational meteorologist will use the height data to construct charts of isopleths of cirrus altitude and thickness to be used in conjunction with the concurrent satellite photograph. He naturally will want, if possible, to know something about all the cirrus he can see in the photograph, and hopefully something about subvisible cirrus. Later, as information and knowledge accumulates, he may be in a better position to utilize fine altitude resolution from a smaller number of samples.

If initial power restrictions do not permit wide-area scanning, the research meteorologist will certainly welcome lidar data taken simply as a series of soundings made along the satellite subtrack. A

downward-pointing lidar capable of firing approximately once per second could generate a cloud altitude and thickness profile based on sample points taken every 3 to 3.5 nmi. This density of data acquisition is greater than that ordinarily achieved in atmospheric sampling and, if used in conjunction with a concurrent television or HRIR picture, could be of great value in evaluating the potential of the lidar and in planning future programs.

The minimum data density which would appear to be worth considering seriously for incorporation into an unmanned satellite even for research purposes would result from a vertical sounding about every 50 to 60 nmi along the orbital track; i.e., approximately one every 18 seconds. If the lifetime of the laser becomes an important consideration, it would be satisfactory to operate such a simple system by command from the ground only during times when interesting cloud situations prevail.

V EQUIPMENT DESIGN FACTORS

A. General

Quantitative values for the various possible tradeoffs in the design of a lidar for space application evolve from study of the lidar equation developed in Sec. V-B.

However it is instructive at this point to list the major contributing factors, the qualitative relationships between them, and the practical boundaries which have been used in compiling the predictions of system performance used in this report. Should a technical breakthrough suddenly reduce the limitation on any one parameter, it is hoped that this section may be useful as a checklist and starting point in evaluating how much total system improvement can be realized before some other limitation takes over.

For the case of a short-pulse ruby lidar, the major specifications can be grouped conveniently into four associated with the transmitter and five for the receiver.

- (1) Transmitter pulse energy should be generally as large as possible, limited by
 - (a) Laser capability
 - (b) Available primary power
 - (c) Reliability
 - (d) Possible eye damage, if beam size is small (See Sec. V-F).

These are interrelated with consideration of

- (a) Pulse repetition rate
- (b) Pulse length.

The value used for design estimates is

$$P_t = 1 \text{ joule per pulse.}$$

- (2) Transmitter pulse length should be short compared to the two-way transit time in the minimum radial dimension of interest in the phenomenon being probed.

For classification of clouds into 500-foot layers, this would specify a maximum pulse length of approximately one microsecond. For probing such volume targets, shorter pulses offer no advantage nor suffer any penalty. It is the total pulse energy which is important. The currently preferred method of obtaining short high-energy pulses is by means of Q-switching the resonant cavity. The pulses which emerge naturally from this mode of operation are very much shorter than one microsecond--typically less than thirty nanoseconds. The value used for design estimates is $t = 25$ nanoseconds.

(3) Transmitter beam size and shape. The minimum beam cross-sectional area near the earth will be limited by:

- (a) Values obtainable with practical ruby rods and collimating optics
- (b) Difficulty of tracking with the receiver field of view
- (c) Possibility of eye damage to observers on earth
- (d) Possibility of missing important information and wasting valuable pulse energy by firing through very small clear areas of no meteorological significance.

The maximum beam cross-sectional area near the earth will be limited by the maximum size of cloud features over which the meteorologist is willing to integrate in determining the value to be assigned to a single sampling point. The transmitter beam size should not be larger than that of the receiver (to prevent energy waste).

Ultimately, there may prove to be some advantage to using specially shaped beams tailored to specific cloud types (e.g., a long thin rectangle for probing cirrus filaments). For the present, no clear need for special shapes is apparent, and simple circular or square cross sections will be assumed. The beam angle used for design estimates is $\theta_t = 0.1$ to 10 milliradians.

(4) Pulse repetition frequency. The PRF should be as great as possible, limited by

- (a) Available primary power
- (b) Laser cooling capacity
- (c) Range ambiguities. A slight complication occurs when the rate exceeds approximately 170 pps, where $1/\text{PRF}$ equals the round trip transit time, but no serious ambiguities occur until $1/\text{PRF}$ becomes less than the round-trip transit time between the top of the sensible atmosphere

(100,000 ft) and the ground. This consideration would limit useful PRF's to less than approximately 20,000 pps.

There is no advantage (in fact there may be some loss) in substituting a series of N smaller pulses, each of energy E/N , for a single large pulse of energy E . (If all pulses occur in a burst shorter than the receiver integration time there will be no loss.)

The minimum rate will be determined by minimum number of sampling points required for full earth coverage. This is independent of satellite altitude. (See Sec. V-D.) The maximum rate used for preliminary system evaluation is $PRF_{max} = 2$ pps (required to provide continuous coverage at 1 data point per degree of latitude and longitude).

- (5) Receiver beam size and shape. For maximum beam energy utilization, the receiving beam cross section should be no smaller than the transmitting beam cross section. The minimum size will be determined by

- (a) Minimum size attainable in the transmitter beam
- (b) Difficulty of tracking with the transmitter beam.

The maximum size will be limited by the background light power intercepted in relation to the signal power returned within the same beamwidth (see Sec. V-B-2 for quantitative discussion).

The choice of beam shape will be determined by the same considerations as for the transmitter beam shape (see above). Certain beam shapes may be preferred in order to facilitate servo tracking of the receiver with the transmitter using fast spot wobbling techniques.

- (6) Receiver aperture size. This should be as large as possible, limited only by mechanical considerations of size, weight, rigidity, and optical efficiency. Since a larger receiver aperture always results in an improved detection probability, even for daylight operation, receiver aperture area may be exchanged for transmitter pulse power.

The maximum value to be used in preliminary design estimates is $A_r (max) = 1.0$ square meter. Note that appreciable reduction in geometric resolution as compared to that usually specified for large optics may be possible and still permit compatibility with the receiver beamwidth requirements discussed above.

(7) Receiver predetection bandwidth. This should be as narrow as possible, limited by

- (a) The point where further bandwidth reduction in practical filters is offset by increased transmission loss
- (b) Frequency variation of the laser, principally due to temperature effects
- (c) Variation of the transmission peak wavelength with direction of the light being filtered. (For currently available interference filters, the shift near normal incidence is approximately $1 \text{ \AA}/\text{degree}$.) This restriction in permissible divergence of the light bundle at the filter implies that the desirable wide-aperture receiving system has a long effective focal length and this in turn restricts the ability to scan over large nadir angles

The minimum value used for preliminary design calculations is $\Delta\lambda(\text{min}) = 3 \text{ \AA}$ to 50 percent response points.

(8) Receiver integration period (range resolution interval). This should be as large as possible, limited by the minimum range resolution desired. The value used for preliminary design estimates is $\Delta t = 2$ microseconds, (corresponding to an altitude cell size of 1000 ft for vertical sounding).

(9) Receiver signal amplitude range and amplitude resolution. The range should be large enough to accommodate the full gamut of possible signal return levels from snow-covered earth to Rayleigh molecular scattering at approximately 10 km elevation. Amplitude resolution should be adequate to record significant variations in cloud densities.

The values used for preliminary design estimates are

- (a) Amplitude range = 60 dB (of received radiation power)
- (b) Amplitude resolution = 1-3 dB.

See Secs. V-B and V-E for further discussion.

B. Power Levels Required for Detection

1. General; the Lidar Equation

As is the case for most radar and communication problems, the specification of the required power for a lidar transmitter involves

consideration of the strength of the desired signal return as compared to the strength of competing background radiation and to fluctuations in the receiver output due to internal system noise. Rather than attempting to work with one all-inclusive system equation, it appears preferable for this discussion to consider first the response of an ideal noise-free receiver to the desired signal alone. We next consider separately the internal noise level and the response of the receiver to various types of background radiation.

In Section V-B-4 we combine two sets of data and use statistical concepts to evaluate the probability of detection of the desired signal.

Figure V-1 shows the geometry of a pulsed lidar system located in space and viewing a distributed target such as a cloud. It is assumed here that the target fills the transmitter beam and is thicker than the pulse length $c\tau$ and that the receiver field of view is at least as large as the transmitter beamwidth.

The "lidar equation" describing the performance of the system defined above in the absence of noise or competing background is:

$$P_r = P_t A_r \frac{c\tau}{8\pi R^2} \beta'_{180} T_o \cdot T_a \exp(-2\sigma R') \quad , \quad (V-1)$$

where

- P_r = received power (watts)
- P_t = transmitted power (watts)
- A_r = effective area of receiving aperture (m^2)
- c = velocity of light (meters/second)
- τ = transmitter pulse length (seconds)
- R = one-way distance between lidar and target (meters)
- β'_{180} = volume backscattering coefficient (m^{-1}) (defined more fully below)
- T_o = transmission efficiency of all optical components in tandem (dimensionless)

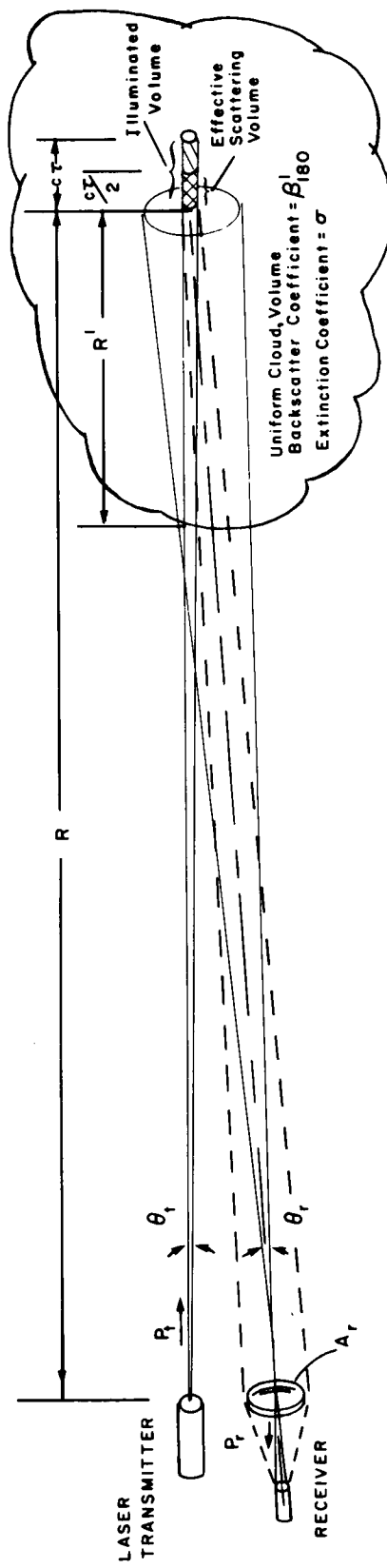


FIG. V-1 LIDAR SYSTEM GEOMETRY

T_a = atmosphere transmission factor accounting for total two-way path attenuation in the region R-R' between the lidar and the region being probed (dimensionless)

$\sigma = \sigma_a + \sigma_s$ = attenuation coefficient within target region (m^{-1})

σ_a = attenuation coefficient due to absorption (m^{-1})

σ_s = attenuation coefficient due to scattering (m^{-1})

R' = penetration distance into the target region (meters)

A few points about Eq. (V-1) are worthy of additional comment. For volume targets, the effective scattering volume (sometimes called the "contributing region") for backscattering is half of the total illuminated volume since because of the two-way travel time the power entering the receiver at any one instant could only have originated from half the length of the illuminated volume.

The volume backscattering coefficient β'_{180} is the value of the volume scattering function for the backscatter angle of 180° .

At least two different definitions are in fairly common use for the factor β'_{180} , resulting in occasional confusion because of numerical values which differ by an annoying factor of 4π . This is unfortunate since β'_{180} is a most convenient parameter to use in exchanging lidar-derived atmospheric data between installations or between equipment engineers and meteorologists. The reader is cautioned to search for the precise definition used for β'_{180} whenever numerical results from different sources are to be compared.

The following convention is used in this report: The product of β'_{180} and the effective scattering volume (the contributing region) is a "radar backscattering cross section," β , defined in conventional microwave radar terminology*--i.e., as if the intercepted power were scattered isotropically. If, as is sometimes done, the volume backscattering

* $\beta = 4\pi \frac{\text{power reflected toward the source/unit solid angle}}{\text{incident power density}}$ (Skolnik, 1962; Van de Hulst, 1957).

coefficient is defined on a per-steradian basis and given the dimensions of meters⁻¹ - steradian⁻¹, the numerical values for this coefficient will be $1/4\pi$ times those used herein.

When the assumption made in Fig. V-1 of a uniform cloud density is not valid--i.e., when σ is not constant for all of R' --the exponential term in Eq. (V-1) must be determined by integration.

The attenuation factor for non-uniform target is $\exp(-2\int\sigma dR')$. Since the total energy per pulse U_t is

$$U_t = P_t \tau \quad \text{joules} \quad (V-2)$$

U_t can be substituted for $P_t \tau$ in Eq. (V-1), whereupon it becomes apparent that for volume targets and for situations where the allowable range resolution is greater than that limited by the transmitter pulse length, the received signal strength P_r is proportional to the total integrated pulse energy, rather than to the peak transmitted power.

Often it is convenient to work with received powers in units of photons per unit time rather than power. This conversion is easily made by employing the identity,

$$1 \text{ photon} = \lambda/hc \text{ joule} \quad (V-3)$$

for the wavelength being used. h is Planck's constant, 6.625×10^{-34} joule-second. By substituting both Eqs. (V-2) and (V-3) into Eq. (V-1), an alternate expression for the lidar equation results.

$$P_r' = \frac{U_t A_r \beta' \lambda T_o T_a}{8\pi R^2 h} \exp(-2\sigma R') \text{ photons/second} \quad , \quad (V-4)$$

where the prime notation indicates that P_r' is expressed in photons per unit time.

In the following sections, the lidar equation will be applied to various cloud models to determine the signal levels to be expected in practical situations.

2. Atmospheric Models and Predicted Waveforms

In this section we postulate several representative cloud situations and apply the lidar equation to derive the corresponding signal waveforms that would be expected from probing this atmosphere with a pulsed ruby lidar located in a 1000 km satellite.

From the point of view of a simple optical radar operating on non-resonant backscattering at some specified wavelength, the actual physical situation existing in the atmosphere can be adequately modeled by two functions, $\beta'_{180}(h)$ the volume backscattering coefficient as a function of elevation, and $\sigma(h)$ the extinction coefficient as a function of elevation. While such a model is uniquely specified by a particular physical distribution of particle sizes, shapes, composition, and number densities, it does not of course follow that the inverse is true. However, the construction of profiles of $\beta'_{180}(h)$ and/or $\sigma(h)$ is about as far as a single-frequency lidar alone can go toward describing the physical situation. This provides a much more precise description than is available from television, photography, or visual observation, and is perhaps the best information interface between the lidar and the meteorologist or cloud physicist.

The specification of either one of the two functions provides a fairly good description since β'_{180} and σ are usually closely related. That is, for a given scattering volume,

$$\beta'_{180} \approx k\sigma \quad . \quad (V-5)$$

When the scattering particles are small compared to the wavelength of the illumination (Rayleigh scattering), $k = 1.5$. The ratio is not constant for larger and non-spherical particles which require the relatively complex calculations of Mie scattering theory, but it seldom differs from unity by more than a factor or two (see Sec. VI).

Thus in the following discussion and throughout most of this report the volume backscattering coefficient β'_{180} will be the principal parameter used to describe the targets being probed.

Figures V-2 through V-5 present four different models, together with the associated lidar returns. The top curve (a) in each figure presents on semilogarithmic coordinates the assumed distribution of β'_{180} as a function of elevation (or time). The middle curves (b), again on semilogarithmic coordinates, show the expected lidar return level at a 1000 km satellite, and the bottom curves (c) present this same information on linear coordinates. The linear coordinate waveforms have been included principally to show the appearance of the return when viewed on a conventional A-scan oscilloscope display, which because of its simplicity is the presentation that has been used for most of the data published to date. It is evident that with the linear A-scan display valuable information would often be lost by compression at the top and lack of resolution at the bottom, and also that it is more difficult to make the mental transition between the signal waveform and the actual distribution of cloud in space. Note that in the semilogarithmic presentation a uniform cloud distribution results in a signal return with a linear negative slope which is directly proportional to the attenuation coefficient σ within the cloud.

The units used on the ordinates of the signal-return waveforms are photons/m²-microsecond and give the signal power density which should exist at the receiving aperture. By multiplying these numbers by the effective receiving aperture area and by the quantum efficiency of the photodetector, the signal output in counts per microsecond is obtained for any specific receiving system. Alternatively, for the higher signal levels where the photoelectron rate is too high to permit digital counting of individual pulses, the waveforms can be thought of as representing the output current at the anode of the photomultiplier.

In Fig. V-1 we have assumed a uniform medium-density cirrus-cloud layer between 26,000 and 31,000 feet (7.9 to 9.5 km), a uniform medium-density stratus layer between 8,000 and 10,000 feet (2.3 to 3.1 km), level grassland at the earth's surface and a Clear Standard Atmosphere at all other elevations.

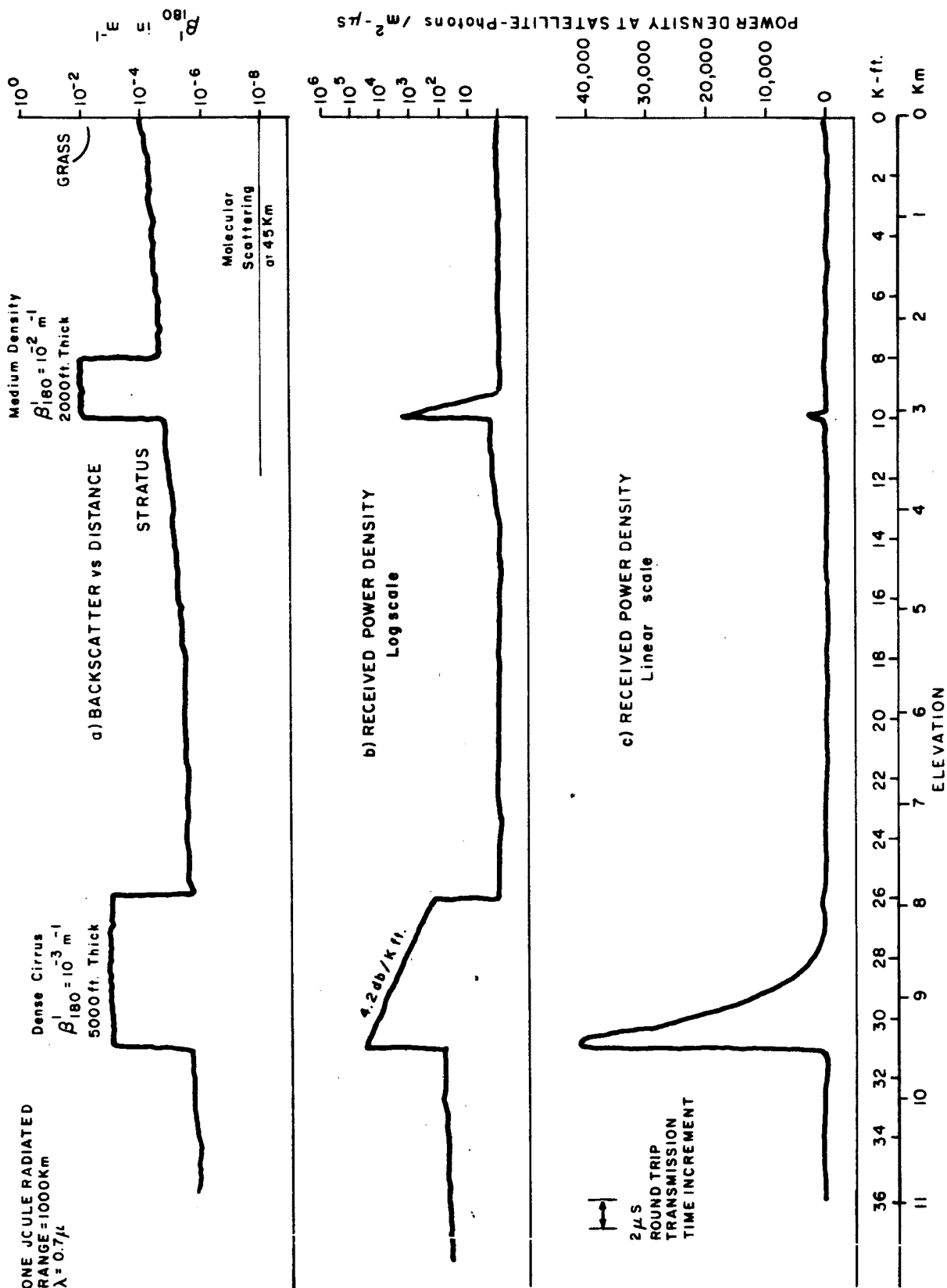


FIG. V-2 PREDICTED LIDAR RETURN: BACKSCATTER DISTRIBUTION FOR MODEL A

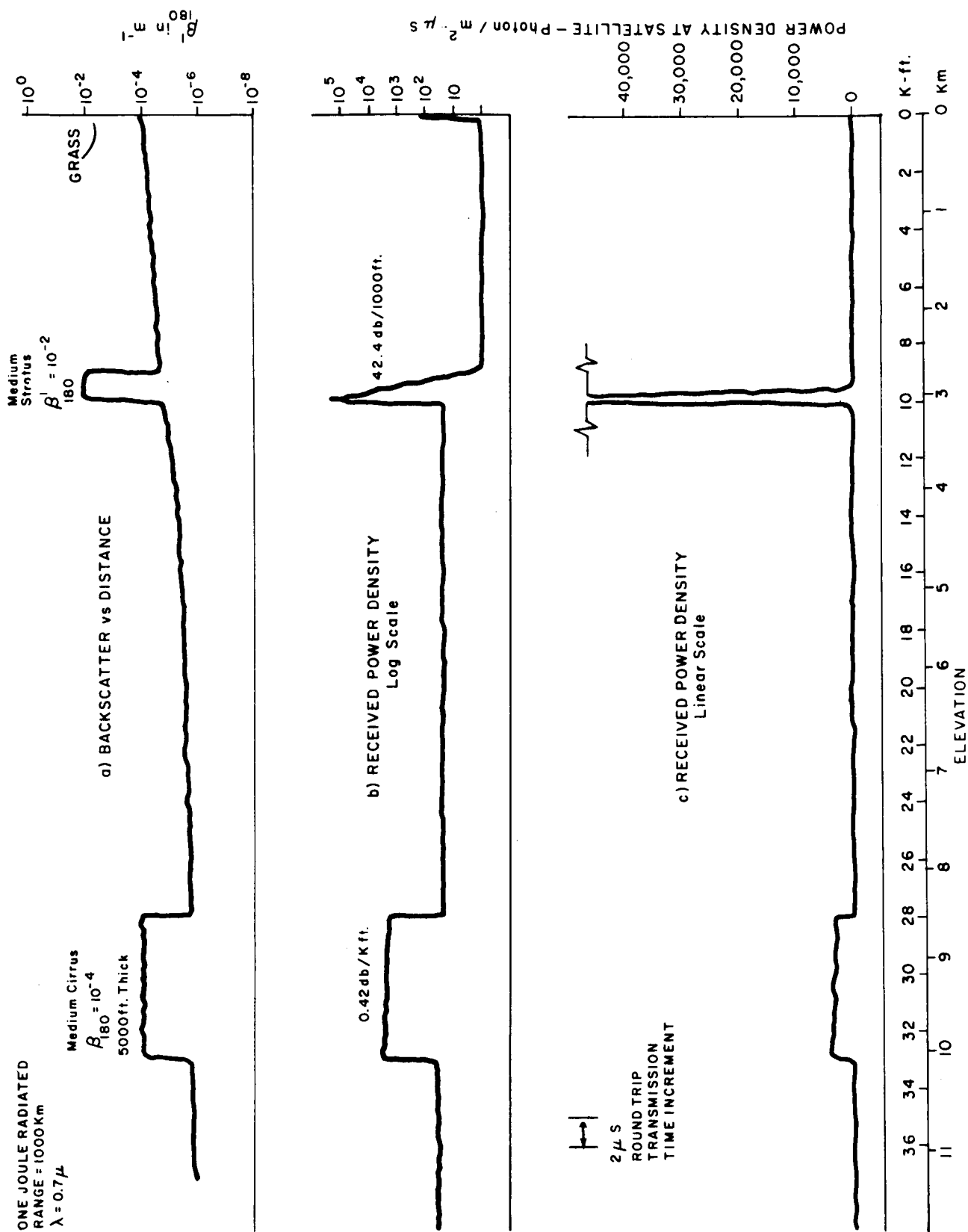


FIG. V-3 PREDICTED LIDAR RETURN: BACKSCATTER DISTRIBUTION FOR MODEL B

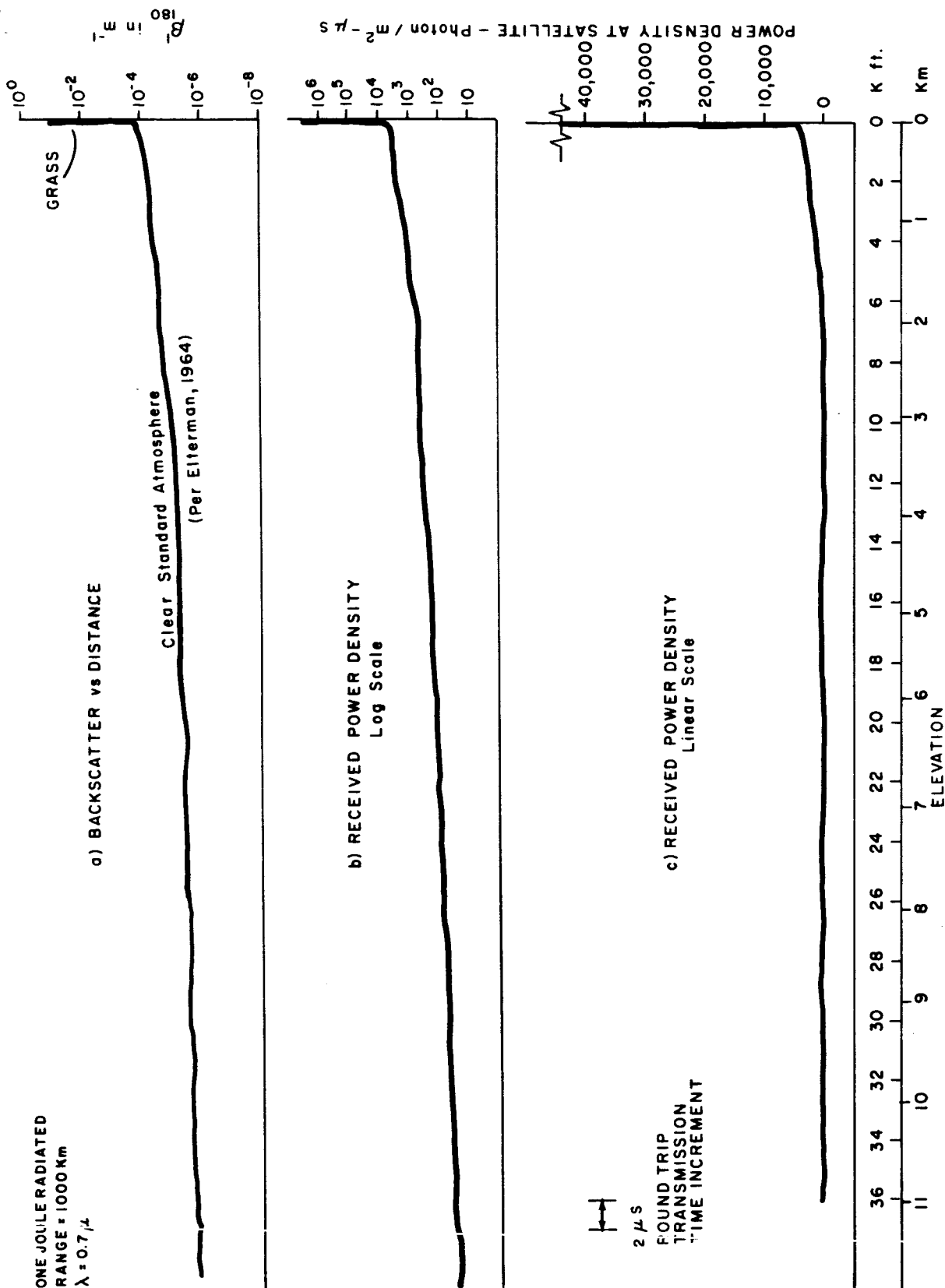


FIG. V-4 PREDICTED LIDAR RETURN: BACKSCATTER DISTRIBUTION FOR MODEL C

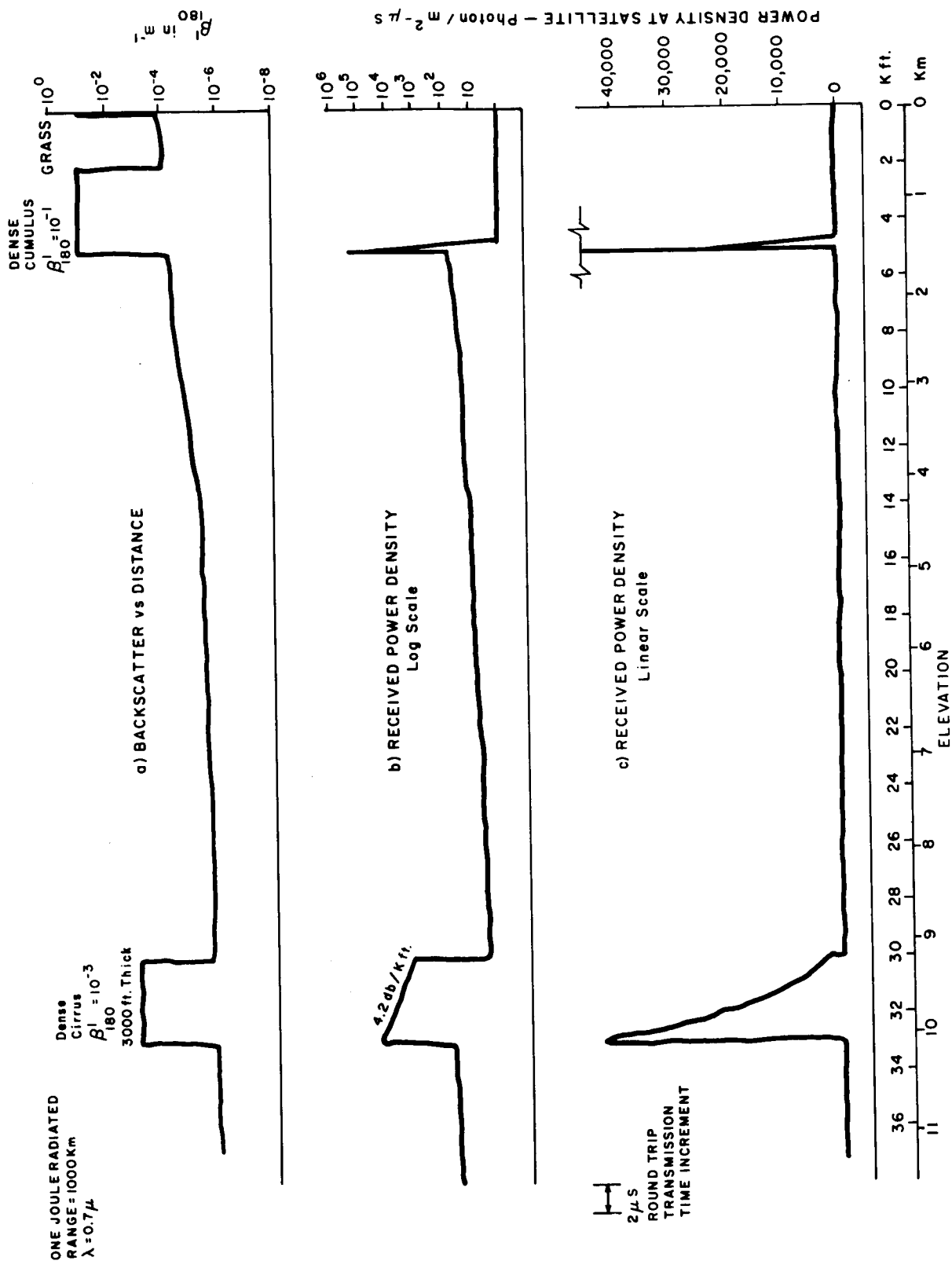


FIG. V-5 PREDICTED LIDAR RETURN: BACKSCATTER DISTRIBUTION FOR MODEL D

Values of β'_{180} for the clouds correspond to those in Fig. VI-2 of Sec. VI. For the clear atmosphere, values were taken from Elterman's model of a Clear Standard Atmosphere (Elterman, 1964).

The first lidar return of significance is received at the satellite (after a total round-trip delay of about 6 milliseconds) from the top few hundred feet of the cirrus layer. For this point the atmospheric transmission term in the lidar equation [Eq. (V-4)] will be essentially unity, so that the power density returned to the satellite will be determined principally by U_t , the transmitted energy, by β'_{180} the volume backscattering coefficient of the cloud, by V , the relative amount of cloud cover intercepted by the beam, and by R , the distance from satellite to cloud.

Since only order of magnitude estimates are required at this point, the calculations will be kept simple by assuming a constant range of 1000 km for all targets, a one-joule transmitted pulse, and $V = 1.0$.

With these assumptions, Eq. (V-4) reduces to

$$\frac{P'_R}{A_R} = 4.18 \times 10^7 \beta'_{180} T_a \exp(-2\sigma R) \frac{\text{photons}}{\text{m}^2 - \mu\text{s}} \quad (\text{V-6})$$

Thus the power density expected back from the top of the cirrus cloud (with $\beta' = 10^{-3} \text{ m}^{-1}$) is $4.18 \times 10^4 \text{ photons/m}^2 - \mu\text{s}^{-1}$, which is plotted in Fig. V-1(b). Returns from the lower portions of the cirrus layer and from any targets below the cirrus top will be attenuated by scattering of photons out of the beam on both the incident and return paths.

Waveforms (b) and (c) were derived by solving Eq. (V-6) using as the atmospheric transmission factor T_a for each point an integrated value obtained by summing scattering losses due to any layers above that point:

$$T_a = \exp -2\sigma \int_{R_1}^{R'_1} \sigma_1 dr + \int_{R_2}^{R'_2} \sigma_2 dr + \int_{R_3}^{R'_3} \sigma_3 dr \dots \quad (\text{V-7})$$

To those accustomed to thinking of transmission engineering problems in terms of "decibels loss per unit distance" it is convenient to recast the signal decay within the cloud as follows:*

$$e^{-2\sigma R'} = 10^{-2\sigma R'(\log e)} = 10^{-2\sigma R'(0.434)} ;$$

$$\frac{\text{signal decay}}{\text{unit distance}} (\text{for two-way transmission}) = -8.68\sigma \frac{\text{dB}}{\text{unit distance}} \quad . \quad (\text{V-8})$$

The following equivalent relations are listed for reference (σ is in units of m^{-1}).

$$\begin{aligned} \frac{\text{signal decay}}{\text{unit distance}} (\text{two-way}) &= -8.68\sigma \text{ dB/meter} \\ &= -8.68 \times 10^3 \sigma \text{ dB/km} \\ &= -2.64 \times 10^3 \sigma \text{ dB/1000 ft} \end{aligned}$$

and since

$$R = \frac{ct}{2} = \frac{3 \times 10^2 t'}{2} = 150t'$$

where t' is echo delay in microseconds and R is one-way range in meters,

$$\frac{\text{signal decay}}{\text{unit time}} (\text{two-way}) = -1.3 \times 10^3 \sigma \text{ dB}/\mu\text{s} \quad .$$

These relations also can be expressed in terms of β'_{180} if, for the various cloud regions one assumes appropriate values of the ratio $k = \beta'_{180}/\sigma$. In sketching the predicted signal waveforms of Figures A through E the following values of k were used:

* While the meteorologist or pure physicist may resist the application of basically telephonic terminology to problems of cloud physics, the occasional use of the term "dB" defined as

$$\text{power ratio (in dB)} = 10 \log_{10} \frac{P_1}{P_2}$$

is felt to be justified because it fills a gap in nomenclature for exponentially decaying phenomena and because much of the instrumentation required for a lidar is calibrated in dB.

Scattering Source	k
Rayleigh	1.5
Water Cloud ($r > 3\mu$)	.625
Cirrus Cloud ($r \approx 120\mu$)	0.625

As discussed more fully in Sec. VII, there is at present considerable uncertainty attached to the value of k for cirrus cloud. A value closer to unity is now felt to be more correct, but since the illustrations in this section were drawn early in the project and there are numerous references to them in other sections, the earlier estimate has been retained here.

Signal returns from the lower cloud and aerosol concentrations were estimated by successively applying Eq. (V-6), using in each case a value for T_a determined by the cumulative losses introduced by all attenuating layers above the altitude being probed.

For example, for the stratus return of Fig. V-2, Eq. (V-6) gives a figure of

$$\frac{P_R}{A_R} = (4.18 \times 10^7)(10^{-2})(7.5 \times 10^{-3}) = 3.14 \times 10^3 \frac{\text{photons}}{\text{m}^2 - \mu\text{s}}$$

for the top portion of the layer, including the effect of attenuation by the higher cirrus layer. The attenuation rate within the stratus layer will be 42.4 dB/1000 ft for a total loss of 84.8 dB ($T = 3.33 \times 10^{-9}$ for 2000 ft stratus).

Similarly, the return from the earth's surface is found by applying Eq. (V-6) and using as the attenuation factor the total loss through the two cloud layers plus 2.2 dB as an integrated value for the remainder of the atmosphere.

$$\begin{aligned} \frac{P_R}{A_R} &= (4.18 \times 10^7)(10^{-1})(1.51 \times 10^{-11}) \\ &= 6.33 \times 10^{-5} \frac{\text{photons}}{\text{m}^2 - \mu\text{s}} \end{aligned} \quad (V-9)$$

Thus, for this cloud situation, the earth return from a one-joule pulse would be well below the quantum detection threshold.

The waveforms for the other assumed cloud situations have been synthesized using a similar procedure.

The signal-return levels read from the ordinates of the (b) portions of these figures can be compared directly with the background light levels tabulated in the following section (V-B-3). They will also provide input data for the detection-probability calculations of Sec. V-B-4.

3. Background Light Levels

The system performance limitations imposed by the extraneous light energy collected along with the desired signals can be investigated by first examining the background power densities which would be expected at the satellite. These data may then be compared with the power density expected at the satellite for various transmitter-target combinations (Sec. III-B-2), using the S/N ratio and detection-probability relations developed in Sec. III-B-4 as criteria for assessing performance.

Except for an inconsequential amount of light generated near the earth's surface by lightning, fires, volcanoes, and man-made sources and except for minor contributions from meteors, the aurora--and the nightglow--all of the stray light entering a carefully designed receiver must necessarily be of astronomical origin and reflected from the earth and/or its atmosphere.

The power density P_s existing at the satellite due to light reflected from the earth will be:

$$P_s = \frac{B_E A_{\text{beam}} \Delta\lambda}{R^2} \text{ watts/m}^2 \quad (\text{V-10})$$

where A_{beam} is the cross-sectional area of the receiver beam pattern near the earth, $\Delta\lambda$ is the effective bandwidth of the optical predetection filter, R is the satellite-to-earth distance, and B_E , the earth's

radiance, is a function of the ambient irradiance I_E falling on the earth and of the nature of the reflecting surface.

Within the accuracy required for this evaluation, the earth and its surrounding cloud cover can be considered as a Lambertian reflector having an effective reflection coefficient r .

Thus

$$B_E = \frac{I_E r}{\pi} \quad \text{watts } m^{-2} \text{-steradian}^{-1} A^{-1} \quad (V-11)$$

where I_E is measured in watts $m^{-2} A^{-1}$.

In the general case, I_E , B_E , and r are functions of wavelength. In this report operation with ruby lasers at the fundamental wavelength of $6943 \text{ } \overset{0}{\text{\AA}}$ has been assumed (except where otherwise noted). Investigation of noise levels at other visible and near-visible wavelengths can be accomplished by multiplying the results for ruby by appropriate wavelength-dependent scale factors. (See Sec. IX.)

Table V-1 lists representative numerical values for I_E , and Table V-2 gives typical values for r .

Table V-1
AMBIENT LIGHT LEVELS AT THE PLANET EARTH
(Duntley, 1948)

	Illumination (ft-candles)	Incident Power Density I_E in Region of $\lambda = 0.7\mu$	
		(watts - $m^{-2} A^{-1}$)	(photons - $s^{-1} - m^{-2} - A^{-1}$)
Full Sunlight	10^4	10^{-1}	3.5×10^{17}
Full Moonlight	10^{-2}	10^{-7}	3.5×10^{11}
Starlight	10^{-4}	10^{-9}	3.5×10^9

Table V-2
EFFECTIVE DIFFUSE REFLECTION COEFFICIENTS
(Gordon, 1964)

Surface	$r(@ \lambda \approx 0.7\mu)$
Snow, dense clouds, salt beds, white sand	0.30 - 1.0
Soil	0.06 - 0.3
Vegetation	0.03 - 0.1
Ocean	0.02

Values of I_E , r , and B_E have been measured and reported by many investigators. Since measured values will vary appreciably in both space and time, and since general descriptors such as "twilight," "starlight," "vegetation," etc. are necessarily inexact, numerical precision beyond two places is seldom justifiable. The important thing is to note the tremendous range of perfectly feasible values which can be encountered (over eleven orders of magnitude for B_E) and to be sure that the decimal point is correctly placed.

Figure V-6, which is a plot of Eq. (V-11), is included as an aid to visualizing this large dynamic range while considering system design tradeoffs affected by the background light level.

The three scales along the right hand margin of Fig. V-6 interpret the values of B_E in terms of background power density at the satellite for the particular case of vertical viewing at 1000 km range, $\Delta\lambda = 3\text{\AA}$, and for three different values of effective receiver field of view (expressed in terms of beam cross-sectional area at the earth.) These values represent solutions of Eq. (V-12):

$$P'_{SE} = B_E \cdot \Delta\lambda \cdot \frac{A_{\text{beam}}}{R^2} \cdot \frac{\lambda}{hc} \times 10^{-6}, \quad (\text{V-12})$$

where P'_{SE} is the power density existing at the satellite due to background radiation within the field of view of the receiver. The primed

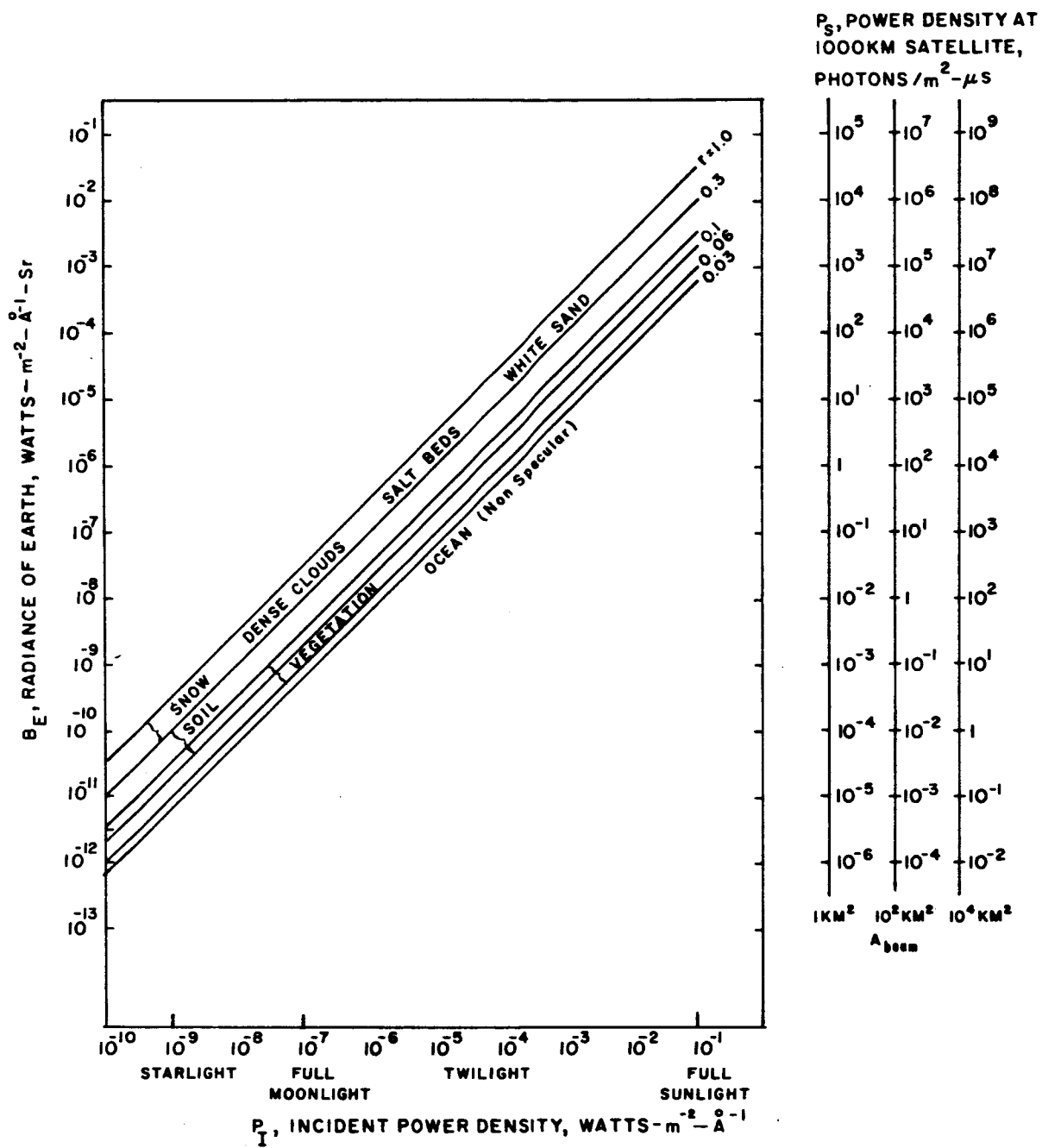


FIG. V-6 BACKGROUND LIGHT LEVELS SEEN FROM SATELLITE

notation indicates that P'_{SE} is expressed in photons $\text{-m}^{-2} \text{-}\mu\text{s}^{-1}$ to make it directly comparable with P'_{SL} , the power density existing at the satellite due to laser echoes.

This presentation clearly points out the folly of becoming overly concerned about precise values of reflection coefficients for earth features when making first design estimates of the amount of background light to be expected. The total gamut from snow to very black surfaces is seen to be quite small by comparison to the changes due to time of day. For example, black asphalt at noon is very much brighter than snow in late twilight. Specular reflections from water surfaces and (less frequently) from the tops of ice clouds will occasionally raise the background level above the values shown in Fig. V-6. However, interference from this source will be rare. Even when encountered, it would not be expected to persist for more than one or two soundings.

4. Probability of Detection as a Function of Signal and Background Levels

For a given background noise level in a particular range interval, the reliability with which a desired signal can be detected and identified will decrease as the signal level decreases. Alternatively, when one is willing to specify a minimum acceptable detection reliability for the system, one can say that there exists a lower limit to the received signal which may be detected. This section discusses the determination of this minimum signal level in terms of the average background noise level, a specific probability of detection, and a specific probability of false alarm* for the case of single-look detection (enhancement of the signal detectability by means of integration over several successive pulses is not considered).

* Probability of Detection = $P(d)$ = the probability that a signal will be correctly identified as a signal; Probability of False Alarm = $P(f)$ = the probability that background noise will be mistakenly identified as signal.

In the case of non-time-varying background illumination, the lidar receiver background photoelectron count per range cell will vary with time according to a Poisson probability distribution about an average value \bar{n} .

The probability of n photoelectrons arriving during a particular range cell is

$$P(n) = \left[\frac{(\bar{n})^n e^{-\bar{n}}}{n!} \right] \quad (V-13)$$

where \bar{n} is the average number of photoelectrons per range cell.

Assume that the receiver has a counting threshold T such that the arrival of T or more photoelectrons will be interpreted as a return signal. The desired condition is that the signal threshold T be set sufficiently above \bar{n} to assure that statistical fluctuations in the background noise will not often be interpreted as signal. This concept is illustrated graphically in Fig. V-7. The probability that the background noise fluctuation will exceed the threshold T (i.e., the false-alarm probability) is defined as

$$P(f) = \sum_{n=T}^{\infty} \frac{(\bar{n}_b)^n e^{-\bar{n}_b}}{n!} \quad (V-14)$$

In the presence of a given average background of \bar{n}_b counts per resolution cell, the threshold T must be chosen to achieve a low value of $P(f)$.

During the reception of a return signal in a particular range cell (i.e., range time interval) the expected or average number of photoelectrons generated in that interval will be the sum of the expected number of electrons due to the signal, \bar{n}_s , and the background noise \bar{n}_b discussed previously:

$$\bar{n}_s + \bar{n}_b = \overline{n_s + n_b} \quad (V-15)$$

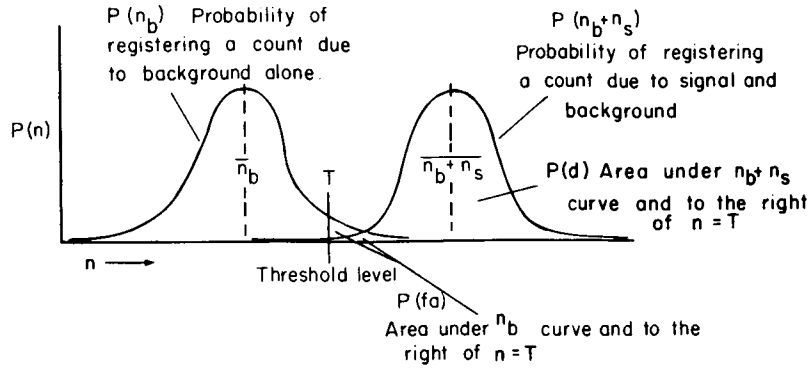


FIG. V-7 DETECTION AND FALSE-ALARM PROBABILITIES

The probability of observing exactly $(n_s + n_b)$ photoelectrons in a particular range cell is given by:

$$P(n_s + n_b) = \frac{\frac{(n_s + n_b)^{n_s + n_b}}{e^{n_s + n_b}} - \frac{(\bar{n}_s + \bar{n}_b)^{n_s + n_b}}{e^{\bar{n}_s + \bar{n}_b}}}{(n_s + n_b)!} \quad (V-16)$$

Similarly, the probability that $n_s + n_b$ photoelectrons will exceed an arbitrary threshold T (i.e., the probability of detection) is given by

$$P(d) = \sum_{(n_s + n_b)=T}^{\infty} \frac{\frac{(n_s + n_b)^{n_s + n_b}}{e^{n_s + n_b}} - \frac{(\bar{n}_s + \bar{n}_b)^{n_s + n_b}}{e^{\bar{n}_s + \bar{n}_b}}}{(n_s + n_b)!} \quad (V-17)$$

Since the threshold T to be used in Eq. (V-17) has been determined by the average background noise \bar{n}_b and a specified value of $P(f)$ in Eq. (V-14), the additional specification of a value for $P(d)$ in Eq. (V-17) will define a minimum value for $(\bar{n}_s + \bar{n}_b)$. Since \bar{n}_b is known, the minimum value of \bar{n}_s is defined by Eq. (V-15).

To summarize, the average background noise level \bar{n}_b and the desired value of false-alarm probability serve to define the value of the counting threshold T . This threshold and the desired value of detection probability will uniquely define the minimum signal level which may be reliably detected with the given values of \bar{n}_b , $P(d)$ and $P(f)$.

Figure V-8 gives a plot of either Eq. (V-14) or Eq. (V-17) as a function of the counting threshold, T.

In Figs. V-9 and V-10, data derived from Eqs. (V-14) and (V-17) are presented in a form which makes it easier to see the dependence of the detection probability on the absolute values of \bar{n}_s and \bar{n}_b . It becomes readily apparent that if one moves up a 45° line of constant \bar{n}_s/\bar{n}_b --corresponding, for example, to increasing either the receiving antenna aperture or the integration time--there always results an increase in the detection probability for a given false-alarm probability. It is also evident from the curves that signals can be detected even in the presence of an equivalent amount of background ($\bar{n}_s/\bar{n}_b = 1$) with a reasonably high degree of confidence--i.e., with $P(d) > 99$ percent and $P(f) < 0.1$ percent--so long as the average number of signal events per integration interval, \bar{n}_s , is greater than about 50.

If one can provide enough transmitter power or a sensitive enough receiver that the average number of signal events per integration interval is on the order of 350, then one can have the same high degree of confidence in the validity of the detection output with a \bar{n}_s/\bar{n}_b of only 0.1.

Comparison of Figs. V-9 and V-10 and examination of the trend in Fig. V-8 reveals that the signal level required for reliable detection is not a very sensitive function of the false-alarm probability for values of the latter below a few percent.

C. Choice of Reporting-Area and Sampling-Spot Sizes

1. General

The specification of an optimum spot size and sampling density for a satellite-borne lidar is one of the most difficult tasks associated with this evaluation. Partial witness to the truth of this assertion is the long and continuing controversy over what is the best compromise between resolution and coverage to be used for observing clouds via satellite-borne television.

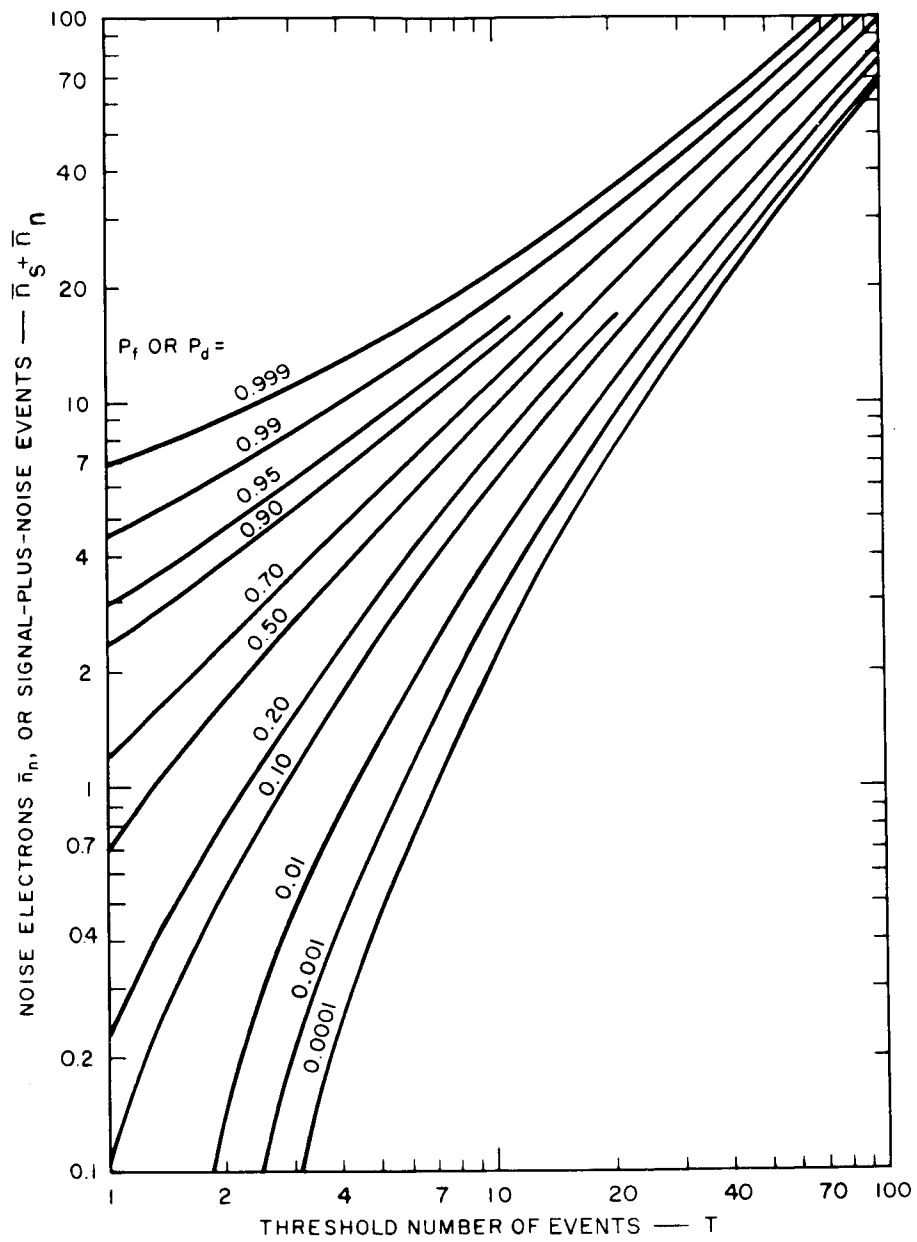


FIG. V-8 DETECTION AND FALSE-ALARM STATISTICS AS FUNCTIONS OF THRESHOLD LEVEL

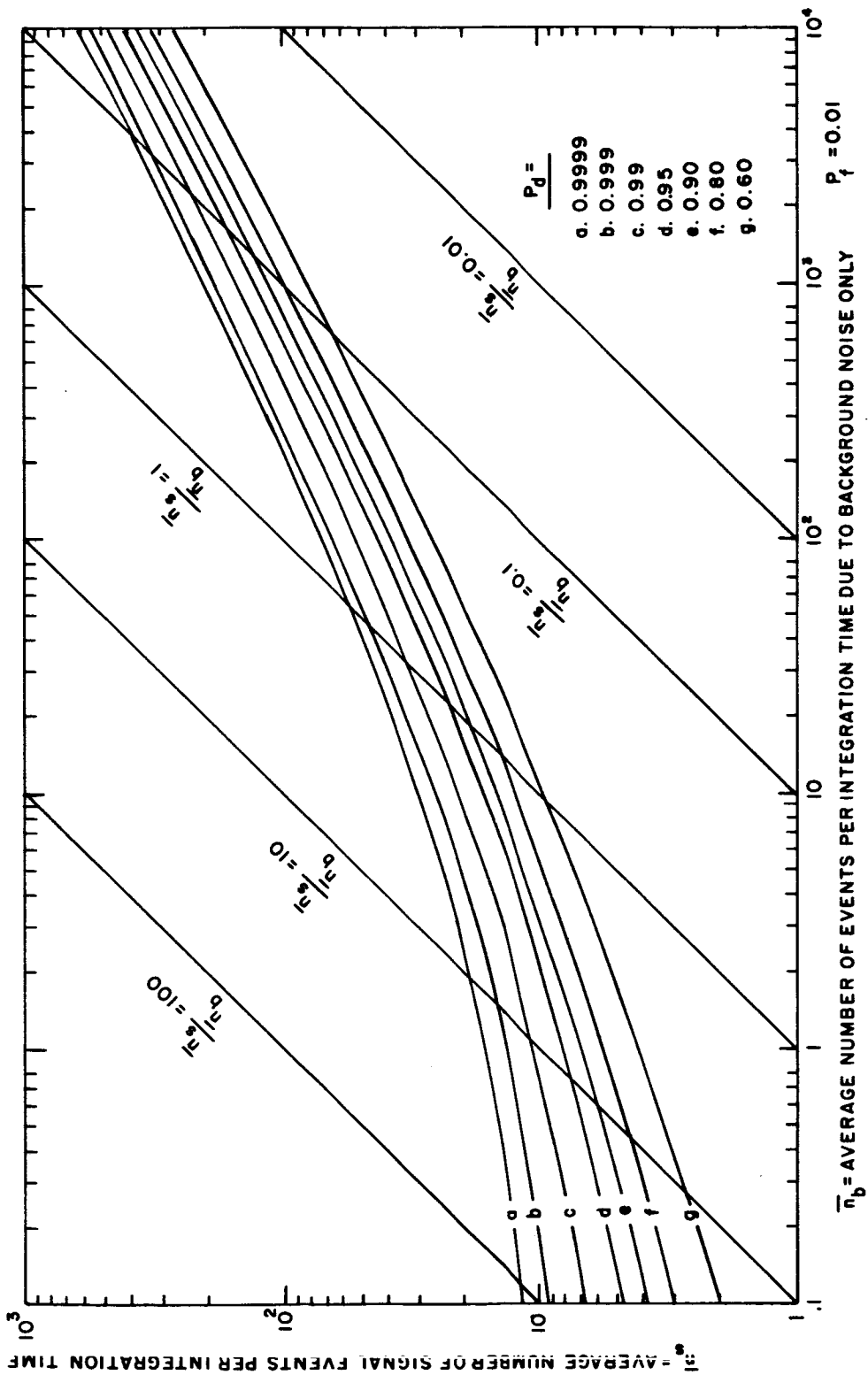


FIG. V-9 SIGNAL LEVELS REQUIRED TO ACHIEVE DETECTION — $P_f = 0.01$

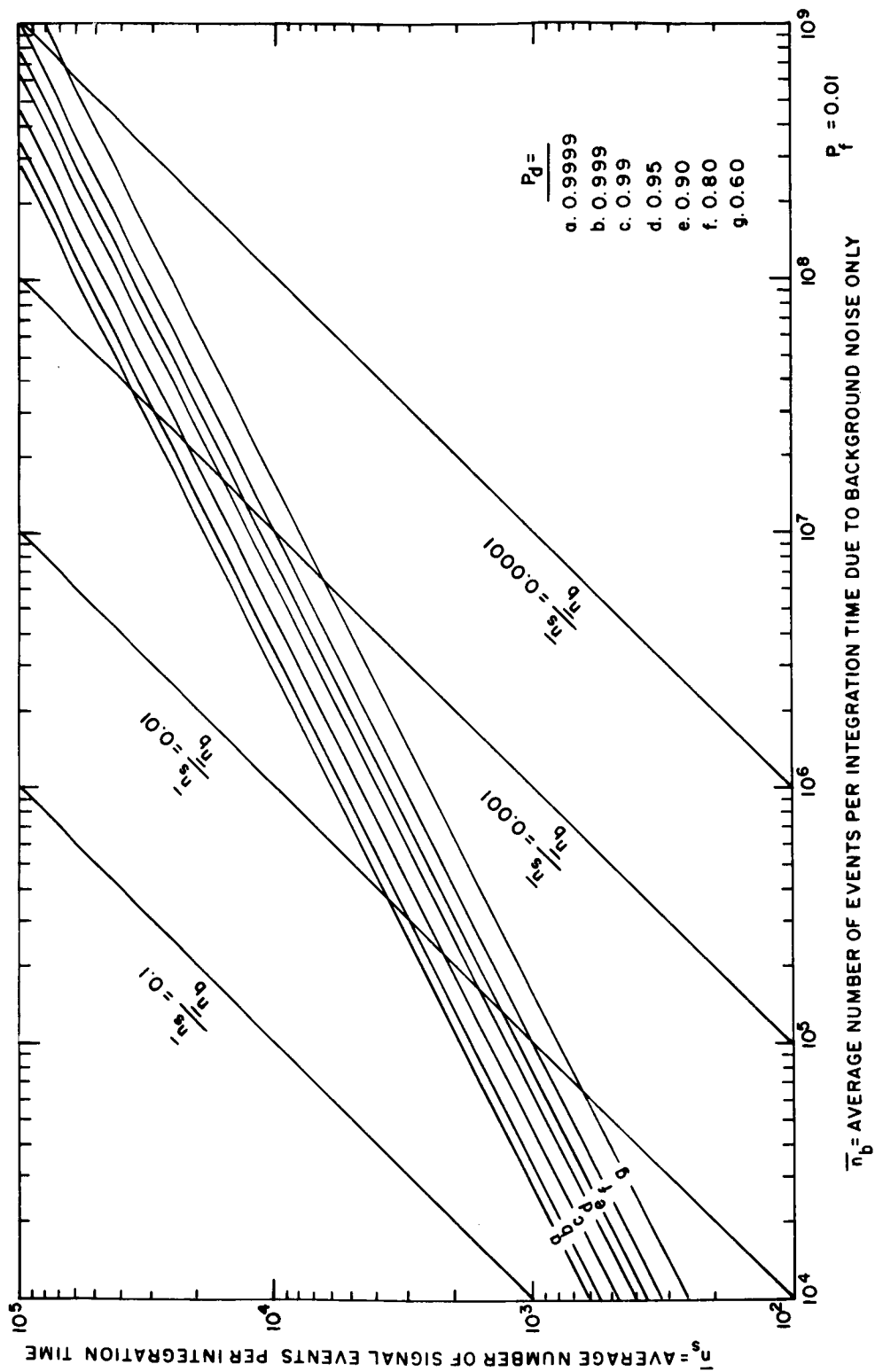


FIG. V-9 Concluded

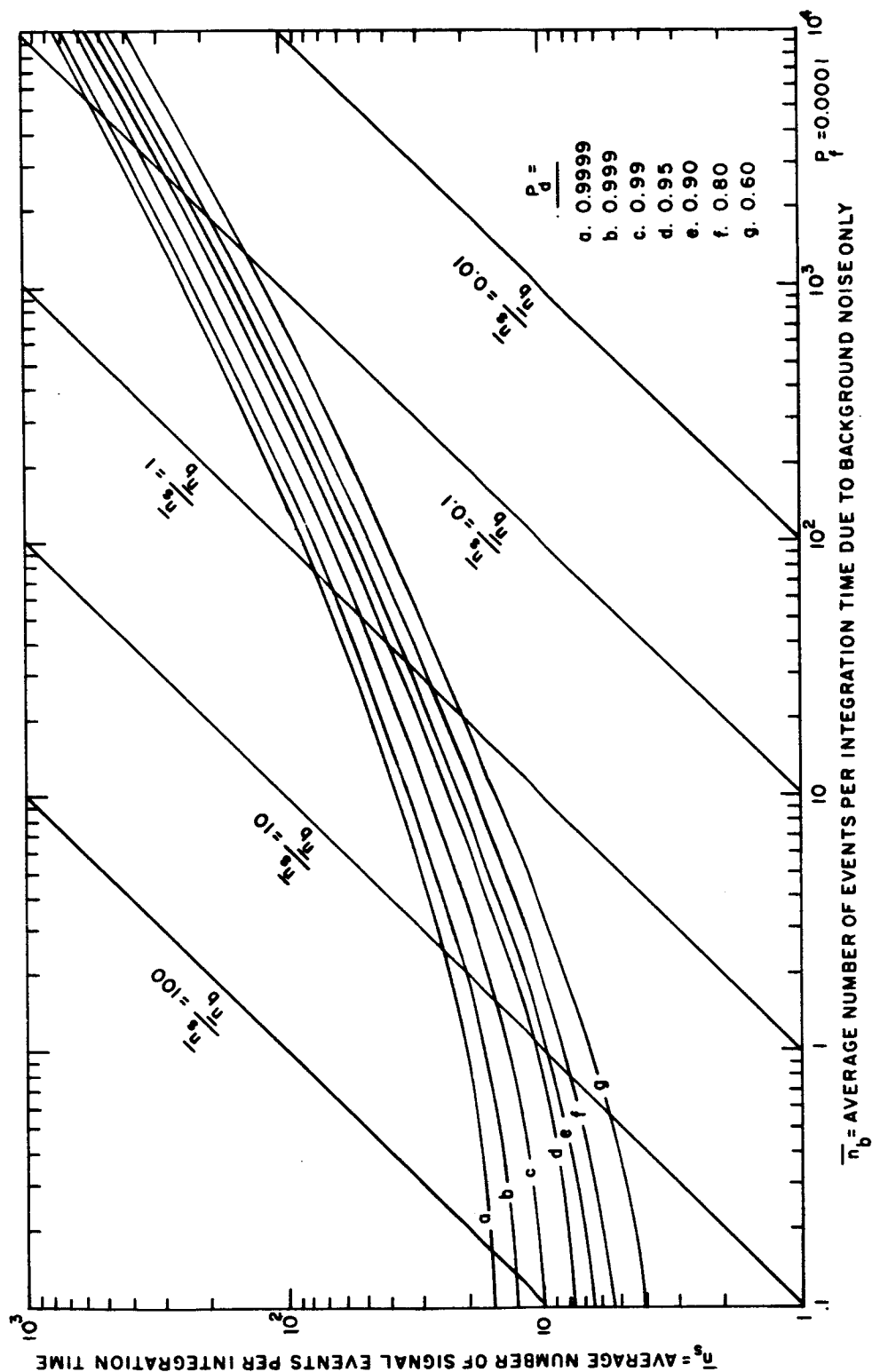


FIG. V-10 SIGNAL LEVELS REQUIRED TO ACHIEVE DETECTION — $P_f = 0.0001$

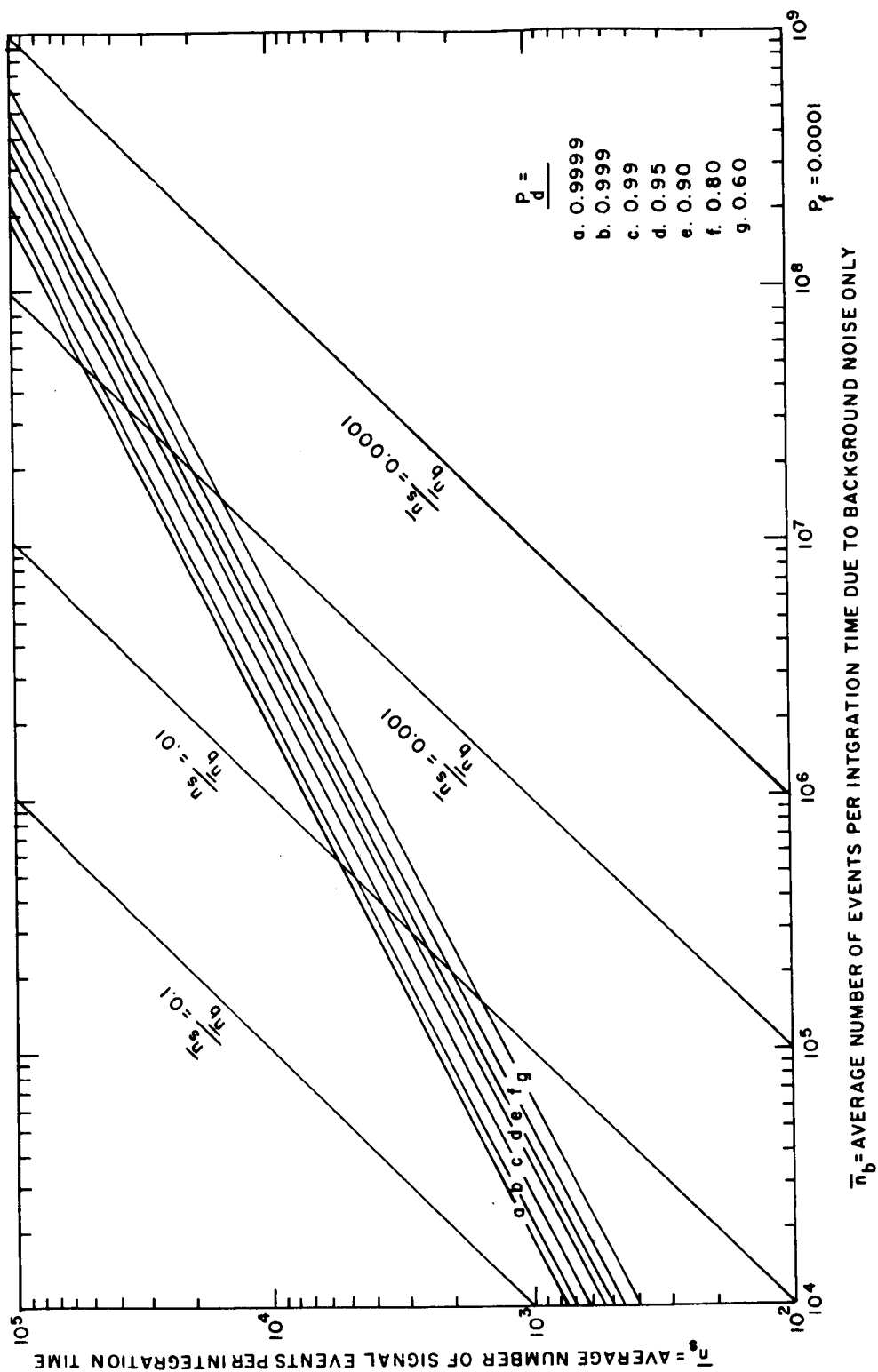


FIG. V-10 Concluded

First, it is important in the lidar case to differentiate clearly between the size of the probing beam and the spacing between soundings taken with that beam. Because of the limited number of soundings possible with an active system, the "reporting area" associated with each sounding will normally be much larger than the area of the actual probing spot. Thus terms such as "definition" or "resolution", unless very carefully defined, tend to be ambiguous and will be avoided here.

2. Reporting Area

The data on extent of cirrus coverage given in Sec. II, the intuition of observers who have worked with thousands of TIROS and NIMBUS pictures, and the experience of numerical weather prediction personnel all point to a desirable maximum reporting-area size of about 100 km on each side. (A rectangular reporting grid is assumed.) This corresponds to approximately 1° of latitude and longitude near the equator.

To obtain this density of data reports requires a lidar sounding rate of 1.86 shots per second, essentially independent of the altitude of the satellite (see Sec. V-D). Fortunately this rate appears to be within reason with respect to current technology in high-power pulsed lasers, at least for ground-based operation. Also, even at 0.1 percent efficiency (a reasonable value for Q-switched ruby lasers) the required primary power for one joule per pulse output would be 1.8 kilowatts which, while high, could be obtained in a satellite if necessary. The chances for significant improvements in laser efficiencies over the next few years, and for the attendant reduction in cooling problems, appear great enough that 1.86 pulses per second will be considered a potentially feasible sounding rate.

3. Spot Size

Technical limitations will place a lower bound on the size of the sampling spot near the earth's surface at about 0.1 km. This figure implies a transmitter beamspread of 0.1 milliradian which is considerably better than that which emerges directly from even a very good ruby rod, but which can be achieved through the use of auxiliary collimating optics. The practical problem of maintaining alignment

between the transmitting and receiving beams in spite of structural variations caused by time and temperature has been reported by almost every group attempting to work with large-aperture systems having beamwidths much less than one milliradian. Some form of automatic servo tracking of the receiver with the transmitter almost certainly will be needed if the 0.1 km spot size is required.

The technical limitations on the largest usable spot size are determined principally by the permissible background light pickup, and one argument for specifying it runs as follows:

- (1) Assume that the lowest signal return that will be of interest is that corresponding to Rayleigh molecular scattering from an elevation of 10 km (very weak cirrus layers will yield returns only slightly larger than this; see Sec. IV).
- (2) For an assumed 1-joule transmitter pulse, either Eq. (V-6) or Fig. V-4(b) gives a value for the expected signal return at the satellite of 80 photons/m² - μ s, or 160 photons/m² for the 2-microsecond integration period (corresponding to a desirable range resolution cell of 1000 feet).
- (3) With a 1 m² receiving aperture and a photodetector quantum efficiency of 5 percent (barely attainable today), the expected signal return from this target would be 8 pulse counts per integration interval.
- (4) Then, using the chart of Fig. V-9, it is found that for a 90-percent detection probability and a 1-percent false-alarm probability, the allowable noise counts from the photodetector should not exceed one count per integration interval. Using the same figures for quantum efficiency and receiver aperture, this corresponds to an allowable background power density level at the satellite of 10 photons/m² - μ s.
- (5) Finally (referring to the background-level chart of Fig. V-6) it is seen that with the assumed 3A bandwidth optical filter, the permissible 10 photons/m² - μ s level is just over that which would be generated by snow in full moonlight if the area of the probing spot were 100 km².

Considering the approximations involved (including the assumption of 100-percent optical and system efficiency) it appears that the largest symmetrical receiver beam which should be considered from a

noise standpoint, even at night, is that which would view an area near the earth approximately 10 km across; this corresponds to a receiving beamwidth of about 10 milliradians.

In Sec. V-D it is shown that an appreciable loss of altitude resolution would result near the edge of a wide scanning swath for beams less than approximately one milliradian wide in the plane of the scan. This suggests the possibility of using a line-shaped scanning aperture having dimensions of approximately 100 km parallel to the orbital track and 1 km perpendicular to the orbital track. However, such a highly elongated scanning aperture would be biased in favor of long filamentary clouds oriented principally in the north-south direction; this approach is therefore felt to be undesirable.

From a meteorological standpoint, the size and shape of the sampling spot must be chosen so that the average or integrated return from the relatively small sample will be most representative of phenomena of interest over the entire reporting area. If the sample size is too small, there is a higher probability of the beam going through holes and giving little or no return from a relatively cloudy situation. If it is too large, strong returns from cloud cells of significant size can be diluted by low or zero return from the surroundings. The statements made in Sec. IV about the desirability of detecting cirrus features on the mesoscale of the thunderstorm cell (3 to 10 nmi or 5.5 to 19 km), together with the data on jet-stream cirrus bands in Fig. IV-1, suggest that the sampling-spot size should be on the order of 1 to 10 km across.

Weighing all of the above considerations, we are led to a recommendation, at least for preliminary system design, of a symmetrical sampling spot 1 to 3 km in diameter.

D. Orbital Considerations

Since it is expected that the lidar would normally be used in close conjunction with other remote sensing devices contained in the same orbiting vehicle it would seem presumptuous to assume that the orbital parameters would be optimized especially for the lidar. Fortunately

most of the design criteria pertaining to orbit selection for television and high-resolution infrared systems are also valid for the lidar.

The ideal orbit for routine meteorological observation appears to be circular, near-polar, and retrograde (sun-synchronous). When provided, in addition, with an earth-oriented platform a satellite in such an orbit provides global coverage with a high degree of day-to-day uniformity in viewing geometry and lighting conditions.

The principal remaining orbital parameters to be specified while still remaining within this general framework are the height and the local time of the ascending node.

These two factors will now be examined from the point of view of satellite-borne lidar operations.

1. Orbital Height

If one assumes that the east-west field of view of a polar-orbiting observational satellite will be designed so that on consecutive orbits the mapped swaths will be contiguous at the equator, then it turns out that the amount of earth area passing through the field of view of the orbiting sensor per unit time is very nearly independent of satellite height. This is because the width of the swath required for contiguous coverage is directly proportional to the orbital period, while the distance covered in the orthogonal or north-south direction is inversely proportional to the orbital period.

Neglecting the oblateness of the earth, the small error caused by precession of the line of nodes, and the small difference between sidereal and solar time, the total possible east-west coverage of all of the swaths of a polar-orbiting satellite will be one earth circumference every 12 hours. On each orbit, one earth circumference of north south-distance will be traversed by the sub-satellite point, and the surface area A capable of being mapped will be very nearly

$$A(1 \text{ orbit}) \approx (2\pi r)^2 \frac{P_S}{12} \quad (V-18)$$

where

r is the earth radius

P_S is the satellite orbital period (in hours)

This approximation differs from the true area coverage only by the ratio of the lengths of the arc and the chord at the equator for one orbital period, and the error is less than 10 percent for swath widths less than 90° .

From Eq. (V-18) it follows that the required mapping rate will be

$$A/t \approx 1.86 \times 10^4 \text{ km}^2/\text{s}$$

regardless of the height of the satellite. This figure, together with the maximum allowable area per sampling point as determined by meteorological considerations, (see Secs. IV and V-C) can be used to find the required lidar firing rate.

Figure V-11 shows the behavior of several pertinent system parameters as functions of satellite height.

Aside from the consideration of generally lower launching cost for lower orbits, the only argument in favor of a low altitude for a lidar satellite appears to be the $1/R^2$ factor in the lidar equation. Since transmitter power will always be at a premium in an active system, the orbit obviously should be no higher than is absolutely necessary to fulfill the other system requirements.

On the other hand, too low an orbit leads to certain difficulties outlined below.

a. Scanning Angle

The maximum east-west scanning angle (i.e., the maximum east-west nadir angle) becomes inconveniently large for low satellite altitudes as shown in curve (a) of Fig. V-11. As a point of reference, "normal" camera lenses are corrected to cover fields of approximately $\pm 20^\circ$. Anything wider than that is considered "wide angle", and is usually achieved by sacrificing some other quality--speed, geometrical accuracy, resolution, etc. The 17 mm, f 4.0 lens used for the vidicon system in NIMBUS satellites has a full field of 49° and was selected

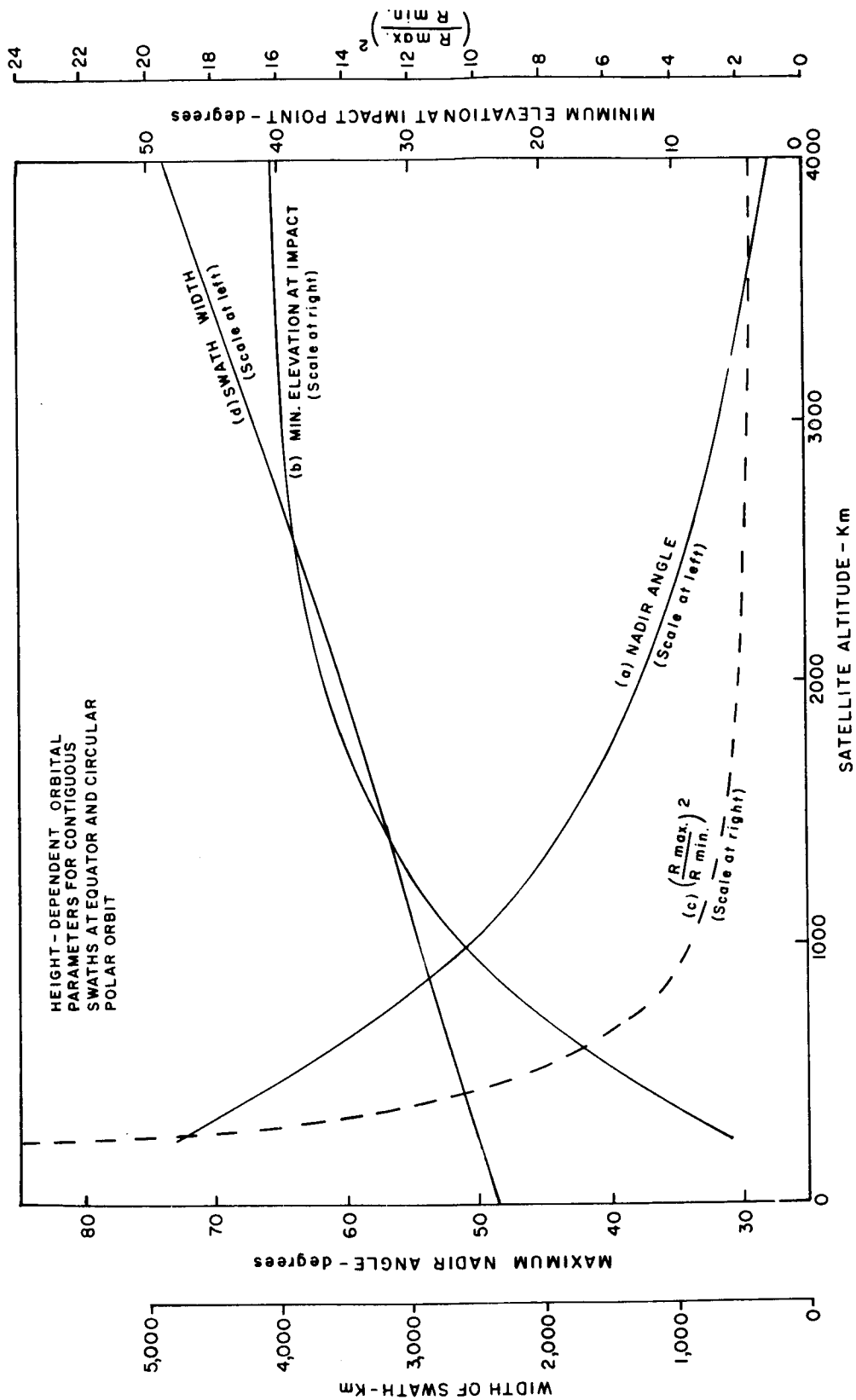


FIG. V-11 HEIGHT-DEPENDENT ORBITAL PARAMETERS

only after thorough study of then available types.* Large scanning angles not only complicate the design of the transmitting and receiving optics; they also call for non-linear corrections to be made in the scanning angle and/or the transmitter firing rate if severe geometric distortion and non-uniform sampling density are to be avoided near the edges of the swath.

Fortunately the sampling rate arrived at from other considerations is slow enough that it is possible to consider a mechanical scan including, for example, cam-controlled corrections on focus, field of view, aiming angle, and receiver gain. Mechanically scanned optics, undesirable as they may seem, do have the ability to achieve more resolution elements per scan line, particularly at wide aperture, than is possible with the best television cameras or even film cameras employing fixed lenses.

Thus a requirement for large scanning angles would not in itself present an insurmountable obstacle.

b. Elevation Angle

The elevation angle for rays arriving at the earth's surface near the edges of the swath becomes very low for satellite altitudes below about 1000 km [see curve (b) of Fig.V-11]. This leads to difficulty in height discrimination as illustrated by the scale drawings of Figs. V-12 and V-13.

In Fig. V-12 the height of a 10 km cirrus layer is so small in comparison with the earth radius that it scales as an imperceptible broadening of the line representing the earth's surface.

Figure V-13 is an expanded view of conditions existing at point B of Fig. V-12, near the extreme edge of the swath for a 1000 km satellite.

The arriving beam from the satellite-borne lidar is depicted as having a width (at least in the plane of the paper) of approximately 1 km. This is about the minimum value that can be expected from both

* Stampfl, 1961.

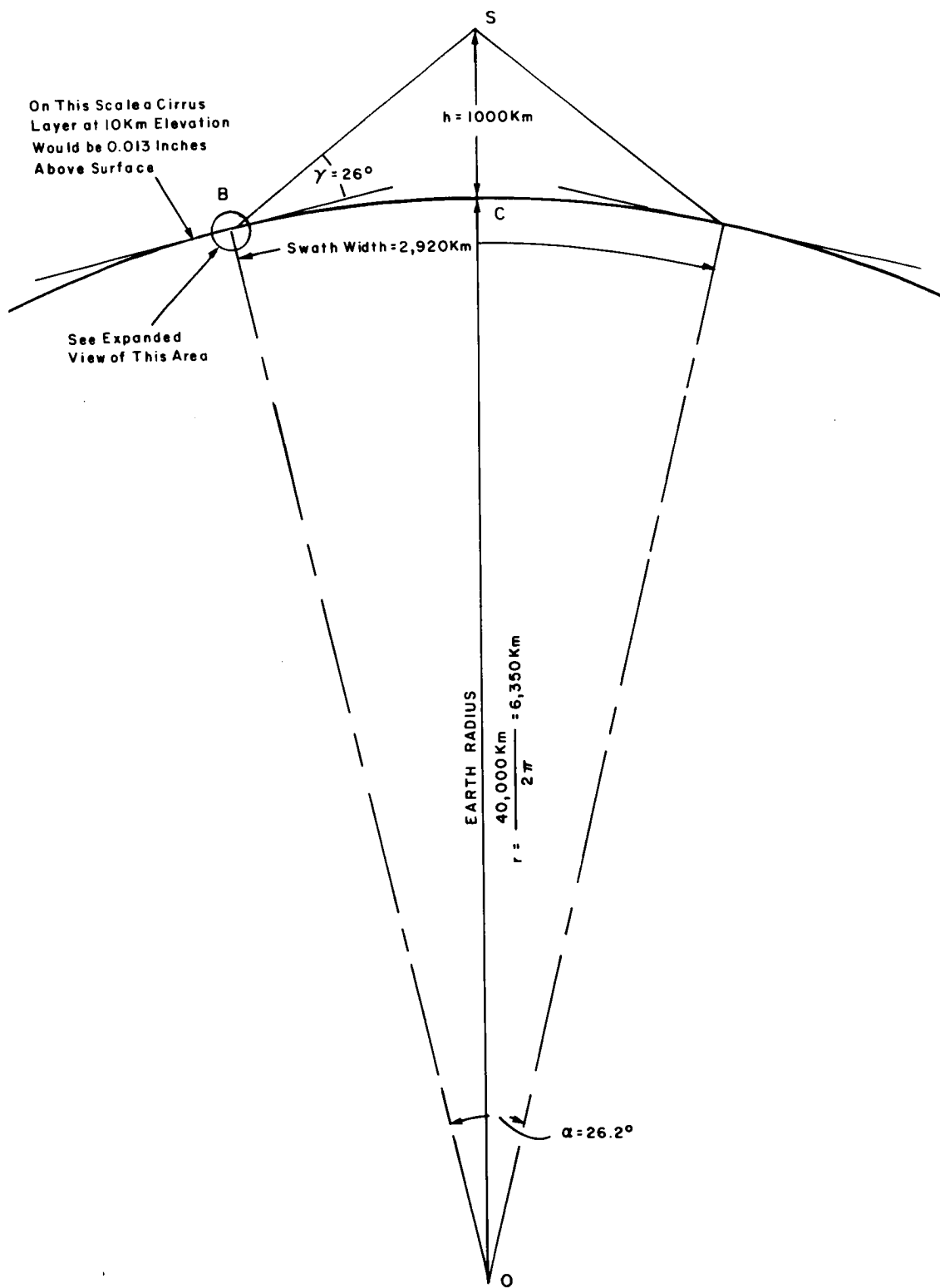


FIG. V-12 VIEWING GEOMETRY FOR SATELLITE AT 1000 km

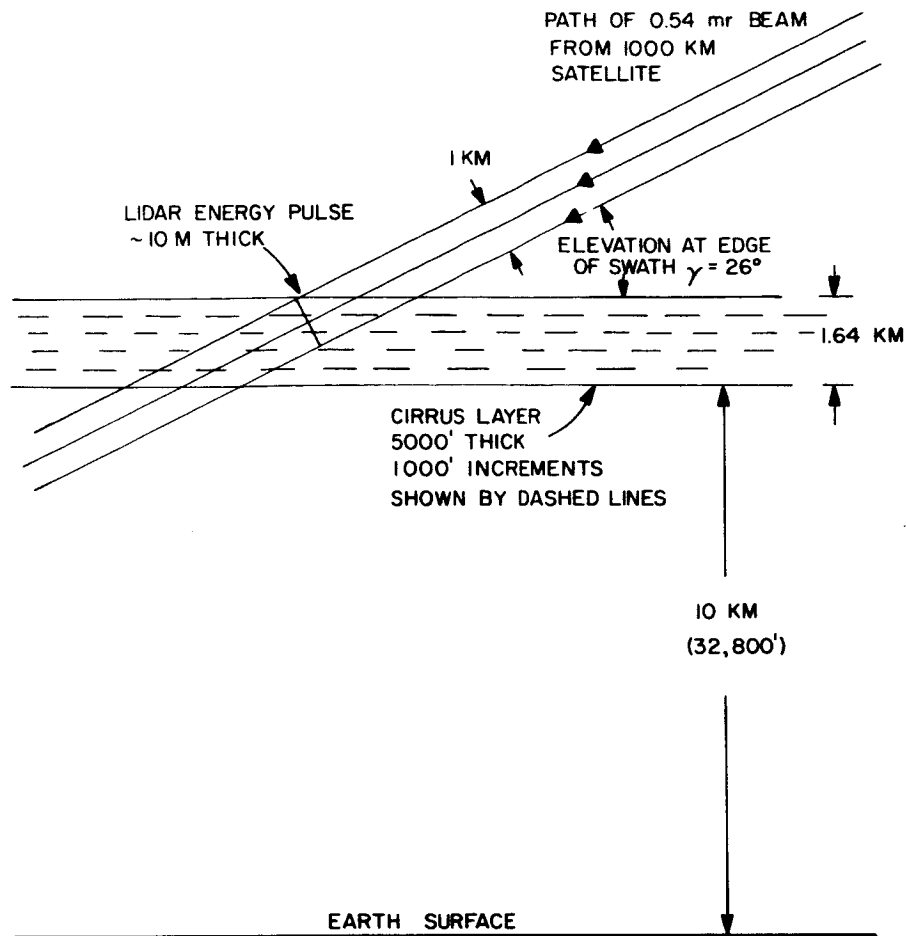


FIG. V-13 BEAM GEOMETRY AT EDGE OF SWATH

meteorological and equipment considerations as discussed in Secs. IV and V-C. The energy pulse from a Q-switched laser, being less than 10 meters long, then resembles a very flat pancake, represented edge-on by the single line in Fig. V-B. It is evident that at any instant the return from this thin disc of energy will be affected by cloud conditions existing over an altitude range of approximately three thousand feet (1 km). Thus for this geometry it will not be possible to realize the desirable condition of having range resolution in 1000-ft (300 meter) increments. A companion effect is that cloud with good vertical development but spotty horizontal coverage could more fully fill the beam and therefore give a stronger return when located near the edge of the swath than when viewed from directly above. These and similar problems were discussed in more detail in Sec. V-C on beam size, but it

is evident here that quantitative results in both range and amplitude will be subject to severe distortion at low incident elevation angles.

c. Signal Variation

The variation in signal strength between targets directly under the lidar and equivalent targets near the edge of the swath becomes very large at low satellite heights because of the $1/R^2$ factor in the lidar equation. Curve (c) of Fig. V-11 plots $(R_{\max}/R_{\min})^2$ as a function of satellite altitude, and shows that for 1000 km height the ratio is 3.5 to 1 and that the factor increases very rapidly for lower orbits. Figure V-14 presents this information in a form somewhat more useful for evaluating the tradeoff between signal variation and absolute signal level. The top curve represents received echo power levels for a given target at the subsatellite point and various satellite altitudes, normalized with respect to the signal at 1000 km range. The bottom curve gives the same data for an echo received via a similar target at the extreme edge of an optimum-width swath and can be used to estimate the minimum signal levels which will be encountered. Since the vertical scale is on logarithmic coordinates, the vertical distance between the two curves is a measure of the variation in received signal level during a transverse scan of a uniform cloud layer near the earth.

d. Variation in Effective Spot Size

The variation in range from center to edge of the swath will result in a variation in the effective spot size of both the transmitting and receiving beams unless some dynamic correction is made. In addition to complicating the specification of system resolution, an increase in spot size is undesirable in that it tends to increase the amount of background light reflected into the receiver, assuming the receiver acceptance angle is correspondingly increased. To a first approximation the background level might be expected to vary as the cross-sectional area in a plane normal to the beam direction, that is, in the same way as $(R_{\max}/R_{\min})^2$, curve (c) of Fig. V-11. This of course assumes that the near-earth radiance will be the same in the oblique direction as it is toward the zenith, an assumption which can only be true in the average, if at all. In any event it appears desirable to specify that the system

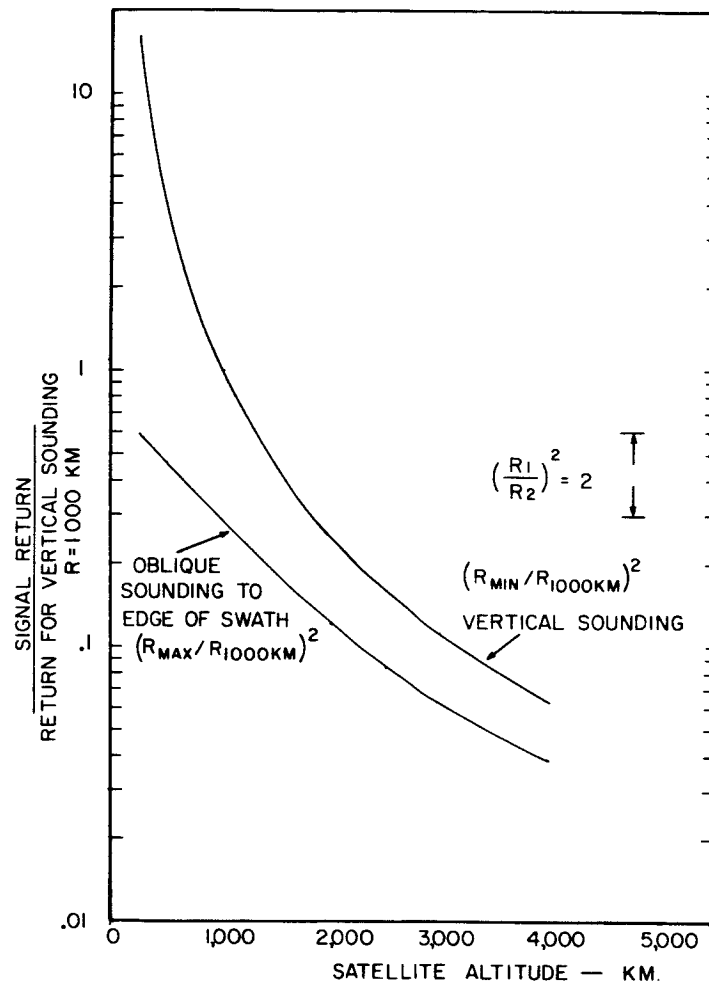


FIG. V-14 ECHO POWER LEVEL AS A FUNCTION OF SATELLITE ALTITUDE

incorporate some form of dynamic control of the beam divergence so that the beam cross section at the point of earth intercept is relatively invariant with deflection angle.

Study of all of the curves of Figs. V-11 and V-14 suggests that an orbital altitude of 1000 km is the minimum which should be used for a lidar satellite expected to give continuous area coverage, and that 1500 to 2000 km would be a much better choice if the required increase in transmitter power can be achieved. Figure V-15 presents for reference a plot of satellite orbital period as a function of height.

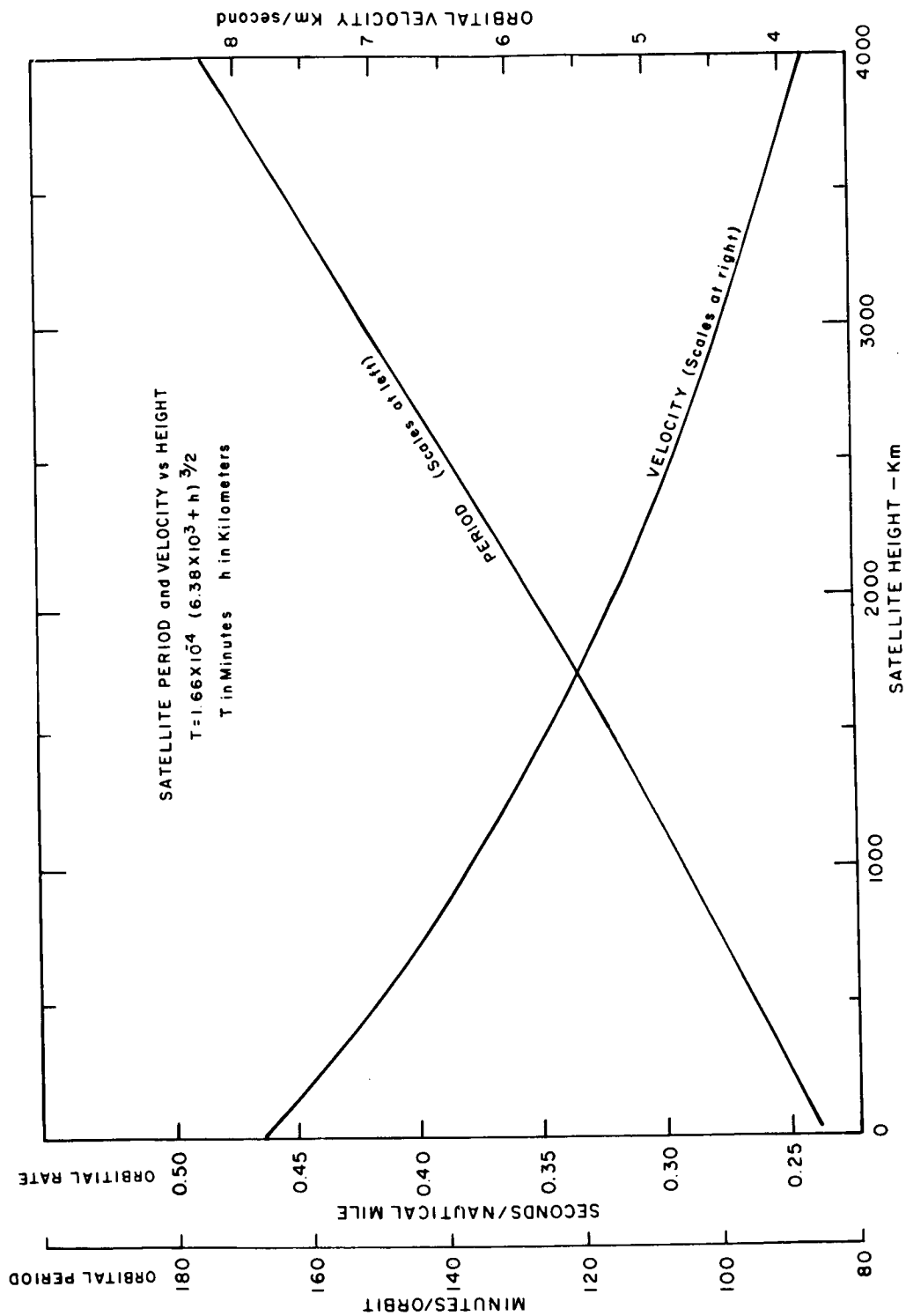


FIG. V-15 SATELLITE PERIOD AS A FUNCTION OF HEIGHT

E. Data Handling and Display

The raw output of the photodetector in the lidar receiver is not in a suitable form either for direct telemetry back to earth or for meteorological analysis. It will be the objective of this section to examine the data quantities and rates, to anticipate what data processing would be desirable, and to suggest appropriate points in the system for discarding, storing, or modifying the time base of the data.

The basic information received at the satellite can be expressed most generally as photon-arrival rate as a function of time, with the useful portion contained in an extremely short time period compared to the interpulse period. For example, the units used in Sec. III-B for plotting the predicted reception of both useful signal and undesirable background noise were photons per microsecond.

1. Data Handling

Conceptually, the receiver output is merely an analog voltage or current, linearly proportional to the photon-arrival rate, and varying as a function of time. Thus the total number of data bits per pulse is expressable by the product of the total number of time increments (range intervals) times a binary representation of the number of possible amplitude increments per range interval. The practical problems which arise in attempting to provide a remote indication of the received signal are:

- (1) The total amplitude range which must be handled is relatively large, so that some form of logarithmic compression is required.
- (2) Detection techniques capable of measuring very low photon-arrival rates currently are severely limited in dynamic range; yet detection techniques having adequate dynamic range currently are too slow or too noisy to be used to measure relatively small photon counts per range interval. Either a technological advance or a composite detection scheme appears to be required.
- (3) It is desirable to provide time-base conversion so that the very high peak data rates generated in real time are smoothed into a relatively modest average rate for storage and telemetry.

To obtain an estimate of the required data rate, we can refer to the predicted waveforms developed in Sec. III-A while keeping in mind quantitative values for the practical restrictions just listed.

2. Number of Range Increments

The minimum range resolution element has been assumed to be about 1000 feet (300 meters) as specified in Sec. III-A. For monitoring of ordinary cloud cover, it appears reasonable to establish a maximum altitude of 100,000 feet (30 km) to be handled regularly. If nacreous or noctilucent clouds are to be monitored, additional data-storage and transmission capacity will be required.

3. Number of Amplitude Increments

Examination of the predicted waveforms developed in Sec. III-A reveals that the power range over which the useful signal component may be expected to vary during any one sounding is somewhere between 10^4 and 10^5 (40 to 50 dB), depending upon the definition of the word "useful." It is also evident that if variations from pulse to pulse in transmitter power output are small enough to be neglected and if conditions are such that the additional received power due to extraneous background light is never more than the maximum signal power--resulting in a maximum power increase of 3 dB--then one can specify upper and lower boundaries on the absolute power levels which would need to be handled by the receiver. These boundaries must be at least 43 dB apart, and preferably 50 dB or more.

In order to accommodate possible drift in transmitter power and/or receiver sensitivity, the system could either be designed for another 10 dB of range on an absolute or dc basis, or alternatively it could be designed to transmit a single code group at the beginning of each lidar pulse which would establish a dc calibration level for all data received as a result of that pulse. A power ratio of 2:1 (3 dB) per amplitude increment is suggested as the maximum step size which should be considered. This would permit one four-bit binary word per range interval to describe the signal over a 48 dB dynamic range; accordingly a minimum data complement per pulse is then estimated to be

$$\begin{aligned}\text{data per pulse} &= \frac{100 \text{ range increments}}{\text{pulse}} \times 4 \text{ bits/range interval} \\ &= 400 \text{ bits/pulse}\end{aligned}$$

This minimum data compliment is found to be low enough that it would appear wise to invest slightly more in the data-handling capability in return for the assurance that the data link would never limit the system performance.

Table V-3 lists the characteristics of three feasible data transmission/storage schemes. The combination in the third column, involving 100 six-bit words per pulse, has easy compatibility with many computer formats and will be assumed for most of the calculations in this report. In practice, perhaps four of the 64 possible code combinations would be reserved for synchronizing and control functions, leaving a nominal 60 dB gamut for the signal.

Table V-3
SUGGESTED DATA-STORAGE/TRANSMISSION CAPABILITY

	Minimum	Alternate	Preferred
Range Increments/Pulse	100	100	100
Data Bits/Range Interval	4	5	6
Power Ratio amplitude increment	2.0 (3 dB)	1.6 (2 dB)	1.26 (1 dB)
Total Dynamic Range	48 dB	64 dB	64 dB
Total Data Bits/Pulse	400	500	600

It should be emphasized that the provision for 60 one-dB steps of amplitude range represents a design goal, not a firm specification as far as the lidar receiver is concerned. As stated previously, achievement of even 40 dB range with 2 to 3 dB accuracy at the required speeds and signal levels is considered to be a significant technical challenge, and performance of this order should still result in a usable lidar system.

The principal reason for desiring a good amplitude resolution and absolute accuracy in the raw data is to permit the best possible transformation into the desired output format of β'_{180} as a function of altitude. As discussed more completely in Sec. V-F-2, this transformation is quite sensitive to amplitude errors in the input data.

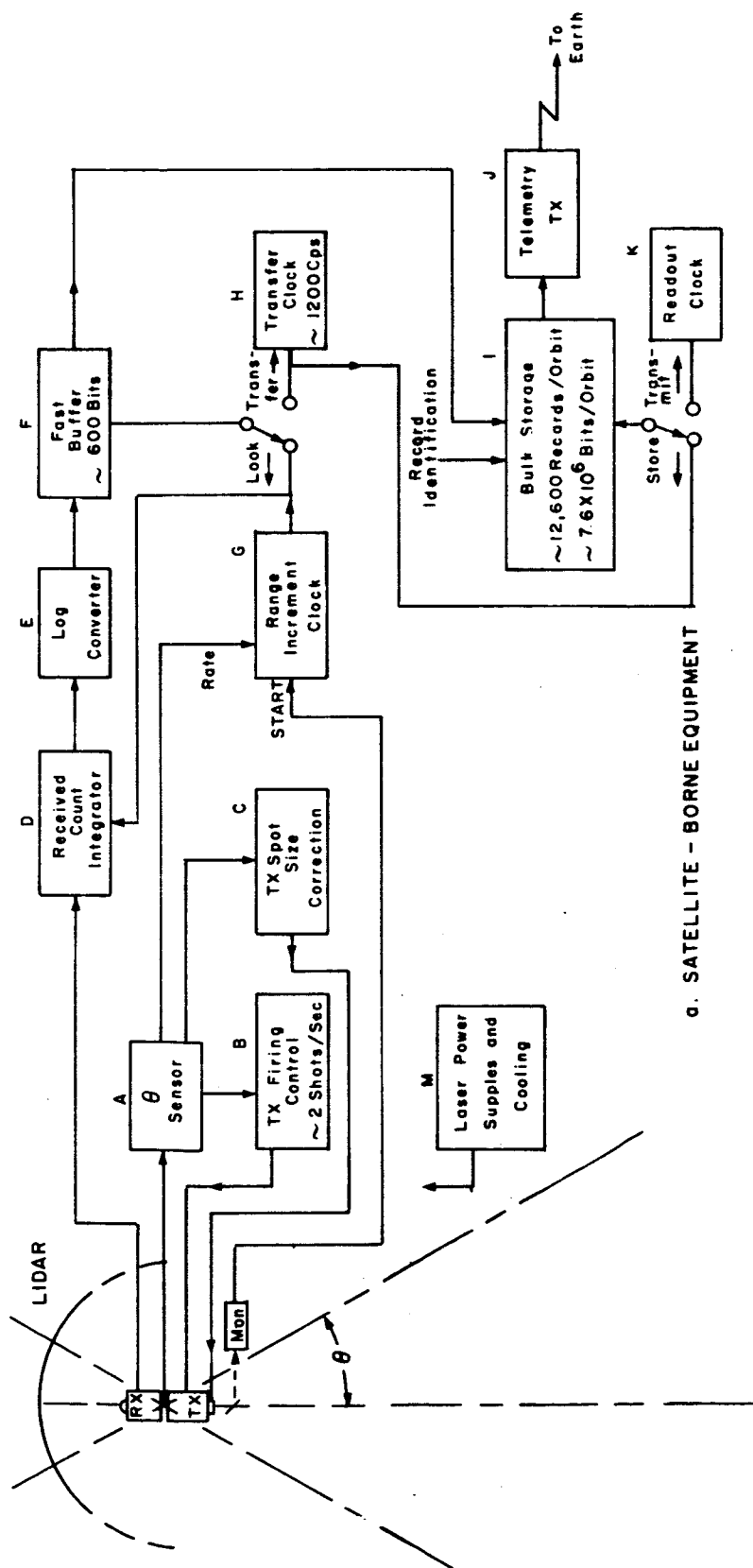
4. Data Processing in the Satellite

It is anticipated that the on-board data processing would be limited to:

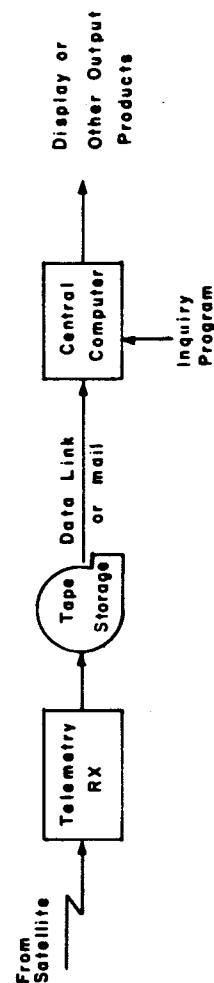
- (1) Derivation of a signal proportional to the received photon rate (analog and/or digital)
- (2) Range integration of the received signal, including correction for slant paths (analog or digital)
- (3) Provision of logarithmic amplitude-response characteristic (analog or digital)
- (4) Time-base conversion (digital)
- (5) Record identification (digital)
- (6) Recording of average background level of each sounding (digital)
- (7) Data storage between polar readouts (digital)
- (8) Transmission to earth (digital)

Figure V-16(a) is a block diagram of the equipment required in the satellite.

The lidar is assumed to scan across the swath at a uniform angular rate under control of the system master clock. "Flyback" could be made essentially instantaneous by the use, for example, of multiple-faceted scanning mirrors. The exact firing time would be controlled by boxes A and B to give soundings uniformly spaced in the east-west direction along the earth's surface. The received signals are integrated over uniform altitude increments and expressed in logarithmic form by boxes D and E. Time periods corresponding to uniform altitude increments near the earth's surface are supplied by box G which provides a slant-range correction for each shot from data supplied by the nadir-angle sensor, box A. It is possible that the design of the receiver would permit $1/R^2$ correction of



a. SATELLITE - BORNE EQUIPMENT



b. GROUND - BASED EQUIPMENT

FIG. V-16 BLOCK DIAGRAM OF DATA-HANDLING COMPONENTS

signal amplitudes for the variation in slant range to be performed at the same time without undue equipment complication. For this discussion, however, it will be assumed that the $1/R^2$ corrections will be handled by the ground-based computer. The approximately 600 bits of data generated by each lidar sounding are buffered by box F which has the capability of accepting data at rates up to three bits per micro-second and outputting at approximately 1200 bits per second under control of the transfer clock, box H.

Because of its required capacity, the bulk storage memory, box I, will probably be either a magnetic tape or a disc. Unless additional telemetry terminals are provided by the time this satellite would be flying, the bulk memory would have to have a capability for storing data from two orbits as is currently done for the Nimbus series.*

Addition of time codes, synchronizing codes, and other record-keeping functions would also be done in the bulk-storage unit.

Not shown on the block diagram but undoubtedly a part of a practical system would be a facility for monitoring the background level received during most of the interpulse period following each sounding and recording this average count rate as one or two six-bit words near the end of each 600-bit record.

During the five to ten minutes that the satellite will be within range of a near-polar telemetry terminal, all of the lidar data taken during the previous orbit--or possibly during the two previous orbits--would be read out of the bulk-storage memory and telemetered to earth by transmitter J.

If the capability were two complete orbits' worth of data in five minutes, the required serial bit rate for data transmission would be 28 kHz. In practice, the lidar data undoubtedly would be multiplexed onto a wider-band, higher-speed data link carrying information from other sensors as well.

* Ref. Stampfl, 1961.

5. Earth Terminal Processing

The lidar product at the telemetry receiving terminal could be a magnetic tape containing approximately 7.6×10^6 bits per orbit [see Fig. V-16(b)]. Assuming 555 byte per inch packing density and six data bits per byte, the data from each orbit would require 190 feet of tape; a typical 3600 ft roll of tape would accommodate lidar data covering about 33 hours of operation.

Depending upon the urgency and the available transmission facilities, the data could then be mailed or transmitted via wire or radio to a central computing facility. The computer would then be used as required to transform the raw data into plots of backscatter coefficient β'_{180} as a function of altitude (see section V-F-2) or into descriptions in terms of inferred physical parameters such as particle size, number density, etc.

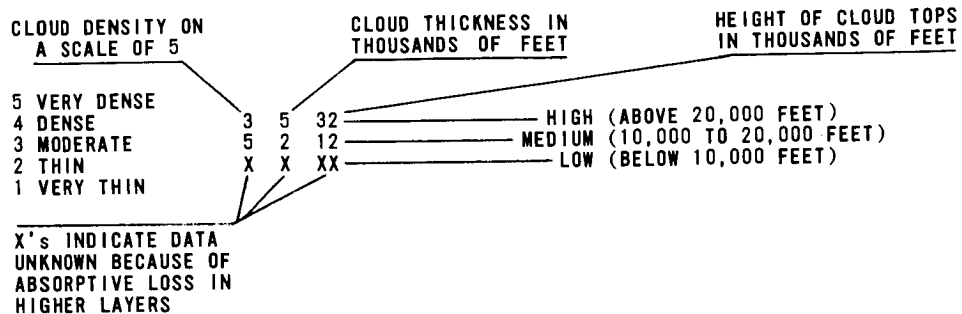
6. Display

The fact that each lidar sounding results in a complete vertical profile rather than a single value complicates the problem of data display. Considering how little is known about how the lidar soundings would be used, it appears unrealistic to attempt to describe an optimum display at this time. However it is very important that we be able to describe one or more suitable displays, in order to permit meteorologists to envision what the lidar might do for them. Ultimately, of course, we look forward to the time when routine forecasting will be done entirely by the computer, and any output maps would be machine-prepared after proper weighting of data from many input sources, possibly including a satellite-borne lidar. In this idyllic extreme, the lidar input would have become so diluted that its individual contribution could seldom, if ever, be recognized by inspection of the output display.

At the other extreme, a cloud physicist performing research on a particular problem in cloud genesis might well be most satisfied with a tabular printout of the raw signal-return levels as a function of time with some set of specified limits on altitude and geographic location. Between these two extremes lie a variety of much more difficult display situations which must be designed to make lidar information available to

a human analyst in predigested, on-call form. Like any good servant, the data should be available when needed but unobtrusive when it is not. One approach would be print in the margin of a television or HRIR print small graphs showing β'_{180} as a function of altitude for critical points in the picture--in much the same way that vertical temperature profiles taken by ground stations located in the picture field are sometimes keyed into the TIROS television pictures (see Fig. A-8, for example).

A 12-digit all-numeric format which could be implemented by computer is as follows:



Altitude and thickness are given in feet rather than meters to reduce the number of digits required for description in useful increments and over a useful total range.

In order to give the reader some impression of the data density involved even in such a highly reduced format, Fig. V-17 shows a TIROS photograph with an overlay gridded in 100 km squares to correspond to the size of lidar reporting areas recommended in Sec. IV-B. Near the center of each square is a number group following the format shown above and representative of the reduced data which might have been obtained from a lidar sounding at a location indicated by the black dot immediately to the left of the number group. The photograph of Fig. V-17, taken over the west coast of Africa, near Cape Blanc, was chosen as an example for several reasons. It was made when the TIROS camera happened to be pointing straight down, which makes it representative of photographs taken from a stabilized platform such as that proposed for the lidar satellite. The optical contrast between the ocean and the desert is great enough to yield a striking

F. Miscellaneous Equipment-Design Considerations

1. Possibility of Eye Damage

One practical upper limit which applies to any space-borne active optical probing system is the power density which can be tolerated at the earth's surface before there is danger of permanent retinal damage to persons on the ground who happen to be looking in the direction of the satellite.

Data on eye-damage thresholds are as yet incomplete, but a figure which is currently in common use is that given in the Laser Safety Bulletin published by the Martin Company (Martin Company, 1965). That bulletin quotes a safety threshold 0.01 joules per square centimeter at the retina for a 30-nanosecond pulse from a Q-switched ruby laser. It is stated that this allows a safety factor of 7 over the damage threshold proposed in a pioneer paper by Geeraets, Ham, et al. (1965). Similar data has recently been published by Peppers (1966).

In the case of an observer on the ground viewing a satellite-borne source, the size of the retinal image will never be smaller than the diffraction-limited spot from the eye lens. This spot will be at its smallest, the intercepted energy will be largest, and the resulting power density at the retina will be greatest when the eye is dark-adapted and its iris wide open. Since the human eye contains enough aberrations that diffraction-limited resolution is never achieved, use of this criterion represents an apparently conservative approach.

On this basis, the maximum radiation field to which humans should be exposed can be computed from the following relation.

$$I_s = \frac{(2.44\lambda f)^2 I_R}{D^4} .$$

Definitions of the symbols and specific values for a Q-switched ruby laser and a dark-adapted eye are:

I_s = energy density allowable at the eye lens; joules/m²
 λ = wavelength of radiation; 0.7×10^{-9} m
 f = focal length of eye lens; 2.3×10^{-2} m
 D = diameter of iris = 7.0×10^{-3} m
 I = permissible energy density on the retinal surface;
 10^2 joules/m².

For these values,

$$I_s = 6.43 \times 10^{-5} \text{ joules/m}^2 .$$

Consequently, as a first approximation and using currently accepted safety thresholds, a nominal 1-joule pulse from a distant point source should be spread over a spot at least 140 meters in diameter if the possibility of accidental eye damage is to be avoided.

The probability of someone actually being in the beam and looking squarely at the satellite at the time of firing is of course extremely low and perhaps can be classed with the danger from falling meteorites, aircraft and satellite debris, etc. On the other hand occasional situations can exist which would greatly enhance the retinal illumination over the value calculated above. Laser beams experience localized focusing in passing through the atmosphere which regularly generate small hot spots at least one to two orders of magnitude more intense than the beam average. One of the most severe remote contingencies that can be imagined is the case of an amateur astronomer staring into the heavens with a large aperture telescope at the instant that a lidar satellite passed through his field of view and fired in his direction.

For the beam angles and pulse repetition rates receiving principal attention in this report, the possibility of eye injury would be strictly probabilistic. That is, there would not be the additional factor of having the observer's attention drawn to the satellite by a series of blinking red lights since he would never be in the beam for more than one pulse. While the eye-damage danger is seen to be low for the energy densities proposed herein for detecting cirrus cloud, the safety margin

is small enough that the danger should be re-evaluated for any proposals requiring appreciably higher transmitter power or smaller beam angles.

2. Errors in Deriving β'_{180} as a Function of Distance

When an existing volume target can be described by two functions of distance, β'_{180} and σ , the power density expected at the receiving antenna for a given incident-power density can be calculated in a straightforward manner from the lidar equation and can be expressed in photons per unit time. Even if only one of the two functions is known, a good approximate prediction of the received power density as a function of time can be obtained by making the simplifying assumption that the ratio between β'_{180} and σ can be approximated by a known constant over each of several regions through the target.

The reverse procedure--that of determining the target distributions, given the receiver power density as a function of time--is more difficult but again can be accomplished if the simplifying assumption is made about the relationships between β'_{180} and σ . The results of this reverse procedure, or inversion, are very sensitive to errors in the input data. Since noise, quantum effects, and other errors in recording and reporting the received signal level are inherent in any practical system and since a plot of β'_{180} as a function of distance and preferably, also of σ as a function of distance is the desired output of the system, a careful error analysis of this inversion procedure appears fundamental to a complete specification of the size and complexity of the required receiving system. Such an analysis has not been made in detail, but a computer model has been prepared and has been used to provide some very preliminary checks that the minimum system constants assumed throughout this study are within reason.

VI BACKSCATTER COEFFICIENTS

A. Predicted Values

The utility of lidar depends upon the fact that small percentages of radiation directed at a target will be returned to a measuring receiver. Quantitative specification of the ability of any target to return some of the incident energy conventionally is done in terms of a "backscattering cross section" which relates the intensity of the return to the energy density of the incident radiation at the target.

In the completely general case, the returned energy may or may not all be at the incident wavelength and it may or may not experience some time delay apart from the normal round-trip transmission time. Depending upon the precision required in the system analysis, the total back-scattering cross section can be broken down into components due to numerous individual contributing effects. It is the objective of this section to examine some of the mechanisms which return energy from atmospheric target volumes and to assign order-of-magnitude values to the various effects.

Energy can be returned at precisely the incident wavelength (neglecting Doppler shifts) via Mie scattering from relatively large aerosol particles, via non-resonant scattering from atoms and molecules (Rayleigh scattering), or via Thompson scattering from free electrons. If desired, the latter two cases can be thought of as special cases of the complete Mie theory. Energy can be returned at wavelengths differing from that of the incident wavelength by processes of wave-particle interaction sometimes classified as fluorescence, phosphorescence, and Raman shifting.* These effects occur to some degree with all atoms and molecules and for virtually all incident wavelengths. The relevant cross sections are

* Brillouin scattering, an extremely weak effect resulting from interaction between electromagnetic waves and acoustic waves, is not considered here.

independent of the amount of incident radiation. When the wavelength of the incident radiation is chosen to correspond precisely to a natural energy-level transition of atoms or molecules within the target volume, the probability of photons being subtracted from the incident beam is greatly increased; i.e., the "coupling" is tighter and more total energy is taken from the beam and reradiated. This is known as resonant scattering, and has the effect of greatly increasing the backscattering cross section both at the incident wavelength and for other wavelengths corresponding to multi-step relaxations within the excited atom or molecule. At wavelengths in or near the optical region the energy return at the Raman-shifted wavelengths will not show useful resonant increases.

1. Rayleigh Scattering

Rayleigh scattering from atoms and molecules is a very important effect from the point of view of lidar satellite design. This is so since its characteristics are reliably predictable, it can always be counted upon as being present from elevations of interest, and (at least for the upper troposphere and lower stratosphere) it represents a convenient reference level with which weaker or more transient effects can be compared.

For wavelengths well separated from the absorption lines of the atmospheric constituents, the Rayleigh scattering cross section C_r of an individual scattering center is given (Van de Hulst, 1957, page 82) by:

$$C_r = \frac{8\pi}{3} \left(\frac{2\pi}{\lambda}\right)^4 \alpha^2 \frac{6 + 3\delta}{6 - 7\delta} , \quad (\text{VI-1})$$

where

- λ = wavelength of incident radiation
- δ = depolarization factor due to the anisotropy of the atmosphere
- α = molecular polarizability of scatterer

Calculations and laboratory measurements (Gucker, 1953) of the factor δ yield a value near 0.035; therefore the fraction $(6 + 3\delta)/(6 - 7\delta)$ is about 1.061. The polarizability α is approximately $2 \times 10^{-30}(\text{m}^3)$. Thus

$$C_r = 3.96 \times 10^{-56} \lambda^{-4} (\text{m}^2) \quad (\text{VI-2})$$

which at the ruby wavelength $\lambda = .694\mu$ is

$$C_r(\lambda=.694) = 1.71 \times 10^{-31} (\text{m}^2) .$$

The total scattering cross section per unit volume of a purely gaseous atmosphere is this elementary cross section multiplied by the number density N_r of molecular scatterers per unit volume.

$$\sigma_r = N_r C_r \quad (\text{VI-3})$$

This quantity is also called the Rayleigh attenuation coefficient. It is that quantity which, when multiplied by the incident power density and the effective illuminated volume, gives the total power scattered in all directions from the incident radiation beam.

For pure Rayleigh scattering it can be shown that $3/8\pi$ per steradian of this total will be scattered back toward the source. As a result of the convention used in defining radar cross sections (See Sec. V-B-1) it follows that for Rayleigh scattering the volume backscattering cross section B'_{180} as used throughout this report can be obtained from:

$$B'_{180} = 4\pi \frac{3}{8\pi} N_r C_r = 1.5 \sigma_r \quad (\text{VI-4})$$

Thus the factor k , which is the ratio of backscattering, B'_{180} , to attenuation, σ , is for Rayleigh scattering a trusted constant ($3/2$) and not subject to the fluctuations encountered when the scattering particles become large compared to the wavelength.

Table VI-1 lists values for N_r from the U.S. Standard Atmosphere, 1962 (U.S. Government Printing Office, 1962) and for B'_{180} [from Eq. (VI-4)] for sea level to 20 km elevation in 1 km increments.

Table VI-1
VOLUME BACKSCATTER COEFFICIENTS β'_{180} FOR RAYLEIGH COMPONENT
OF ATMOSPHERIC SCATTERING

Height (km)	N_r (m^{-3})	β'_{180} (m^{-1})
0	2.55×10^{25}	6.55×10^{-6}
1	2.31×10^{25}	5.94×10^{-6}
2	2.09×10^{25}	5.38×10^{-6}
3	1.89×10^{25}	4.86×10^{-6}
4	1.70×10^{25}	4.38×10^{-6}
5	1.53×10^{25}	3.93×10^{-6}
6	1.37×10^{25}	3.53×10^{-6}
7	1.23×10^{25}	3.15×10^{-6}
8	1.09×10^{25}	2.81×10^{-6}
9	9.71×10^{24}	2.50×10^{-6}
10	8.60×10^{24}	2.21×10^{-6}
11	7.59×10^{24}	1.95×10^{-6}
12	6.49×10^{24}	1.67×10^{-6}
13	5.54×10^{24}	1.42×10^{-6}
14	4.74×10^{24}	1.22×10^{-6}
15	4.05×10^{24}	1.04×10^{-6}
16	3.46×10^{24}	8.90×10^{-7}
17	2.96×10^{24}	7.60×10^{-7}
18	2.53×10^{24}	6.50×10^{-7}
19	2.16×10^{24}	5.56×10^{-7}
20	1.85×10^{24}	4.75×10^{-7}

2. Mie Scattering

A type of scattering of key interest in the design of a cloud-ranging lidar is Mie scattering from particulate matter having dimensions appreciably larger than the wavelength of the incident radiation. For such particles the elementary scattering cross section C_p is about twice the geometrical cross section.

The scattering pattern does not resemble the symmetrical-dipole pattern of Rayleigh scattering, but can be quite irregular and complicated (Middleton, 1958; Van de Hulst, 1957; Deirmendjian, 1964). The pattern is a function of the particle-size-to-wavelength ratio distribution, dielectric characteristics, and particle shape.

Usually Mie scattering is predominately forward rather than backward with the result that the factor k , in the relation $B'_{180} = k\sigma$ is often less than unity. SRI calculations for a random distribution of water spheres having radii greater than 3 microns give an average value of 0.625 for k .

This value, together with the aerosol distribution is Elterman's Clear Standard Atmosphere (Elterman, 1964), have been used in computing values for the aerosol contribution to total β' for various elevations as plotted in Fig. VI-1. (The value $k = 0.625$ is most accurate for water spheres, but is a reasonable approximation for other aerosol components.)

From this figure it is apparent that even on "clear" days (horizontal visibility of about 25 km at sea level for the Elterman model) the aerosol backscattering predominates over the molecular backscattering for all elevations below 4 km (13,000 ft).

The total backscattering coefficients, β'_{180} , of Fig. VI-1 are then the minimum values which would be encountered by the lidar satellite and they represent a baseline above which reflections from clouds and all other transient phenomena must rise.

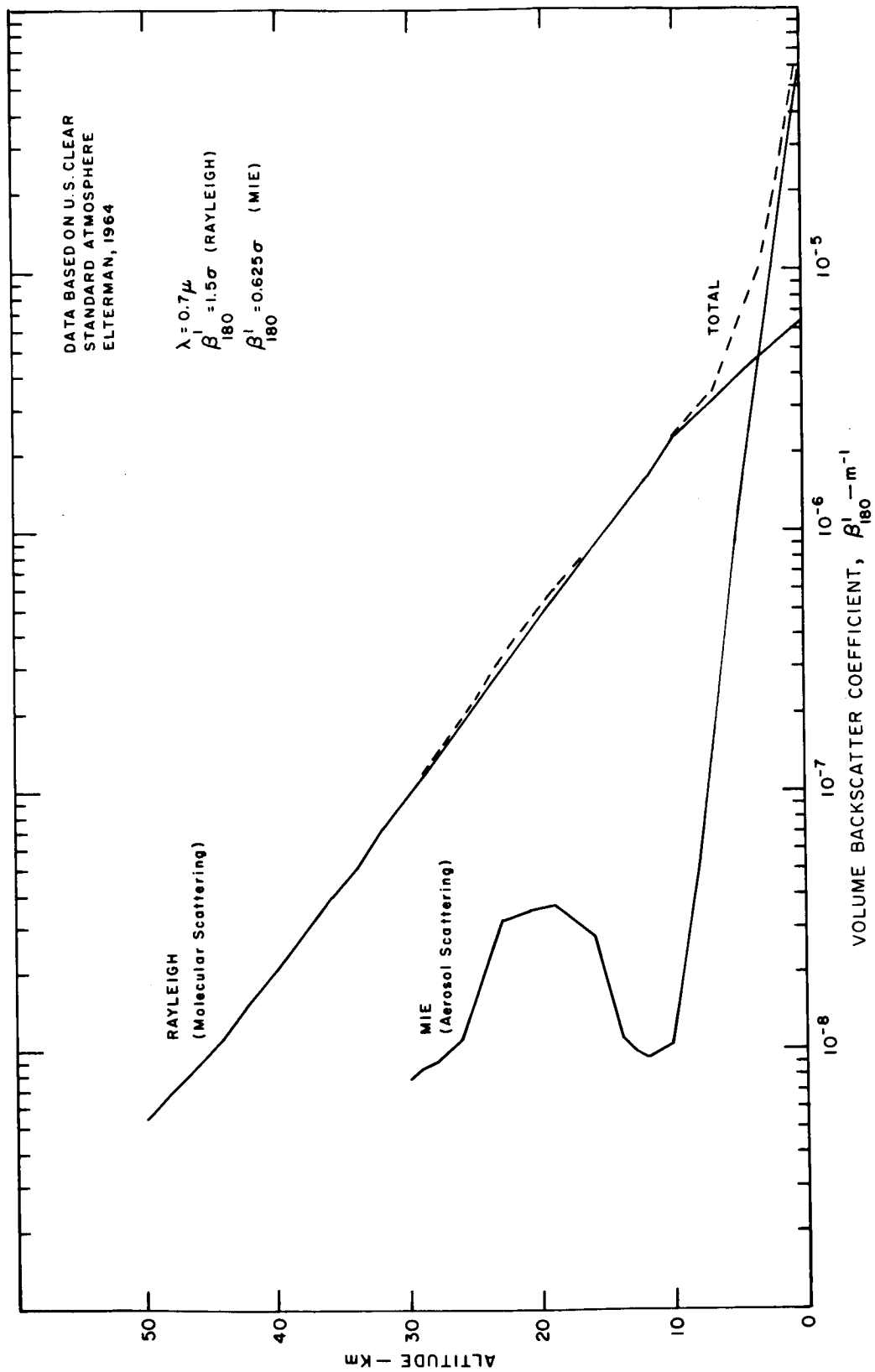


FIG. VI-1 VOLUME BACKSCATTER COEFFICIENTS FOR A CLEAR STANDARD ATMOSPHERE

Table VI-2 lists a range of typical water-cloud and haze conditions, together with the associated computed aerosol attenuation coefficients, and anticipated volume backscatter coefficients, β'_{180} , under the assumption that $k \approx 0.625$.

These values are also displayed graphically in Fig. VI-2.

Table VI-2
PREDICTED VOLUME BACKSCATTER COEFFICIENTS FOR WATER CLOUDS AND HAZES

Condition	Average Radius, a (μ)	N_p (cm^{-3})	σ_p (m^{-1})	β'_{180}	k
Dense Water Cloud	10	200	3.2×10^{-1} to 1.6×10^{-2}	2×10^{-1} to 1×10^{-2}	0.625
Light Water Cloud	20	10	1.6×10^{-2} to 4.0×10^{-3}	1×10^{-2} to 2.5×10^{-3}	0.625
Thick Haze	4	50-200	4.0×10^{-3} to 1.1×10^{-3}	2.5×10^{-3} to 7×10^{-4}	0.625
Moderate Haze	2	50-200	1.1×10^{-3} to 4.8×10^{-3}	7×10^{-4} to 3×10^{-4}	0.625
Light Haze	1	500	4.8×10^{-3} to 1.6×10^{-4}	3×10^{-4} to 1×10^{-4}	0.625

3. Electron Scattering

The formula for Thompson scattering from a free electron is:

$$C_e = \frac{8\pi}{3} r_o^2 ,$$

where

$$r_o = \frac{e^2}{4\pi\epsilon_0 mc^2} ;$$

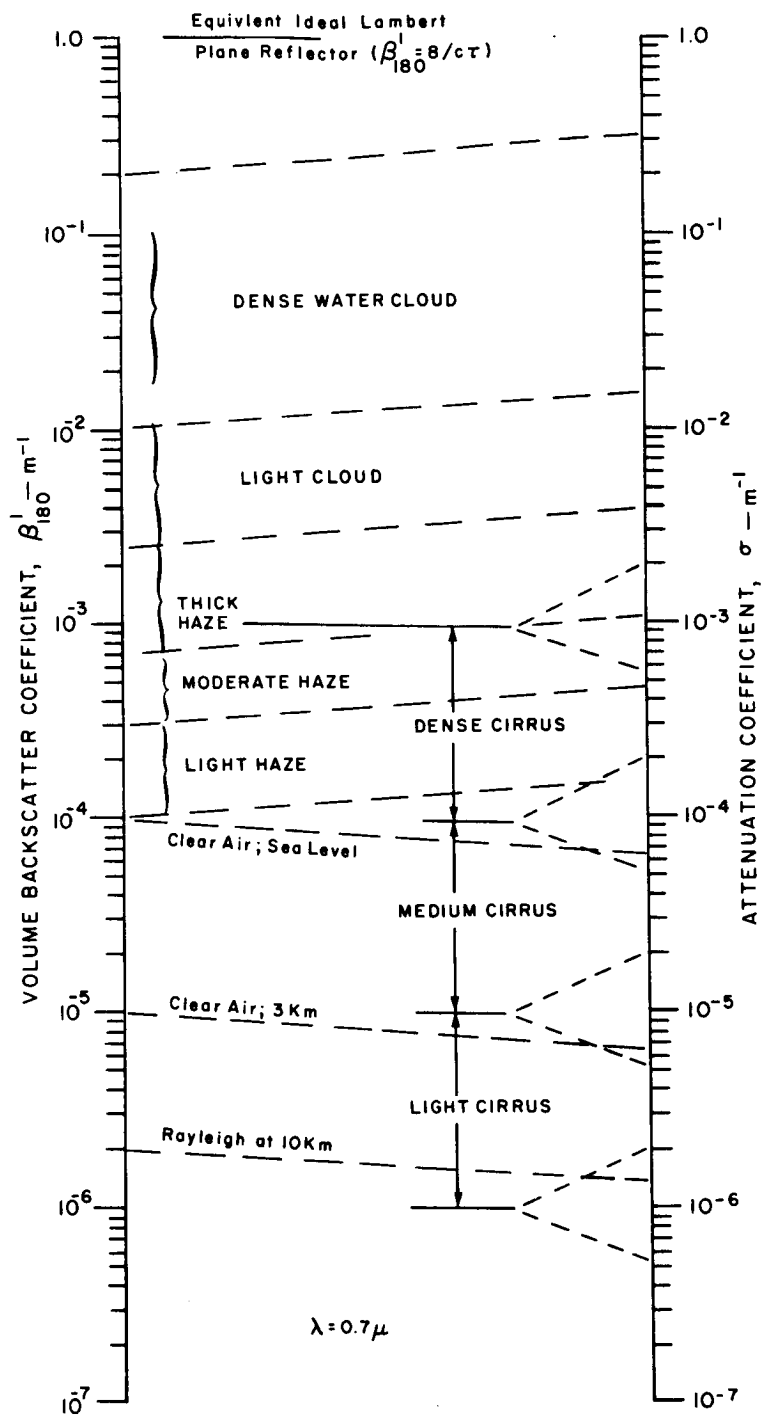


FIG. VI-2 BACKSCATTER AND ATTENUATION COEFFICIENTS
FOR VARIOUS CLOUDS AND HAZES

e is the electronic charge, ϵ_0 is the dielectric constant of free space, m is the electronic mass, and c is the velocity of light.

The value of C_e is

$$C_e = 6.7 \times 10^{-29} \text{ m}^2 .$$

Maximum electron densities in the F region are on the order of 10^{12} electrons/cm³, and the polar scattering pattern is the same as for Rayleigh. Thus, the maximum volume backscattering pattern coefficient β'_{180} expected from free electrons in the path between the satellite and earth is

$$\begin{aligned} \beta'_{180} &= k N_e C_e \approx 1.5 \times 10^{-12} \times 6.7 \times 10^{-29} \\ &\approx 10^{-16} \text{ m}^{-1} . \end{aligned}$$

Free-electron scattering is thus seen to be ten orders of magnitude below Rayleigh scattering from 10 km elevation (the approximate lower threshold of sensitivity for the proposed lidar system) and its effect either as a potential target or as background noise should be completely negligible.

4. Raman Scattering

Raman scattering is discussed in some detail in Sec. X. Raman cross sections are typically about 3 to 4 decades lower than Rayleigh cross sections for the same gas.

5. Fluorescence

Fluorescent radiation occurs when atoms or molecules, excited by an external source, decay toward their ground states, usually after a time delay on the order of 10^{-8} seconds or less. This radiation may take place at any of several wavelengths, depending upon the atom and its level of excitation.

Unless enhanced by operating with an excitation wavelength at or near a resonance line, the cross sections for fluorescent effects will be smaller than those for the Raman effect in targets of meteorological

interest. Thus, they appear to be of doubtful utility. No suggestions for utilizing nonresonant fluorescence have come to the attention of the authors.

6. Resonant Scattering

When the incident radiation frequency corresponds exactly with one of the natural atomic molecular resonances of an atmospheric constituent, individual particle scattering cross sections are obtained which are many orders of magnitude larger than Rayleigh cross sections for the same conditions. In addition to the problem of precise frequency control, however, a number of conditions regarding the density of the resonant species and of the surrounding gas must be satisfied in order to realize the effect. The quantitative evaluation of resonant scattering is quite involved and has not been attempted herein, other than to determine that the maximum expected volume backscatter coefficient β'_{180} for a typical natural resonant effect (ionized nitrogen N_2^+ at 400 km elevation) is about 10^{-12} to $10^{-15} m^{-1}$. It thus resides on the scale between Raman scattering and Thompson scattering and is well below the detection threshold of the lidar systems considered herein. Larger resonant-backscattering coefficients are encountered in the upper atmosphere following high-altitude nuclear blasts. While some of these data appear in open literature* most are classified. A fairly detailed treatment of resonant scattering from both natural and nuclear-weapon causes is given in reference.†

B. Experimentally Determined Volume Backscatter Coefficients for Cirrus Clouds

The vast majority of lidar cloud signatures which exist in the SRI files and, to our knowledge, in any other similar collection contain only qualitative information. A number of different methods have been used at various times to provide some degree of absolute amplitude calibration. However, in spite of continued refinement of techniques, one or more items from a long list of practical difficulties usually have

* Latter and Le Levier (1963).

† Vassiliadis (1965).

precluded obtaining even order-of-magnitude estimates of backscatter coefficients at the time when the most interesting cloud situations were available. For example, differential thermal expansion in the equipment has made it very difficult to correlate calibrations made at night (when they are easiest and most accurate) with data obtained during the day. Only during the final weeks of the work reported herein have equipment and technique improved to the point where it now appears possible to provide reliable and consistent amplitude calibration, day or night.

In brief, the presently preferred method is to operate with beam-widths and optical bandwidths narrow enough and with sufficient transmitter pulse energy that when the transmitter and receiver beams are properly coaligned one is sure of having enough return from the relatively reliable Rayleigh molecular backscatter from (nearly) clear air at a suitably chosen high altitude to clearly override the background noise. Unknown targets are then compared in amplitude against this reference. Tentatively, the region around 10 km elevation appears to be a good choice.

This elevation is only slightly above the so-called isopycnic level at about 8 km where atmospheric densities usually do not deviate by more than 1 or 2%, regardless of season or location (Handbook of Geophysics, 1965, page 3-23). In addition, the data of Elterman (1964) indicate that the contribution to backscatter from particulate matter normally is at a minimum at about 10 km, where it is less than 1% of the gaseous backscatter component (see Fig. VI-1). Even allowing for occasional increases in the aerosol content by a factor of ten, and without any knowledge of prevailing pressure soundings, it then appears that we can count on knowing the volume backscatter coefficient of air in this region to $\pm 10\%$ or better. This is significantly better accuracy than is achievable by extrapolation from calibration measurements carefully made on ground-based targets and is considered adequate for present purposes.

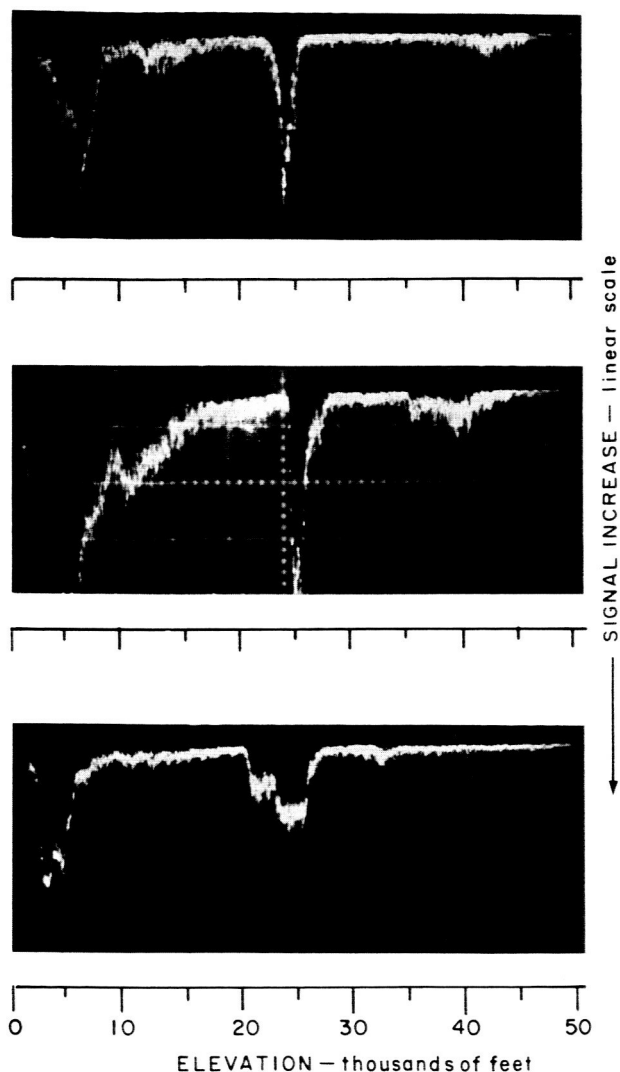
Since other targets roughly ten to one hundred times larger can then be compared directly to this return, no measurements need be made of transmitted power, calibration attenuators, or low-altitude atmospheric absorption.

The method requires lidar beamwidths and optical bandwidths narrow enough to insure that with the available transmitter power the Rayleigh return will be measurably above the background noise when the transmitter and receiver beams are properly coaligned. The SRI Mk II lidar now has this capability. It also requires that a patch of clear air be found at approximately the right elevation. By using the (uncalibrated) lidar waveform as a guide, location of a suitably clear region normally has not been a problem.

Using this technique we obtained during the week of 14 March 1966 what we believe to be the first daytime measurement of backscatter coefficients and vertical extent of very weak cirrus clouds when conventional daytime visual observations also were possible. Figure VI-3 shows A-scope traces taken on an afternoon when both clearly visible and marginally visible cirrus was present. Figure VI-4 is a photograph of the lidar and of the general cloud situation taken during the run. For the particular waveforms shown in Fig. VI-3, the laser was fired when visible cloud was in the field of view. Other shots fired between conspicuous clouds and into light blue sky produced returns from only the higher, less dense layer which was apparently quite uniform and which persisted all afternoon. On the day of the run, the pertinent lidar characteristics were:

- Transmitter wavelength, $6943\overset{\text{O}}{\text{\AA}}$
- Transmitted energy, 0.3 joule per pulse (Q-switched)
- Transmitter beamwidth, 0.3 milliradian
- Receiver field of view, approx. 1.5 milliradian
- Receiver optical bandwidth, $12.5\overset{\text{O}}{\text{\AA}}$
- Overall optical efficiency, approx. 10 percent.

With these constants, the photoelectron count due to background light was 11 to 15 pulses per microsecond, which accounts for over half the "fuzz" on the waveform baselines above 30,000 feet. Subsequent transmitter-receiver convergence techniques permitted the receiver viewing solid angle (and consequently the background noise) to be reduced by almost an order of magnitude. While this improvement does not make too much difference in the appearance of the A-scope display on the scale shown in Fig. VI-3, it does greatly facilitate comparing signal levels



TIME: 1320 PST
 LIGHT CIRRUS VISIBLE OVERHEAD
 RETURN FROM 23-25,000 ft. CORRESPONDS
 TO $\beta'_{180} \approx 2.0 \times 10^{-4} \text{ m}^{-1}$
 RETURN FROM 42-44,000 ft. CORRESPONDS
 TO $\beta'_{180} \approx 1 \times 10^{-5} \text{ m}^{-1}$

TIME: 1408 PST
 LIGHT BLUE SKY GENERALLY OVERHEAD
 LIGHT CIRRUS DIRECTLY OVERHEAD
 RETURN FROM 25-28,000 ft. CORRESPONDS
 TO $\beta'_{180} \approx 2 \times 10^{-4} \text{ m}^{-1}$
 RETURN FROM 36-44,000 ft. CORRESPONDS
 TO $\beta'_{180} \approx 2 \times 10^{-5} \text{ m}^{-1}$

TIME: 1626 PST
 TRANSLUCENT CIRRUS OVERHEAD
 RETURN FROM 21-27,000 ft. CORRESPONDS
 TO $\beta'_{180} \approx 2.0 \times 10^{-4} \text{ m}^{-1}$ (peak)
 RETURN FROM 31-33,000 ft. CORRESPONDS
 TO $\beta'_{180} \approx 1.0 \times 10^{-5} \text{ m}^{-1}$

AFTERNOON OF MARCH 17, 1966, MENLO PARK, CALIF.

VERTICAL SCALE: 50 mv/div FOR TOP TWO TRACES
 100 mv/div FOR BOTTOM TRACE
 ACROSS 50Ω PMT ANODE LOAD RESISTOR

ELEVATION = 90°
 CLEAR BLUE SKY; BRIGHTNESS =
 1000-1500 ft. LAMBERTS
 VISUAL OBSERVATION: UNIFORM, LOW DENSITY
 CIRRUS AT HIGH ALTITUDE; 4/10 COVERAGE OF LOWER
 CIRRUS LINES OF MEDIUM DENSITY

FIG. VI-3 LIDAR RETURNS FROM MEDIUM AND WEAK CIRRUS SYSTEMS



FIG. VI-4 MK II LIDAR AND CIRRUS-CLOUD SITUATION OF 17 MARCH 1966

by pulse counting. Use of this procedure has now made it clear that marginally visible cirrus layers, one or two km thick, can have volume backscatter coefficients at ruby wavelength of even less than 10^{-5} m^{-1} . It has also become very apparent how imprecise is the description "marginally visible". On one occasion, a weak cirrus shield with $\beta'_{180} \approx 10^{-5}$ and thickness 1000 to 2000 feet persisted through the day with little change as monitored by the lidar. However, the visibility to human observers on the ground varied from subvisible to definitely overcast, depending upon the sun angle, low-altitude haze conditions, and possibly other factors. It was evident that color contrast plays an important role in defining the daytime visibility of cirrus and should be considered in any serious attempt to correlate lidar data with visual observations.

The strongest consistent returns measured from cirrus heights to date correspond to $\beta'_{180} \approx 1 \times 10^{-3} \text{ m}^{-1}$ as determined by the attenuated return from a ground-based plywood test target at equivalent range. Occasional brief echoes of very high amplitude have been noted near the bottom or top boundaries of cirrus layers. It has been presumed that these may result from chance specular reflections from flat-plate ice crystals floating principally horizontally, like falling leaves. A similar explanation has been given for the "sun-dog" or "under-sun" effect often observed when flying over some forms of cirrus. Boeing investigators reported this phenomenon to be so strong as to damage their thermocouples during infrared measurements of cirrus (Boeing Company, June 1962).

Lidar reflections from low-level water clouds usually have been strong enough to cause severe overloading in the photomultiplier, and very little quantitative data are yet available on these clouds. However, attenuation coefficients (or extinction coefficients, as they usually are known when measured in luminous units) have been measured in the past by numerous investigators for water clouds and hazes, and the lidar returns appear to be not markedly different from what would be expected from the relation $\beta'_{180} = k\sigma$, where k has a value of approximately 0.6.

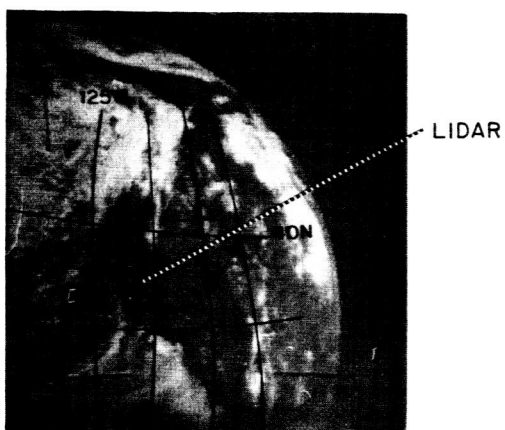
The values of β'_{180} given in Fig. VI-2 are being used at SRI as the best currently available working estimates for all types of clouds and hazes in the visible region. It is hoped that the data can be refined appreciably in the near future.

C. Three-Day Lidar Test Run to Monitor Visible and Subvisible Cirrus

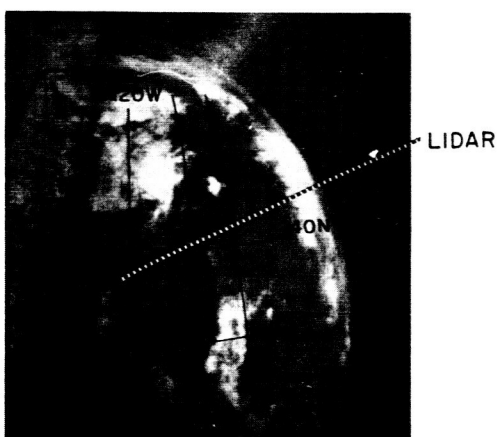
An extended test run was performed midway through the project in an attempt to learn whether lidar-measurable but subvisible cirrus cover might be more common than originally anticipated. While the results were largely negative, the experiment is briefly described here for completeness. At the time these measurements were made, the lidar characteristics were such that cirrus corresponding to $B'_{180} \approx 10^{-4} \text{ m}^{-1}$ would have had to be present in order to be visible above the daytime noise level. At night, however, the system would have been capable of detecting anything more than four or five times the Rayleigh return level up to 50,000 feet elevation.

The lidar at the SRI facility in Menlo Park was fired along the vertical once each hour during the three-day period from noon on 20 July 1965 until noon on the 22 July 1965. During this period a series of migratory cyclones were moving slowly eastward around the northern periphery of a large subtropical anticyclone in the eastern Pacific [Fig. VI-5(d)]. It was anticipated that lidar returns from cirrus were forthcoming as one of these cyclones, accompanied by multiple cloud layers (including cirrus) was approaching the area at the start of the period. However, the storm veered eastward before reaching this far south so that only haze and a few widely scattered low stratus clouds (normal conditions for the area) were observed during the period. The vertical lidar beam did not intercept any visible clouds during the three days of observations.

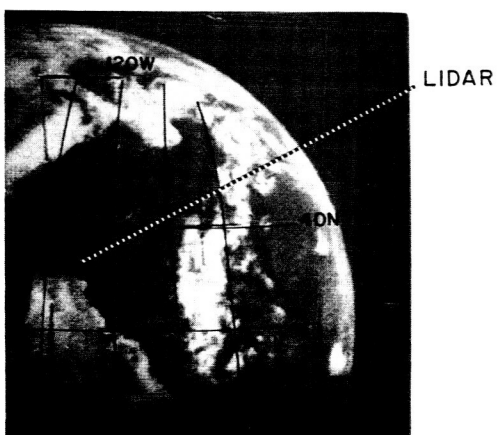
The bright cloud areas immediately to the north of the San Francisco region in the pictures made by TIROS IX as it passed overhead [Fig. VI-5, (a)-(c)] approximately outline the areas of multiple cloud layers associated with this and other storms in the series mentioned above. Note that the



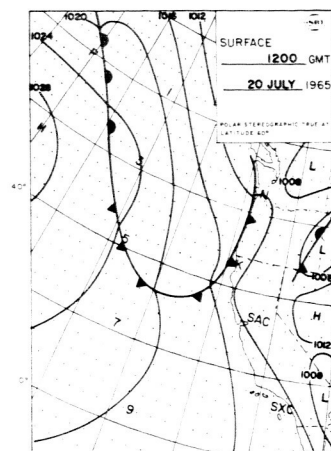
(a) ORBIT 2167 FRAME 6
1643GMT 20 JULY



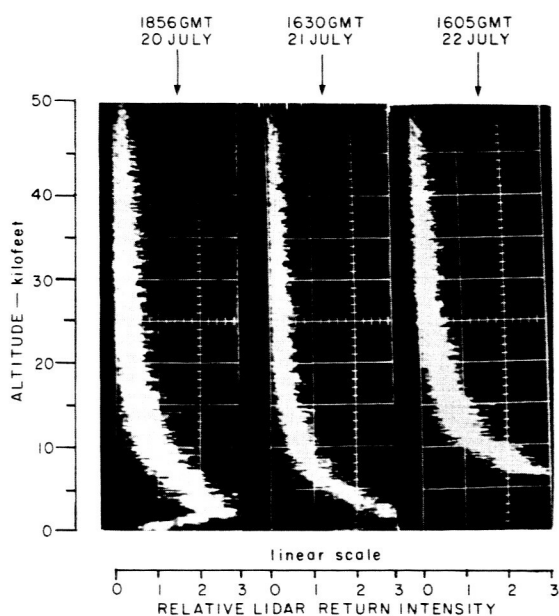
(b) ORBIT 2179 FRAME 5
1634GMT 21 JULY



(c) ORBIT 2191 FRAME 5
1625GMT 22 JULY



(d) SURFACE CHART



(e) LIDAR RETURNS AT TIMES CLOSE
TO TIROS IX PICTURES

FIG. VI-5 TIROS IX PICTURES, LIDAR RETURNS, SYNOPTIC CONDITIONS
FOR 20-22 JULY 1965

cloudiness near the San Francisco area has a dull appearance. This is characteristic of satellite-viewed fog or low clouds.

Figure VI-5(e) shows lidar return as a function of altitude when the lidar was fired close to the times that TIROS IX was photographing the area on each of the days during the period. No returns from clouds above 10,000 feet or below 50,000 feet are indicated, although intensity of return does increase significantly below 10,000 feet, particularly on the last day of the period. This more intense low-level return was due to the normal increase in particulate concentration near the surface. The further increase in low-level return at 1605 GMT on 22 July was caused by the stagnation of the air near the surface during the preceding 24 hours which allowed the particulate concentration there to increase significantly.

VII AN APPLICATION OF SATELLITE-LIDAR DATA TO INFRARED RADIATION STUDIES

A. Introduction

Aircraft have observed thin ice-crystal clouds that are often invisible from the ground and cannot be seen on daytime cloud photographs from weather satellites (Appleman, 1961). The frequent occurrence at night of thin layers of cirrus that were undetectable by visual means has been established with observations from a ground-based lidar (SRI, private communication).

The effect of tenuous cirrus clouds on the outgoing infrared radiation from the earth's surface and the lower troposphere was first suggested on the basis of measurements made with balloon-borne radiometers (e.g., Gergen, 1957; Riehl, 1962).

Zdunkowski (1965) demonstrated by means of a computational model that visually transparent cirrus clouds can appreciably effect the interpretation of long-wave radiation measurements of the type that have been obtained from the medium-resolution radiometers of TIROS (e.g., Channel 1, 6.0 to 6.5 μ and Channel 2, 8 to 12 μ).

The purpose of the following presentation is:

- (1) To show the effect of two cirrus-cloud models on the interpretation of various infrared radiation measurements that are being planned for the Nimbus meteorological satellite series
- (2) To show how cirrus clouds of the type described by the two models can be detected by a satellite-borne lidar
- (3) To demonstrate how lidar data on tenuous cirrus clouds can be converted into estimates of correction factors to be applied to long-wave radiation measurements from satellites.

B. Computed Effect of Ice Crystal Clouds on Infrared Radiation Measurements from Satellites

1. Selection of Cirrus-Cloud Model

We wish to consider a cloud model that represents large-scale thin ice-crystal clouds of the type that produce the 22° halo. These thin ice clouds (e.g., cirrostratus) are observed very frequently in advance of frontal cyclones. Minnaert (1954) states that "the most observant see halos on 200 days a year." When the optical phenomenon of the halo cannot be observed (on a moonless night or in the presence of a low-level haze) the thin cirrostratus may go undetected. Thus, thin ice clouds associated with the halo must occur even more frequently than actual observations of the halo indicate.

All clouds giving rise to halos are believed to be composed of regularly shaped ice crystals that are randomly oriented. The random orientation of the regularly shaped ice crystals (hexagonal prisms) permits the adoption of a cloud model consisting of monodisperse spherical ice particles to which an effective radius is assigned.

The cloud model used in this study has spherical ice particles with an effective radius of 120 μ . This value is essentially that used by Zdunkowski, and is also very close to the effective radius listed by A. M. Borovikov et al. (1965) for ice crystals in altostratus clouds (121 μ). The number densities used are those suggested by Zdunkowski for visually transparent ($2 \times 10^{-3} \text{ cm}^{-3}$) and for visually semi-transparent ($2 \times 10^{-2} \text{ cm}^{-3}$) cirrus clouds that have a thickness of 1000m. The measurements by Borovikov et al. give an average number density of $2 \times 10^{-3} \text{ cm}^{-3}$ for ice crystals in altostratus clouds. The 1000m thickness is in good agreement with the seasonal mean thickness values for cirrus clouds as determined from the data of Project Cloud Trail (Stone, 1957), and is also compatible with a thickness of "a few thousand feet" for a visually semi-transparent cirrus cloud cited by Blau and Espinola (1965). Table VII-1 summarizes the physical dimensions of the two ice cloud models.

Table VII-1
CLOUD MODELS USED IN COMPUTATIONS

	Model I High Visual Transparency	Model II Medium Visual Transparency
Effective Radius (a)	120μ	120μ
Number Density (N)	$2 \times 10^{-3} \text{ cm}^{-3}$	$2 \times 10^{-2} \text{ cm}^{-3}$
Thickness (H)	1000m	1000m

2. Computations of Transmission and Absorption

For the two cirrus-cloud models specified above, the total attenuation due to both absorption and scattering processes is computed as a function of wavelength for the infrared region of 3.0μ to 200μ. The real and complex parts of the refractive indices for ice used in the computations are those given by Kislovskii (1959) for $T = 10^{\circ}\text{C}$.

The total attenuation coefficient σ equals the sum of the attenuation coefficients due to scattering and absorption:

$$\sigma = \sigma_s + \sigma_a$$

where

$$\sigma_{s,a} = \int \pi a^2 Q_{s,a}(a,n)n(a)da.$$

In this expression $\pi a^2 Q_{s,a}$ is the total scattering (s) or total absorption (a) cross section, as the case may be, for a single sphere of radius a and refractive index n . $n(a)da$ represents the number of ice spheres of radius a in the interval da . For cloud models I and II

$$\sigma_{I,II} = \pi(120\mu)^2 Q(120\mu,n)N_{I,II}.$$

The efficiency factors for scattering and absorption ($Q_{s,a}$) are obtained from the Mie scattering theory by averaging over the radius interval $a_1(\Delta a)a_2 = 110\mu(1\mu)130\mu$. Results are applied to the effective radius

$a = 120\mu$. The correction introduced by Zdunkowski [$Q_s^* = Q_s - 2/(Q_s + Q_a)$] is applied to Q_s in order to account for that part of the scattered radiation that is diffracted into the forward direction and that should be added to the transmitted radiation. Thus for the visible wavelengths when no absorption takes place, $Q_s = 2$ and $Q_s^* = 1$.

Figure VII-1 shows the fraction of the incident infrared beam radiation that is lost due to both scattering and absorption [$1 - \exp(-\sigma H)$] and that fraction which is lost due to absorption only [$1 - \exp(-\sigma_a H)$] for cirrus-cloud models I and II. The total attenuation amounts to 10 to 15 percent of the beam radiation incident on cloud model I and to 60 to 80 percent of the beam energy incident on cloud model II. The importance of absorption is evident. Except for the "window" regions near 5μ and 7μ , 80 percent or more of the total energy attenuated from the incident beam is attenuated due to absorption between 3.0μ and 100μ . It is the large absorption of the cloud models in these infrared wavelengths that warrants a further study of their effect on infrared radiation measurements from satellites.

For the visible wavelengths the transmissivity equals 91 percent for model I (assumed visually highly transparent) and 40 percent for model II (assumed semi-transparent).

3. Approximated Effects of Cloud Models on Infrared Measurements from Satellites

The effects of the attenuation and absorption of infrared radiation by the two cloud models on the interpretation of satellite measurements of long-wave radiation that originates from sources below the cloud level ($\sim 200\text{mb}$), can be approximated. To do this, a "target" black-body radiation source of temperature T_B is placed below the cloud model and the upward hemispheric flux of radiation, in various infrared spectral regions, is attenuated as it passes through the clouds. The transmitted plus the cloud-emitted radiation is then converted to the temperature T_e of an equivalent black-body. Differences between T_e and T_B are a measure of the effects that the cloud models have on the interpretation of satellite measurements of long-wave radiation emitted by the earth's

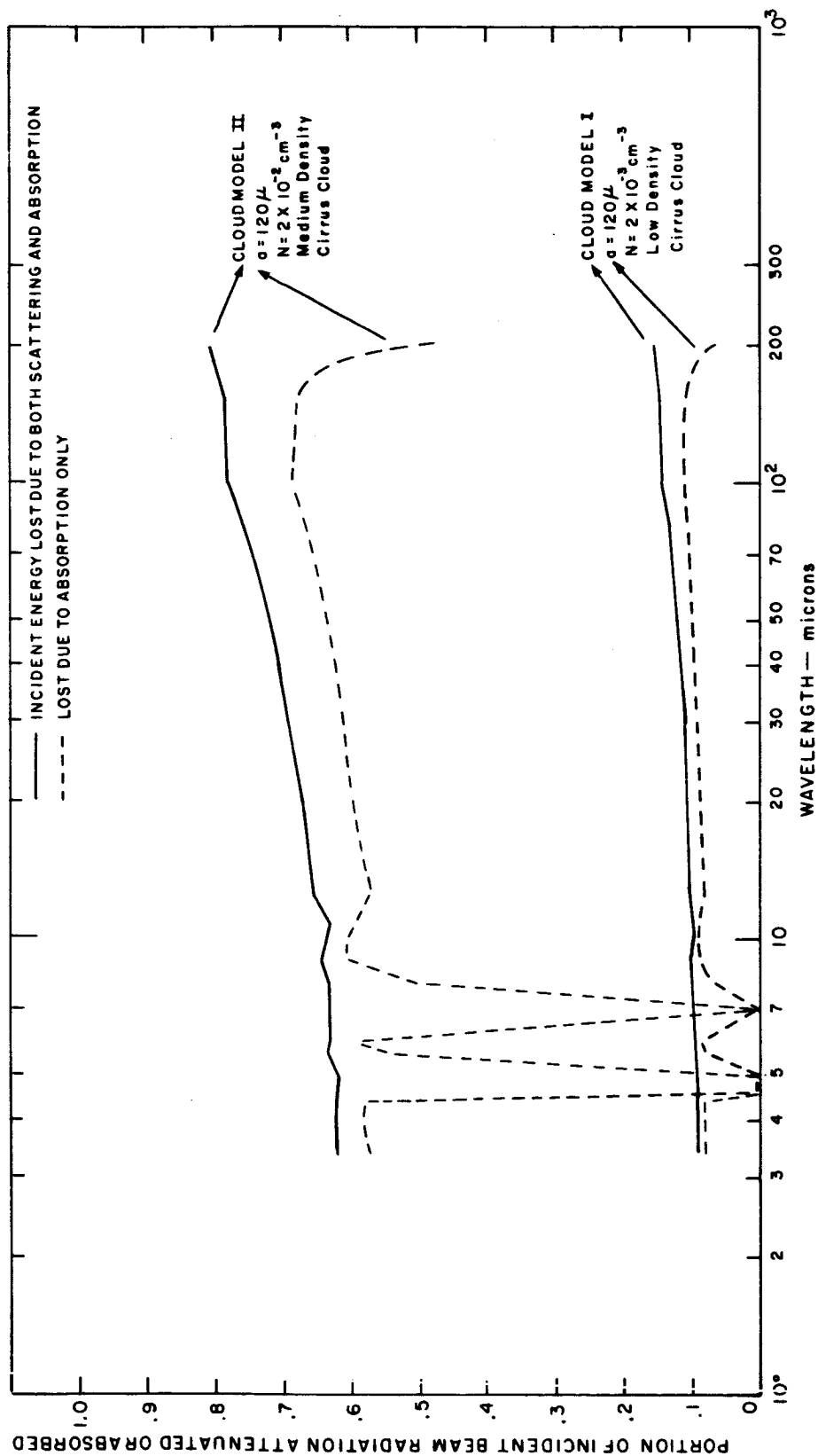


FIG. VII-1 INFRARED ATTENUATION AND ABSORPTION FOR CLOUD MODELS I AND II

surface and the lower troposphere. The attenuation is computed by applying the attenuation factor $e^{-\sigma H}$ which involves the simplifying assumption that the upward hemispheric flux from the "target" black body arrives at the lower cloud boundary as beam radiation. The cloud-emitted radiation is computed from Kirchhoff's Law taking an emission temperature of 230°K (-43°C) and an absorptivity equal to $1 - \exp(-\sigma_a H)$. This value of the absorptivity is correct only for small values of σH such that $\exp(-\sigma_a H)$, $\exp(-\sigma_s H)$, and $\exp(-\sigma H)$ can be expanded into series keeping first order terms. The absorptivity can be obtained in this fashion for cloud model I, but not for model II. Computations will therefore be limited to cloud model I. Considering the large absorption (approximately 60 percent of the incident beam energy), cloud Model II is highly opaque to long-wave radiation and the effect on identifying infrared emission sources located below such a cloud is obvious.

Figure VII-2 shows a comparison between T_B (the true temperature of a "target" black-body radiation source located below cirrus-cloud model I) and T_e (the temperature deducted from infrared measurements made above the cirrus cloud) for four infrared regions and two black-body temperatures. The infrared regions are selected to coincide with the nominal bandwidths of various sensors that will be placed in the Nimbus B and C meteorological satellites (expected to be launched in late Summer of 1967 and Spring of 1966, respectively). The selected "target" black-body temperatures of 300°K and 250°K correspond to the average terrestrial temperature and the average mid-tropospheric temperature, respectively. Table VII-2 lists the selected infrared regions together with the meteorological information to be deduced. Also listed is the essential information of Fig. VII-2, i.e., the approximate errors ($T_B - T_e$) in the determination of the "target" black-body temperature due to the interference by a visually highly transparent cirrus cloud of the type represented by cloud model I. It can be seen from Fig. VII-2 and Table VII-2 that for a "target" black-body temperature of 300°K, the difference between T_{300} and T_e is 2 to 3 degrees for the spectral region 3.5 to 4.0 μ and increases gradually to 7 to 8 degrees for the wavelength region 14 to 16 μ . For a black-body temperature of 250°K, a steady

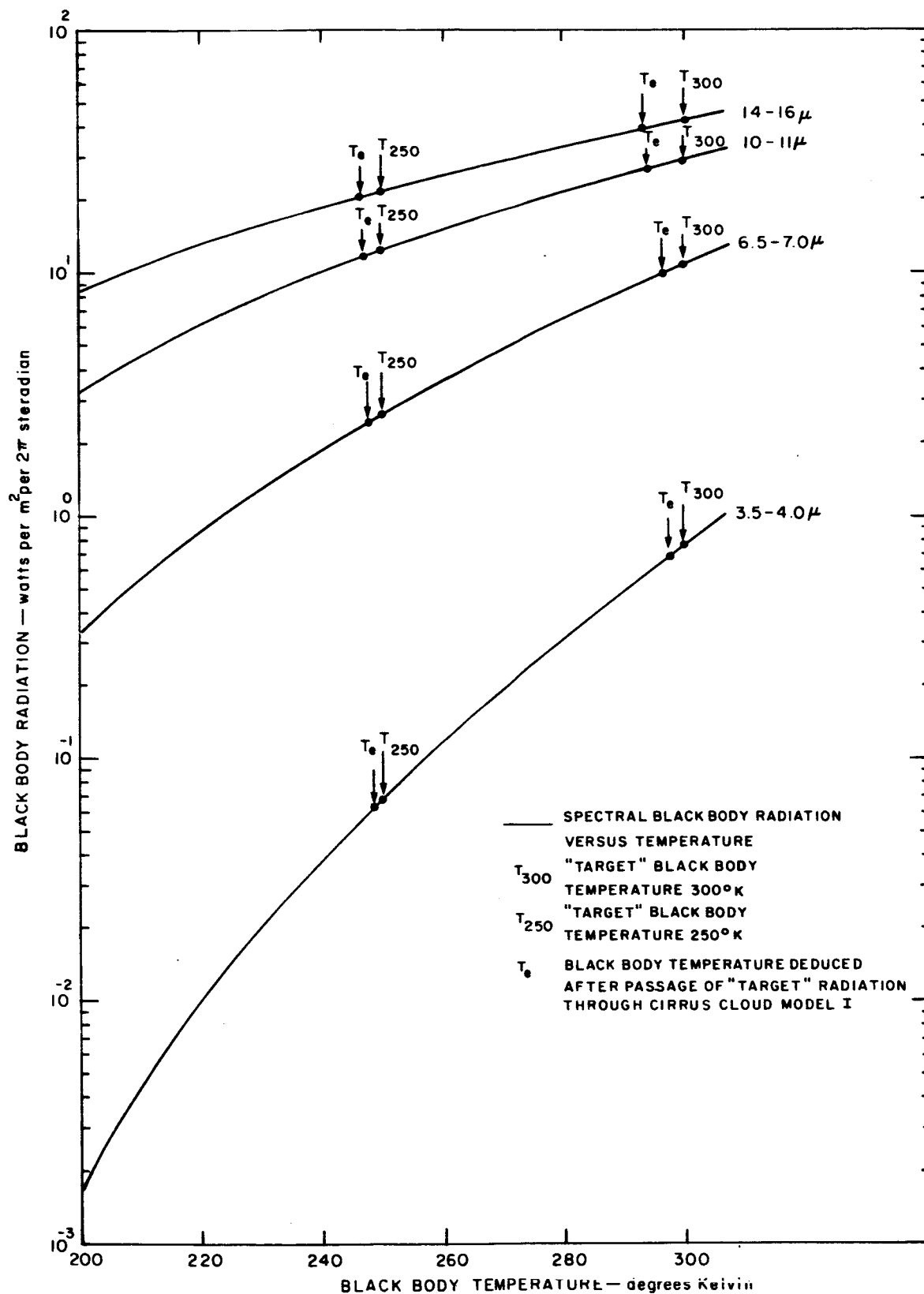


FIG. VII-2 ERRORS IN DETERMINATION OF BLACK-BODY TEMPERATURE DUE TO INTERFERENCE BY TENUOUS CIRRUS CLOUD

Table VII-2

ESTIMATE OF ERRORS IN DETERMINATION OF "TARGET" BLACK-BODY TEMPERATURES
FROM SATELLITE ALTITUDE DUE TO INTERFERENCE TENUOUS CIRRUS CLOUD

IR Bandwidth in Microns (Nimbus B,C)	Nature of Band	Meteorological Information to be Deduced	Approximate Error in "Target" Black-Body Temperature Due to Interference by Tenuous Cirrus ($T_B - T_e$)	
			"target" black-body temperature 250°K	"target" black-body temperature 300°K
3.5-4.0	Atmospheric Water-Vapor Window	Night-time cloud photography, cloud-top temperature, surface temperatures	1-2	2-3
6.5-7.0	Atmospheric water-vapor absorption band	Atmospheric water-vapor distribution	2	4
10-11	Atmospheric window	Earth surface temperatures	2-3	6-7
14-16	Carbon dioxide absorption band	Atmospheric temperature distribution	3-4	7-8

increase of $T_{250} - T_e$ with wavelength is again shown but differences are less than at 300°K, ranging from 1 to 2 degrees at 3.5 to 4.0 μ to 3 to 4 degrees at 14 to 16 μ .

C. Detection of Cirrus-Cloud Model I by Satellite Lidar

In order to evaluate the capability of a satellite-borne lidar to detect cirrus clouds of the type described by cloud model I, it is necessary to compute the lidar pulse energy that is scattered back to the receiver by this cloud model. For this purpose a volume backscattering coefficient β'_{180} is defined as:

$$\beta'_{180} = 4\pi \int \pi a^2 i_{180} n(a) da$$

where $i_{180} = (\lambda^2/8\pi^2)[i_1(180^\circ) + i_2(180^\circ)]$ = the flux scattered per unit solid angle in the 180° direction for a single sphere of radius a and for unit flux incident on the geometrical cross section πa^2 . $i_1(180^\circ)$ and $i_2(180^\circ)$ refer, respectively, to the intensity of radiation vibrating perpendicular and parallel to the plane through the directions of propagation of the incident and scattered beams.

The validity of the assumption that a cirrus cloud can be represented by a concentration of homogeneous ice spheres with perfectly smooth surfaces becomes critically important when the volume backscattering coefficients β'_{180} for such cirrus clouds are to be computed at optical wavelengths (e.g. $\lambda = 6943\text{\AA}$) on account of the phenomenon of the glory (Van de Hulst, 1957). The variation in the angular scatter efficiency i_ϕ in the region of the glory (i.e. the region near $\phi = 180^\circ$) is shown in Fig. VII-3 for a Mie-scattering sphere with a radius of 120 μ and a refractive index of 1.33*. The wavelength considered is that of the ruby lidar ($\lambda = 6943\text{\AA}$). The bright "rings" increasing in intensity toward a sharp maximum at $\phi = 180^\circ$ are evident. The magnitude of the

* The glory phenomenon as defined in this paper is due to the variation in the angular scattering efficiency near 180° shown in Fig. VII-3 and is therefore not restricted to refractive indices between $\sqrt{2}$ and 2.

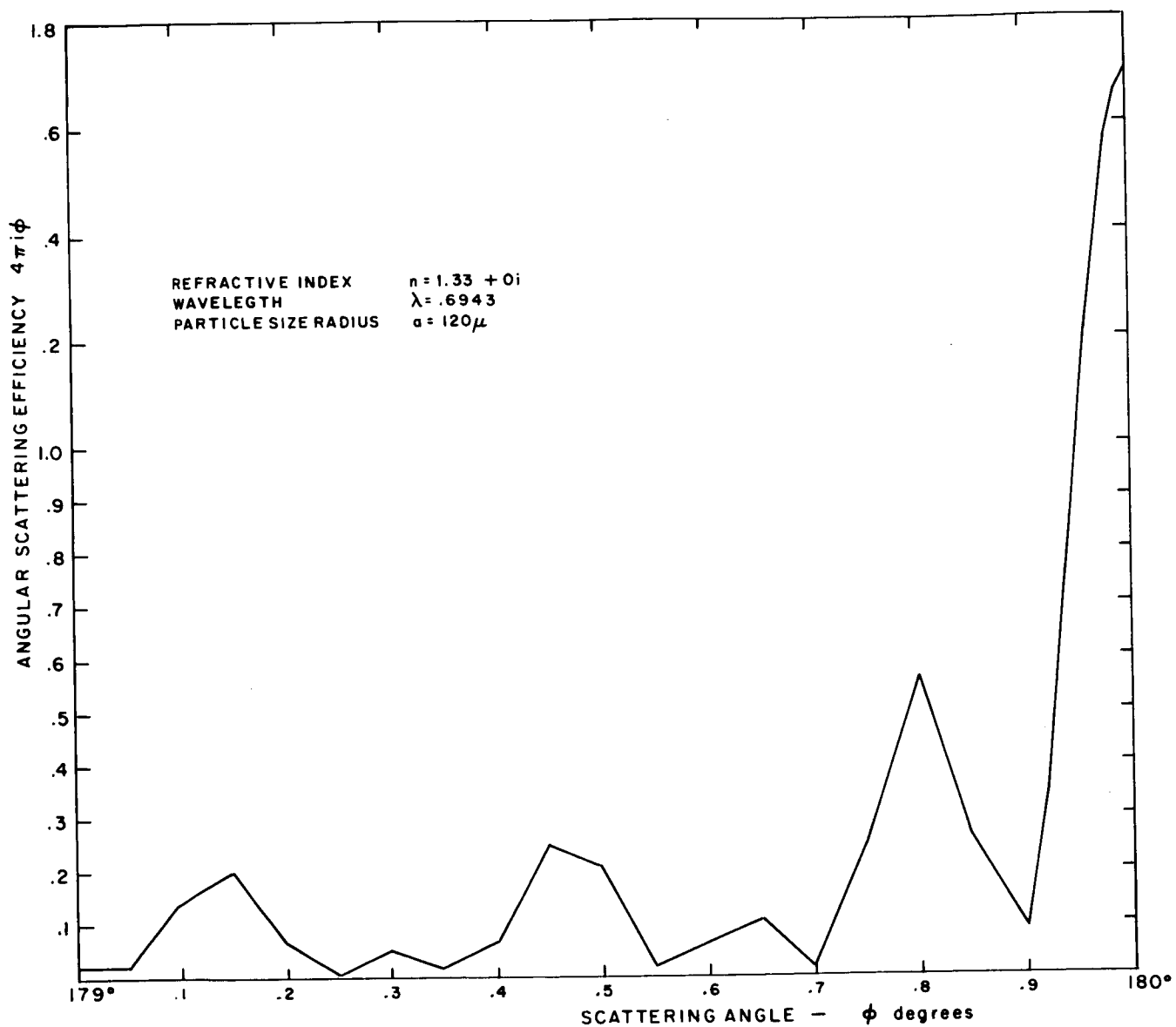


FIG. VII-3 ANGULAR SCATTERING EFFICIENCY IN REGION OF THE GLORY

large maximum at 180° is greatly dependent on the radius of the sphere. Figure VII-4 shows graphically the variations of $4\pi i_{180^\circ}$ between $a_1 = 120\mu$ and $a_2 = 120.44\mu$. The graph is constructed by joining with straight lines values of $4\pi i_{180^\circ}$ computed for intervals of $\Delta a = 0.01\mu$.

It is evident that the glory phenomenon leads to large values of the computed backscattering coefficient β'_{180} .

Although the glory enters prominently into the explanation of the exceptionally high radar backscattering cross sections obtained from large hailstones (Probert-Jones, 1964), Van de Hulst cites a single reference that gives evidence against the existence of an optical-wavelength glory phenomenon in ice clouds. More evidence should be obtained by comparing the backscattering coefficients deduced from the lidar-signal return of cirrus clouds with those predicted on the basis of cirrus-cloud models such as model I.

If tenuous cirrus can be represented by cloud model I--i.e. if the glory phenomenon is accepted--a backscattering coefficient can be computed from the exact Mie equations. In this case an average value of the quantity $4\pi i_{180^\circ}$ over a narrow range of radii will be applied. Figure VII-5 shows such average values for three narrow ranges of radius centered at approximately 100μ , 120μ and 140μ . It can be seen that the variation with small changes in effective radius is quite small. Adopting the average value of 2.85 for $a = 120$ to 122μ , the volume backscattering coefficient β'_{180} for cloud model I ($\lambda = 6943\text{\AA}$) can be written as:

$$\beta'_{180} = 2.85\pi(120\mu)^2 N_I = 2.58 \times 10^{-4} \text{ m}^{-1}.$$

The extinction coefficient σ_I is equal to

$$\sigma_I = Q_s^* \pi (120\mu)^2 N_I = 9.04 \times 10^{-5} \text{ m}^{-1} \quad \text{for } Q_s^* = 1,$$

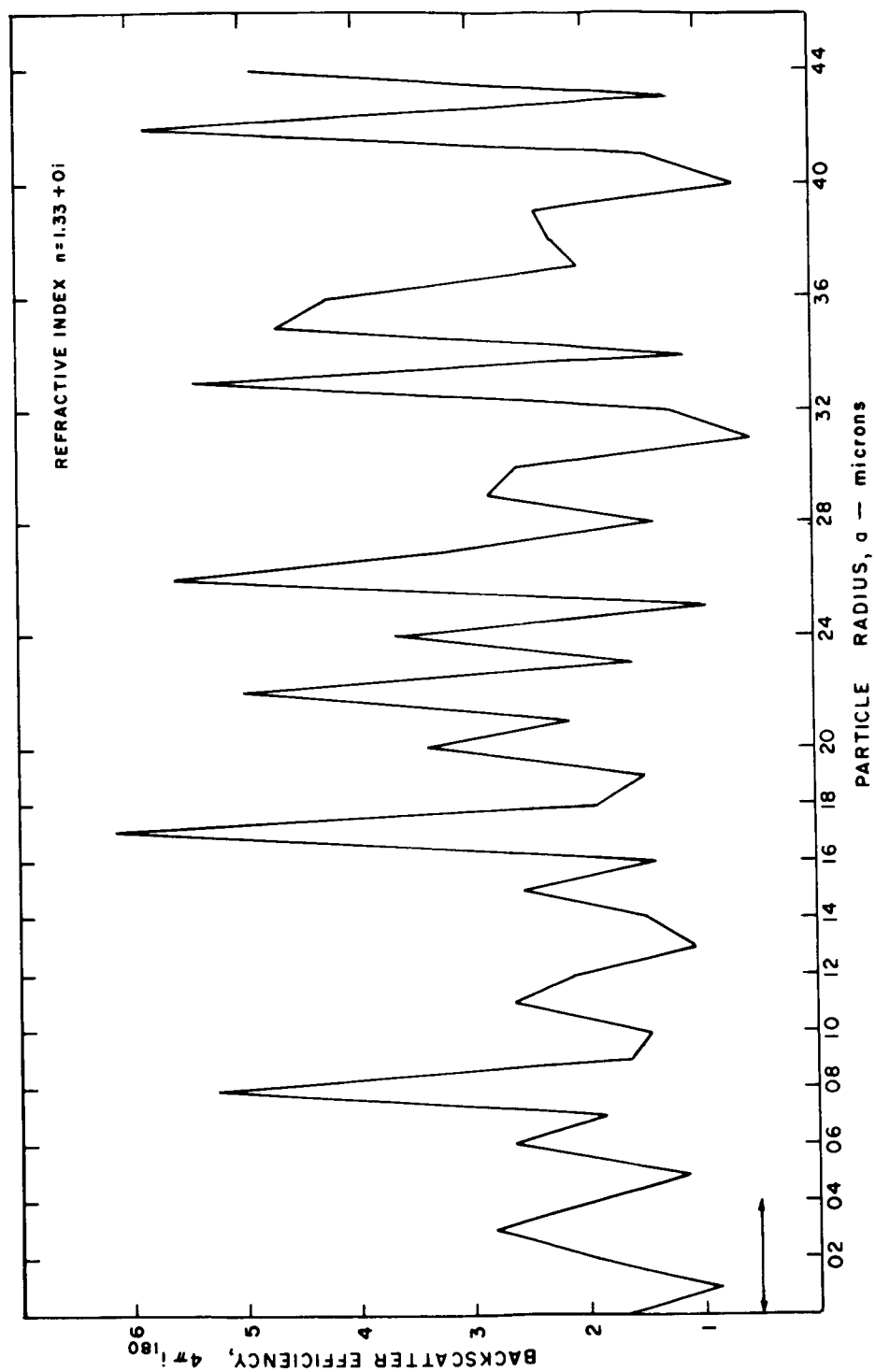


FIG. VII-4 BACKSCATTER EFFICIENCY AS A FUNCTION OF PARTICLE RADIUS

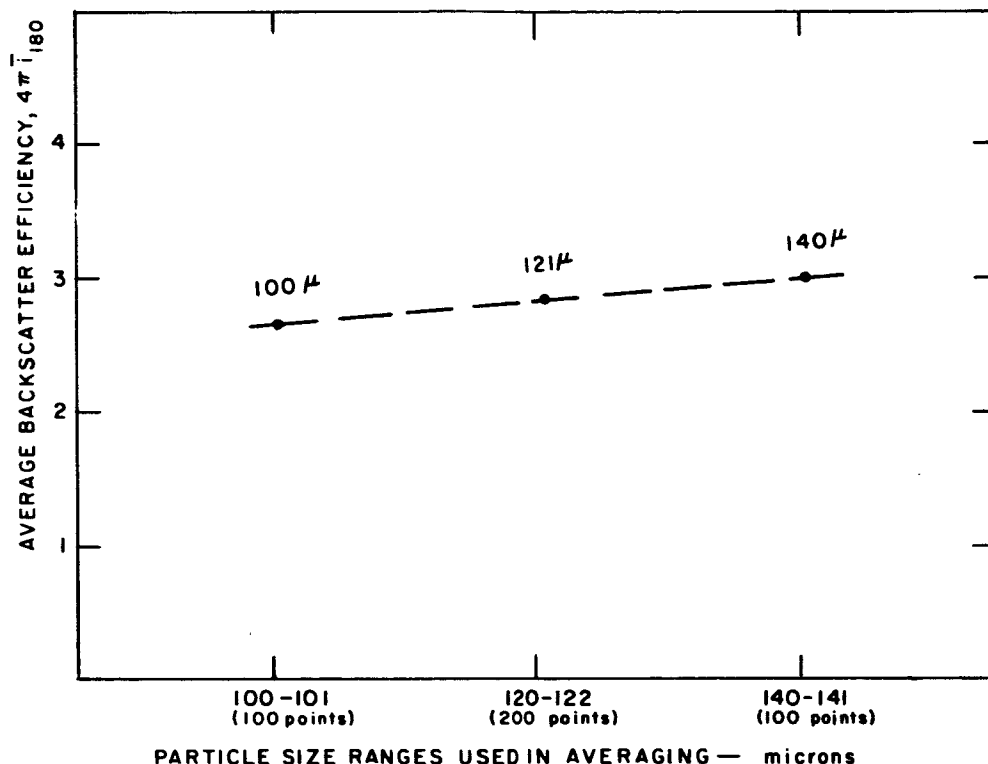


FIG. VII-5 AVERAGE BACKSCATTER EFFICIENCY FOR THREE RANGES OF PARTICLE SIZE

so that

$$\frac{\beta'_{180}}{\sigma_I} = 2.85 \quad .$$

If we cannot apply the angular scattering patterns of large spheres in the Mie theory near and at $\phi = 180^\circ$ to the ice crystals of cirrus clouds, the following alternatives can be considered.

- (1) The backscattering pattern given by the theory of geometrical optics (ray tracing) can be applied. In this case the effect of the glory is not accounted for. Adopting the scattering pattern of a very large water drop given by Van de Hulst (p. 232) the backscattering coefficient β'_{180} for cloud model I can be written:

$$\begin{aligned}\beta'_{180} &= 0.098\pi(120\mu)^2 N_I \\ &= 8.86 \times 10^{-6} \text{ m}^{-1}\end{aligned}$$

The extinction coefficient σ_I would remain equal to $9.04 \times 10^{-5} \text{ m}^{-1}$ so that

$$\frac{\beta'_{180}}{\sigma_I} = 0.098$$

- (2) It can also be assumed that the large (compared with the wavelength) particles of a cirrus cloud distribute the reflected and refracted part of the scattered radiation uniformly in all directions (isotropically) while the diffracted part remains concentrated into a narrow forward angle. In this case

$$i_{180^\circ} = \frac{1}{4\pi}$$

and

$$\beta'_{180} = \pi(120\mu)^2 N_I = 9.04 \times 10^{-5} \text{ m}^{-1} ;$$

also

$$\sigma_I = \pi(120\mu)^2 N_I = 9.04 \times 10^{-5} \text{ m}^{-1} \quad \text{for } Q_s^* = 1 .$$

Thus

$$\frac{\beta'_{180}}{\sigma_I} = 1$$

- (3) It can be assumed that the ice crystals of cirrus clouds represent large spheres whose surface elements are diffuse reflectors following Lambert's law. The scattering pattern of such spheres as computed by Schoenberg is given by Van de Hulst (p. 112). Assuming 50 percent surface

reflectivity and an isotropic distribution of the refracted part of the scattered radiation, the volume backscattering coefficient β'_{180} can be written as:

$$\begin{aligned}\beta'_{180} &= 4\pi \left(2.667 \frac{0.50}{4\pi} + \frac{0.50}{4\pi} \right) \pi(120\mu)^2 N_I \\ &= 1.66 \times 10^{-4} \text{ m}^{-1}\end{aligned}$$

The factor 2.667 is the "gain" of the Lambert-reflected radiation relative to isotropic scattering in the direction $\phi = 180^\circ$ as given by Van de Hulst. The extinction coefficient σ_I equals

$$\sigma_I = \pi(120\mu)^2 N_I = 9.04 \times 10^{-5} \text{ m}^{-1}$$

and the ratio

$$\frac{\beta'_{180^\circ}}{\sigma_I} = 1.84$$

A comparison of β'_{180° , σ , and their ratio as determined from the lidar return of tenuous cirrus clouds, with the various values computed above would greatly enhance our understanding of the backscatter characteristics of cirrus clouds. Such understanding could in turn help to define the type of model that can represent cirrus in studies that involve infrared radiation. The waveforms representative of cloud model I (with the various backscatter characteristics) that could exist at the satellite-borne lidar receiver under various conditions of background lighting can be predicted using the outline of Sec. V-B-2 and the values of β'_{180} and σ_I given above.

D. Conclusions

In order to demonstrate an application of satellite-borne lidar data on tenuous cirrus clouds to meteorological problems that involve infrared radiation, an attempt was made to approximate the errors that arise when temperatures characteristic of the earth's surface and the

lower troposphere are determined from satellite measurements when tenuous cirrus clouds are present.

The computational model used is simple and more sophistication is necessary although more accurate information on the shape and size distribution of ice crystals in cirrus clouds and on the refractive index of ice may have to be obtained first. The validity of the assumption that the cirrus clouds can be represented by a number of ice spheres with a uniform effective radius in order to compute bulk transmission and absorption, should be more objectively examined with a comparison between actual lidar observations and predicted values of the volume backscattering coefficients and extinction coefficients. The refractive indices for ice used in the computations were limited to a temperature of -10°C which is much warmer than the temperature of $<-40^{\circ}\text{C}$ that is generally assigned to ice clouds. Kislovskii states the effect of lower temperatures on the refractive index qualitatively as follows:

Upon cooling, the band near 3μ increases significantly in intensity (the reflection attains a maximum of 12 percent). The weak reflection band near 6μ becomes even weaker. The band near 12.5μ shifts toward the short-wavelength side.

These remarks imply that the absorption may have been larger than computed in the region $10-11\mu$ and smaller in the region $6.5-7.0\mu$.

At this point it may be warranted to speculate on a quantitative application of the lidar data. If the total extinction $e^{-\sigma H}$ of the lidar signal by the cirrus cloud, and its total geometric thickness H are retrieved from the basic lidar data, an average or "effective" value of $\pi a^2 N$ can be determined when it is assumed that, for the wavelength of the lidar ($\lambda = 6943\text{\AA}$)

$$\sigma = Q_s^* (\pi a^2 N)_{\text{effective}}$$

where $Q_s^* = 1$.

Furthermore, if upon impact of the lidar pulse on the cloud boundary an accurate value of β'_{180} can be determined, the ratio β'_{180}/σ represents an average value of the quantity $4\pi i_{180^0}$ shown in Fig. VII-5, provided the backscatter from a cirrus cloud can be represented as that from a concentration of ice spheres that scatter according to the Mie theory. This average value can in turn provide a "fix" on an average "effective" radius a , using a precomputed graph such as that shown in Fig. VII-5. Because of the small variation in the average value of $4\pi i_{180^0}$ with effective radius, a high degree of accuracy is required in the determination of β'_{180} and σ . With the derived quantities (a , $\pi a^2 N$) and correct values of the refractive index of ice, the total extinction and absorption cross sections can be computed with the help of the Mie theory for various infrared regions of interest. Correction factors (e.g. black-body temperature corrections) to be applied to satellite measurements of infrared radiation can then be estimated as discussed in Sec. II-B and Sec. II-C.

When preliminary lidar observations disagree with values of the volume backscattering coefficient and the extinction coefficient as computed from the Mie equations, a dependence of β'_{180} on the effective radius can no longer be maintained in the case of geometric optics, isotropic scattering and Lambert reflection, and other ways must be found to obtain a reliable value of effective radius for further computations in the infrared wavelengths.

VIII CURRENT LASER TECHNOLOGY

The specific lasers and types of lasers considered in this report are, by and large, those that were typical of the state of the art when this study began. However, substantial advances in the development of these lasers have occurred during the course of the work, and new and fascinating developments have resulted in new types of lasers. Furthermore, there is every reason to believe that the pace of such developments will continue, at least into the near future.

Q-switched ruby lasers have not yet been surpassed in peak power output, however. Short pulses in the gigawatt (10^9 watts) region are reported even in the unclassified literature, i.e., approximately 10 joules in 10-nanosecond pulses.

Typical of the performance of recent high-repetition-rate solid-state ruby lasers is the following small Siemens & Halske system:

Material	Ruby 1 × 1/8 inch
Threshold for lasing	2.5 to 3.5 joules
Pump pulse energy	3 to 15 joules
Pulse repetition rate	60 to 120 pps
Output power, average	1.6 watts
Output power, peak	60 watts (not Q-switched)
Efficiency	0.2 percent
Pump pulse length	2 ms

About an order of magnitude increase in overall efficiency can be realized in low-threshold neodymium-doped crystal lasers such as calcium tungstate or yttrium aluminum garnet (YAG), which lase in the infrared region around 1.06 microns. All of these materials can be continuously pumped and then Q-switched at high repetition rates with little reduction in the efficiencies realized for continuous (CW) operation, as long as the time between subsequent pulses is comparable to the fluorescent lifetime in the material.

Hundreds of watts of average power output have recently been demonstrated in at least two lasers. The first was demonstrated by Union Carbide using Nd:YAG at 1.06 microns, by pumping with a vortex-stabilized plasma torch. Such a system could presumably be Q-switched at high repetition rates. The overall efficiency is still low (the order of 0.2%), although it can be improved somewhat by straightforward techniques. Perhaps more interesting is the carbon dioxide (CO_2) laser, in which hundreds of watts of average power in a single mode have been achieved with efficiencies in excess of 10 percent. The output is in the far infrared at 10.6 microns, fortuitously in an atmospheric window. Mode-selecting techniques have been demonstrated that can tune the laser to discrete lines within the 9.2 to 9.8 μ and 10.2 to 10.8 μ bands. Because of the relatively longlifetimes, this system can also be Q-switched at high rates with large gains in peak-to-average powers, but at the expense of multi-mode operation. In principle, properly designed mode-selection techniques would solve this problem. The CO_2 laser is in a class called "molecular" lasers, an area that is receiving intensive study at the moment, and an area in which one can confidently expect rapid, even spectacular, developments in efficient lasers.

Another type of laser that is of great potential interest for satellite applications is the injection laser. Normally these are semiconductor junctions in which the recombination radiation produced by injecting current across the junction is used to produce lasing action in an optically resonant cavity. In general these devices are quite small, producing low peak powers, and many of them require low temperatures. However, they can be very efficient, on the order of 10 to 30 percent, which is of great importance in space applications. It is entirely possible that the total energies and powers required may be achieved in a suitably designed array of junctions.

For satellite applications, the possibilities of optically pumping laser materials using solar radiation is particularly attractive. This was recognized early in the course of laser R&D efforts, and a good deal

of development work has already been accomplished, principally by the following groups:

Electro-Optical Systems, Inc., Pasadena, Calif.

Radio Corporation of America, Camden, N.J.

American Optical Company, Southbridge, Mass.

It is expected that average output power on the order of 1 watt could be realized from Nd:YAG with a 30-cm diameter solar collector.

Substantial improvements in the performance of existing lasers are also to be expected in the near future. For instance, doping Nd-crystals with additional ions such as chromium has produced substantial improvements in efficiency by effectively broadening the useful absorption bands of the material, permitting better utilization of black-body pump radiation. Better quality crystals, more efficient and reliable flash lamps, and better coupling to the laser materials are all engineering developments that can be expected to further improve the picture.

IX NONRUBY LASERS

A. General

The possible utilization of laser wavelengths other than ruby would involve equipment performance tradeoffs as well as atmospheric-propagation considerations. If the choice is limited to laser sources capable of high peak output powers, three predominant selections are: neodymium-doped glass (1.06μ), the second harmonic of neodymium-glass (0.53μ) and the second harmonic of ruby (0.347μ). Some of the factors fundamental to system performance are depicted as a function of wavelength in Fig. IX-1. These factors are relative, and are normalized to the performance of a ruby lidar. Values of relative performance (K) greater than unity at a particular wavelength indicate improved overall system performance with respect to ruby; values of less than one indicate inferior system performance.

The curves of detector quantum efficiency for various photocathodes (Marked S-1, S-5, S-17, S-20) illustrate the marked variation in this parameter with changes in operating wavelength.

B. Internal Noise

An important consideration regarding the selection of a detector which is not shown in Fig. IX-1 is the internal noise levels of the various detectors. The internal noise level is a function of the type of cathode material, the cathode area, and the temperature. In general, detectors employing an S-20 photosurface tend to have internal noise levels 1 to 2 decades lower than tubes employing S-5 or S-17 photocathodes, and 3 to 4 decades lower noise level than S-1 photocathodes.

The curve of background noise power illustrates the marked decrease in this quantity (and hence an increase in system performance) as wavelength is increased above ruby. However, as wavelength is decreased below ruby (to 0.53μ for example) system performance is not markedly degraded.

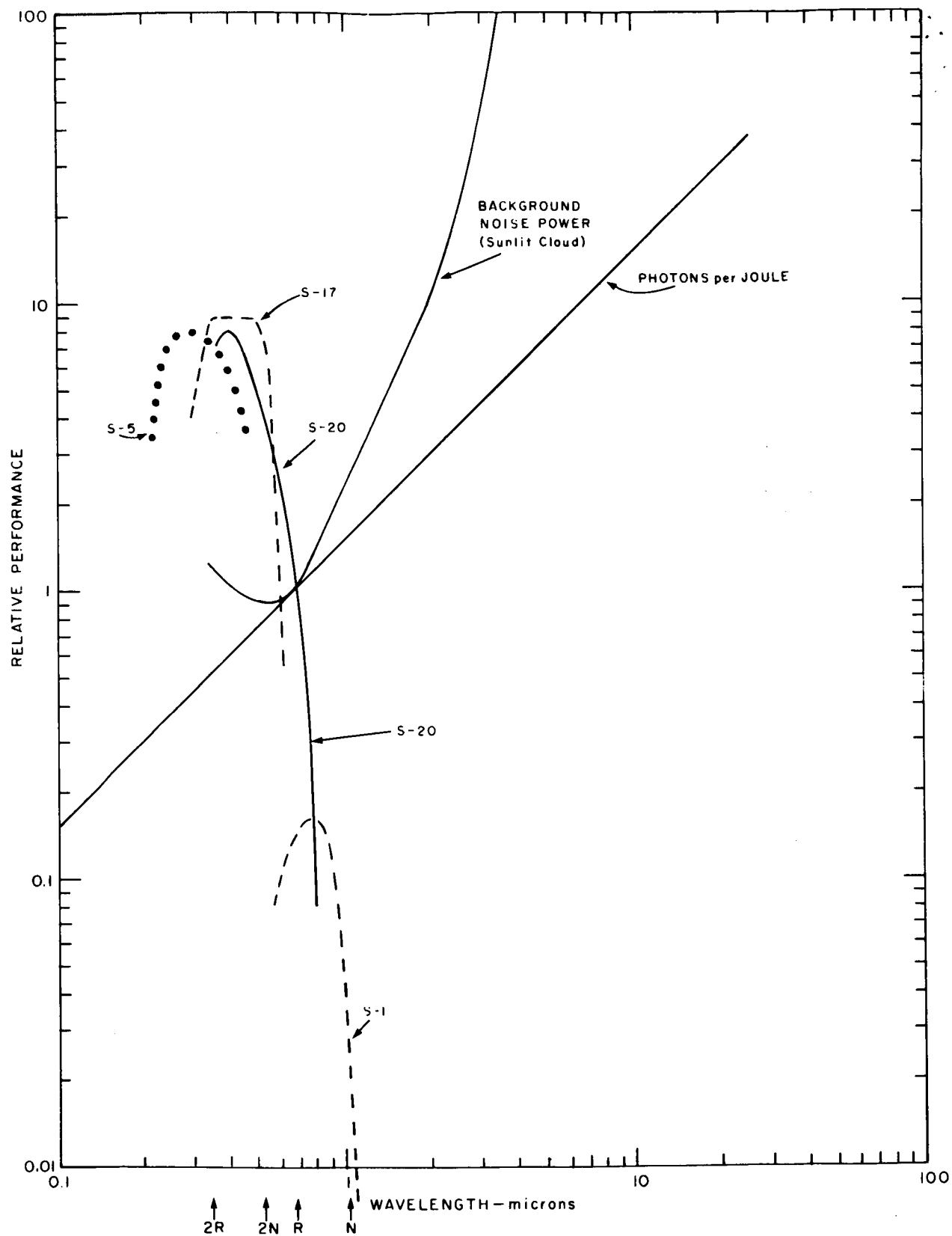


FIG. IX-1 LIDAR SYSTEM DESIGN FACTORS AS FUNCTIONS OF WAVELENGTH

The curve of photons per joule indicates the relative quantization or "granularity" of both signal and noise. This granularity affects the detection probability, since if more measurable events are received per integration period, the statistical basis for estimating true signal and background levels is improved.

It must be emphasized that in the absence of a detailed description of the two systems whose performance is to be compared, the use of Fig. IX-1 will yield only a general, qualitative answer. The reason for this lack of accuracy lies in the fact that the ultimate criterion of system performance is the maximization of detection probability. In order to make use of the detection criteria discussed in Sec. V, a knowledge of absolute value of received signal and background noise must be available; hence system parameters must be defined before a detailed comparison of system performance can proceed. For example, a qualitative comparison between ruby (6943\AA) and the second harmonic of neodymium (5300\AA) may be accomplished in the following way.

Assume a reference ruby system whose performance is such that 20 signal counts and 10 noise counts are produced in a particular range cell. Referring to Fig. V-9(a), for a false-alarm probability of 0.01, 20 signal counts and 10 noise counts will produce a detection probability between 0.95 and 0.99.

Further assume a 5300\AA system with a peak power output equal to the ruby system. Referring to Fig. IX-1, the quantum efficiency has increased by a factor of 4, the number of quanta per joule has decreased by 0.79, thus producing 63 signal counts in the particular range cell.

Regarding the background noise, Fig. IX-1 shows the 5300\AA system performance degraded by 0.9 (i.e. an increase of background noise of 1.11). The changes in quantum efficiency and the number of quanta per joule are 4 and 0.79 respectively, the number of noise counts in the particular range cell will be 35.

Referring again to Fig. V-9(a), 63 signal counts in the presence of 35 noise counts will produce a detection probability in excess of 0.9999.

However, the previous assumption of a second harmonic system with a peak power output equal to the ruby system infers a 100 percent conversion efficiency of the KDP second harmonic crystal. At present, a realistic conversion efficiency is about 15 percent. Taking into

account this loss inherent in producing the second harmonic would decrease the number of signal counts from 63 to 9.

The detection-probability curves of Fig. V-9(a) then show that 9 counts of signal in the presence of 63 counts of noise will produce a detection probability less than 0.6. Thus, for equivalent primary power input, the performance of the 5300Å ruby second-harmonic laser will be inferior to that of a 6943Å lidar of the same general design.

C. CO₂ Laser

The power levels, both pulsed and CW, which have recently been obtained from a CO₂ laser operating at 10.6μ suggest that a lidar operating at this wavelength may have some value, if certain equipment limitations can be overcome.

For example, output power levels of 100 to 300 watts are presently obtainable only with a continuous replacement of the gas mixture in the laser cavity. The operating lifetime of the laser is therefore presently limited by the volume of gas available.

Another problem which may limit the usefulness of a 10.6μ lidar in orbital applications is choice of available detectors. For wavelengths greater than approximately one micron, photoemissive detectors (such as photomultipliers) are no longer effective, and photoconductive detectors must be used. Typical detectors which are sensitive in the 10.6μ region include mercury-doped germanium and copper-doped germanium. The quantum efficiency of these detectors is very high, approaching unity; however, the internal noise of these detectors at 10.6μ is approximately 4 to 5 orders of magnitude greater than that of typical photo-emissive detectors operating in the visible portion of the spectrum. Additional complicating factors are that both detectors must be cooled to cryogenic temperatures; also, the speed of response of the mercury-doped germanium detector (approximately 1 μs) may be too slow for some lidar applications.

X USE OF SATELLITE-BORNE LASERS FOR PURPOSES OTHER THAN MEASURING NONRESONANT BACKSCATTER AS A FUNCTION OF RANGE

A. General

With increasing frequency, suggestions may be expected to appear in the literature for remote probing of various atmospheric parameters through the use of satellite-borne laser systems of much higher sophistication than would be required for the relatively simple task of measuring nonresonant backscatter as a function of range. It can certainly be argued that in contemplating the launching and powering of an active optical system, one should examine the incremental cost of having it perform as many functions as possible. On the other hand, any system purporting to provide information of meteorological utility must ultimately withstand the test of whether the data could be obtained more accurately or less expensively by other means, including pure prediction on the basis of past experience. There appears to be general agreement that this implies measurement precision on the order of 1 percent for pressure and density and of 1°K for temperature.

In this section two proposals, perhaps typical of others requiring relatively precise spectrographic techniques, are reviewed.

B. Multiple-Frequency Systems

The possible advantages of using more than a single transmission and reception wavelength have been pointed out by several authors. For pulsed systems, the achievement of harmonically related wavelengths is made relatively simple through the use of non-linear effects in certain crystals, such as KDP. Other wavelengths may be obtained with Raman-shifting materials at the laser output. A well-defined approach, employing frequencies relatively close to each other, has been proposed by White, Carrier, and Nugent (1965).

In their method, the required transmitter frequencies are obtained by Raman shifting. From there on, the signals are handled much as if there were two independent pulsed lidars.

One half of the system is intended to operate in the clear of any absorption lines, with the other half at the center of an isolated absorption line of the molecular species being sampled. The return from the selectively absorbed lidar will show greater attenuation than the lidar operating outside any region of selective absorption. A detailed analysis of the differences in attenuation will, in principle, give information as to the temperature and density of the gas as a function of altitude.

A fairly involved derivation is presented, which leads from the lidar equation for intensity versus range, through a variety of approximations, to a final result in the form

$$\frac{S(T)}{\sqrt{T}} = \frac{\pi\alpha K}{2K_{02}} \frac{d[\ln Y(x)]}{dx}$$

where $S(T)$ is the absorption-line strength as a function of absolute temperature T , $\pi\alpha K/2K_{02}$ is a constant which may be evaluated in the laboratory or calculated, and $d[\ln Y(x)]/dx$ is the derivative, with range, of the logarithm of the ratio of the lidar intensities at a given range. The intent is to obtain a measured number representing the right-hand side of the equation, and then to find the value of T which makes the left-hand side equal to that number (values of $S(T)/\sqrt{T}$ would be tabulated as a function of T in advance).

This apparently simple result hides a number of considerable difficulties. These arise from the nature of the approximations used in the derivation, certain physical problems not mentioned in the derivation, and instrumental difficulties. It should be remembered that these are problems in the face of measurements of very high precision (1 percent or 1°).

The approximations made in the derivation involve neglect of off-line absorption, variation of Rayleigh and Mie scattering cross sections and angular distributions over small wavelength intervals ($5\text{--}10\text{\AA}$), etc. These approximations are usually justifiable, but most of them are not necessarily true to better accuracy than 1 percent. Thus the composite result is, on these grounds, likely to be in error by at least 1% or more.

A potentially serious physical problem is that resulting from the shift of the line center with pressure; it appears that absorption lines both broaden in width and shift their centers proportionately with pressure; the center shift is thought to be about 75 percent of the line width at any pressure. Thus the wavelength of the line center will vary significantly with altitude, and a transmitted lidar pulse will not stay at the center of a line as it changes altitude (nears the earth from a satellite). This vitiates the result given above by invalidating certain steps in the derivation of that result.

It also appears that $S(T)$, which must be known in advance, is different in form for different molecules, and frequently may not be very strongly dependent on temperature. This implies that a small error in evaluation of the right-hand side of the equation above would lead to a larger error in determining the value of T corresponding to that evaluation (i.e., a 1 percent error in $d[\ln Y(x)]/dx$ could lead to about 5 percent error in T).

By far the greatest difficulty comes in implementing such a system for incorporation in a satellite. Since the demands for frequency measurement and control are of great (0.01\AA or better on the laser output at all times during output and for repeated shots), a much more sophisticated system than presently available is necessary. The demands for precision measurement of the returned signal are equally difficult to meet. In addition, the most careful laboratory determination must be made of several physical parameters entering into the final results. These instrumental difficulties are recognized by the authors of the suggested technique, but it is not clear that they will be overcome in the foreseeable future.

The measurements of density and pressure, in the proposed system, follow from the results of temperature measurements, and since further measurements and analysis must be accomplished to obtain these parameters, the same difficulties apply to these measurements.

In summary, it seems unlikely that any operationally meaningful system of this sort, with sufficient accuracy to be competitive with present measurement techniques, will be forthcoming within a reasonable period. Much additional work needs to be done experimentally to justify the method in principle before serious consideration for satellite operation appears warranted.

C. Raman-Scattering Measurements

For the atmospheric physicist or meteorologist, Raman scattering in the free atmosphere offers a potential for remote measurements of certain atmospheric parameters, particularly density and temperature; at least one proposal has been made for incorporating such a probe into a meteorological satellite (Cooney, 1965). In this section, a brief discussion is given concerning the nature of Raman scattering and the advisability of its use in a satellite system.

Raman scattering is differentiated from Rayleigh scattering by the fact that the wavelength of Raman-scattered radiation is different from the incident radiation wavelength. This shift or wavelength can be described from the point of view of a wave-molecule interaction or a particle (photon)-molecule interaction.

From a wave point of view, the shift is due to the mixing of the incoming wave (at a "carrier" frequency) with an oscillating change of polarizability of a molecule. For a molecule with constant polarizability, the scattered radiation is due to oscillations of polarization induced by the incoming wave. Simple molecules, however, have natural vibrational and rotational motions, whereby the polarizability is not constant, but varies slightly in an oscillatory fashion. The natural frequency of polarizability change mixes with the frequency of the incoming wave to produce a scattered wave with the "carrier" frequency and sum and

difference frequencies simultaneously placed on both sides of the carrier. The magnitude of the shift depends on the natural frequencies of the molecular oscillations.

From perhaps a simpler point of view, the shift may be pictured as particle-molecule interaction. On one hand, a photon may interact with a molecule, transferring to the molecule enough energy to raise it to an excited state. The photon then leaves with less energy. On the other hand, a photon may interact with a molecule already in an excited state, and the molecule may deliver energy to the photon. The molecule then drops to a lower state, and the photon leaves with increased energy. If the energy of the excited state is $E = h\nu_r$ then the two types of photons will have energy $E_0 \pm E$, and frequencies $\nu_0 \pm \nu_r$, where $E_0 = h\nu_0$ is the energy of the incoming photon. In general it will only be possible to excite one vibrational state or several rotational states, because of the limited energy of the photon and the decreasing probability of interaction with increasing energy. In this picture, Rayleigh scattering refers to elastic interaction, where the photon interacts but no energy transfer occurs.

By whichever picture one uses, Raman-scattered radiation consists of energy at a central frequency (that of the laser) and at frequencies symmetrically displaced on both sides of center. The relative intensity of the lines occurring to the side depends on the number of molecules found in an excited state, which in turn depends on local temperature. The absolute intensity of these lines depends on the molecule. For very symmetric molecules it is largest, and for complex molecules weak; in very few cases, however, does the intensity exceed 10^{-3} or 10^{-4} times the Rayleigh-scattered intensity. This difference of three or four orders of magnitude is a serious obstacle in the way of using the Raman effect for meteorological probing from a satellite.

The two most significant applications probably are measurements of density and temperature. Density would be measured by measuring the returned power and deducing the density from a known single-molecule cross section.

This is the same procedure as for an ordinary lidar sounding except that with sufficient care it would be possible to exclude the contribution of the aerosol component, since observations of the scattered component would be made at wavelengths where only a particular molecule would be capable of delivering energy. The "with sufficient care" reservation could be quite significant, however, since compensation would somehow have to be made for the one-way transmission losses through aerosol-laden air for the incident beam and then back over the same path at a different frequency.

Temperature measurements are proposed in terms of the relative intensities of the shifted lines on both sides of the carrier frequency.

The remote measurement of temperature, by methods other than inference from pressure and/or density measurements, is an attractive goal. In principle Raman scattering allows such a measurement. This method revolves about the measurement of the relative power of displaced lines on either side of the center frequency.

The relative intensity of these lines depends on the temperature, as described, since the number of molecules to be found in an excited state depends on the absolute temperature. The line at frequency $\nu + \nu_r$ will be due only to photons having interacted with an excited molecule. The line at $\nu - \nu_r$ is due to photons interacting with molecules in the ground state. The ratio of molecules in an excited state with excitation energy E_r to those in the ground state is

$$\frac{N_r}{N_o} = \left(\exp \frac{-E_r}{kT} \right) = \left(\frac{h\nu_r}{kT} \right)$$

(for nondegenerate excited states). T is the absolute temperature, k is the Boltzmann constant. This ratio is then the ratio of intensities for the two displaced lines, assuming the cross section for inverse reactions are equal.

$$T = \text{const} / \ln(I_1/I_2)$$

where I_1 is the intensity (power) of the longer-wavelength line and I_2 is the intensity of the shorter-wavelength line (integrated over a suitable number of rotational lines).

The error in such a measurement of T is found by differentiating the above expression on both sides and dividing by T . This fractional error has the form

$$dt/T = (dR/R)(1/\ln R)$$

where R is the ratio I_1/I_2 . This is close to saying that the fractional error in temperature measurement is equal to the fractional error in measurement of the intensity ratio.

Now if the intensity ratio can be measured to an accuracy of n percent, then the temperature accuracy is $2.73 \times n(^{\circ}\text{K})$, since one is talking about absolute temperature. Thus 10-percent intensity accuracy gives 27° temperature accuracy. The difficulties of making measurements accurate to better than 10 percent are obvious; what would be desirable, in fact, is measurements to less than 1-percent accuracy in ratio, allowing temperature measurements to within 2°K , to make the method competitive with current techniques. The difficulty of making good statistical measurements on small numbers of photons is compounded by the fact that the two lines being observed may be as much as 2000\AA apart, demanding careful calibration of sensitivities, etc.

The conclusion is again that a very large effort, in terms of equipment sophistication and power requirements, would be required to achieve useful results. The required transmitter power, even if it could be achieved, puts the system into the area where eye-damage considerations become important (see Sec. V-F-1) unless the beam is spread so much that finding a suitably cloud-free hole to fire through would become a problem.

Direct methods in common use measure densities (of the molecular component) with accuracies of about 1 percent to 10 km and 10 percent to 100 km. Ordinary lidar is potentially more accurate at high altitudes (perhaps 5 percent). At considerable cost a Raman lidar could single

out a particular type of molecule and map its density with altitude. This would be true only for N_2 and O_2 , however, since the densities of any other molecular species are simply too small for accurate detection (their returns would average perhaps 10^{-6} to 10^{-8} of Rayleigh returns).

Thus the possible usage for density measurement would appear to be limited to mapping of O_2 and N_2 densities with an overall accuracy of perhaps 5 percent at best.

The cost would be that of providing 1000 to 10,000 times as much transmitter power as would be required to make similar soundings of the combined aerosol-molecular backscatter.

Temperature measurements present the same limitations and problems, with the added requirement of greater precision in measurement of signal power to achieve the same accuracy (5 percent) in temperature determination.

D. Polarization Measurements

The fact that the output of a lidar system may readily be completely polarized, implies that perhaps new information could be drawn from polarization measurements, with little additional effort in system design.

In the simplest kind of scattering situation (e.g., scattering from water spheres or single atoms with isotropic polarizability) polarization is unchanged in scattering. For molecules or larger particles with anisotropic polarizability (or irregular shape), the direction of polarization is altered by the scattering process.

In lidar observations of molecular gases, one would see a continuous background cross-polarized component due to molecular depolarization. (For air, this cross-polarized component would always be about 3 percent of the ordinary component.) Superimposed on this would be any effects due to particulate matter with depolarizing effects. The quantitative measurement of this additional depolarization, however, cannot give information as to the type or number of particles responsible for it. Thus, the utility of the information made available is limited.

Essentially, the observation of cross-polarized components allows one to discriminate between water clouds with spherical droplets and dust or particulate aggregations, because of their different depolarizing capabilities.

The advantages of this discrimination, for a meteorological satellite, seem to be few. The particular applications one might consider would be discrimination between dust or cirrus clouds and spherical-droplet clouds, and discrimination against dust or water particles in the measurement of densities of molecular or particulate components of the atmosphere.

The SRI Mk II lidar was equipped for polarization measurements, but spurious signals (presumably resulting from internal reflections) have prevented effective use of this feature to date. To our knowledge no other experimental lidar program currently makes use of polarization, so that even the effects described above lack experimental verification. Until some more elaborate use is proposed and demonstrated, the principal value of a polarized receiver appears to lie in its ability to halve the background light power passed on to the photodetector.

XI COMPETING METHODS OF MEASURING CLOUD-TOP ALTITUDES

A technique has recently been devised for the determination of cloud-top altitude by measurements from a satellite of reflected solar radiation in and near the 7600⁰A band of oxygen (Saiedy, Hilleary, and Morgan, 1965; Wark and Mercer, 1965). The ratio of measurements can be used to describe the transmittance through the oxygen in the intervening sun-cloud-satellite path. Since the mass distribution of oxygen is known, the attenuation can be interpreted in terms of pressure at the reflecting surface. Even if errors in measurement and uncertainties in computations of oxygen transmission are tolerable, scattering and absorption in the cloud and their variations with cloud type and thickness introduce significant effects on the deduced geometrical top height. After a critical cloud thickness is exceeded, only very small changes in spectral albedo are associated with large additional penetrations through thicker clouds. More theoretical work is needed to reduce the uncertainty caused by penetration of each cloud type for arbitrary illumination and view angles, and by the effect of aerosols in the path above the cloud top. Since statistical information on temperature-height variation is available, it is not clear that the deduced cloud-top pressures from daytime oxygen transmission measurements will be significantly superior to the equivalent temperature-height deduced from an infrared-window measurement. For example, the standard deviation of temperature in the troposphere at 40°N in North America is only about 6°C in any given season, or the equivalent of about 1 km deviation in height.

The biggest difficulty in most of the remote-sensing techniques is the unknown effect of tenuous (usually subvisible) cirrus cloud. Here the lidar offers a distinct advantage in its capability for specifying top heights and thicknesses of all tenuous clouds, as well as heights and backscattering properties of other clouds.

XII CONCLUSIONS AND RECOMMENDATIONS

A. Conclusions

Present state-of-the-art limitations on power output will preclude high-resolution cloud mapping on a global basis by lidar alone. However, when used in conjunction with television or high-resolution infrared-imaging sensors, the unique and highly accurate ranging capability of the pulsed lidar would permit useful monitoring of the atmosphere--particularly of the high cloud cover--with a realizable number of soundings per orbit.

Of the numerous meteorological uses which have been suggested for a satellite-borne lidar, two stand out as being potentially capable of yielding data of very considerable operational and research significance within the practical bounds imposed by equipment which might be placed in orbit within the next few years with some reasonable expenditure of effort. These are:

- (1) To aid in the continuous monitoring of cirrus-cloud cover over the earth.
- (2) To assist the interpretation of infrared radiometry measurements from satellites--principally by resolving ambiguities in altitude of the targets and by providing measures of atmospheric transmission between the radiometer and the targets.

These two applications are related, in that cirrus-cloud cover presents one of the most troublesome sources of error in atmospheric radiometry.

Cirrus-cloud concentrations of meteorological interest, capable of introducing several degrees of error into radiometric determinations of temperature, can be so weak as to be characterized by optical backscatter cross sections only barely larger than those due to pure Rayleigh molecular backscattering at the elevations where cirrus is found (6 to 14 km). The sensitivity of the satellite-borne lidar should preferably be made great enough to permit reliable detection down to that level.

Achievement of the required order of performance appears barely possible using some extension of presently known pulsed ruby lidar techniques. Even so, the most useful performance will be achievable only at night when background light caused by reflected sunlight is at a minimum.

This limitation is not as serious as it might be since both high-resolution infrared and high-sensitivity (starlight-illumination) television are capable of providing the required companion pictures at night, and since major cirrus systems are normally large and persistent enough that nighttime-only sampling would still provide useful data. During daylight, the same lidar system would permit detection of returns from the earth itself or from the tops of large, relatively dense clouds. With experience, these additional data might be used effectively. Daylight performance equalling that described in this report for use at night is not completely beyond reason, but the considerable additional effort required does not appear warranted for an initial program.

Exclusive of the radiometric aspects, the principal projected uses for lidar monitoring of cirrus-cloud cover are extensions of techniques which have been developed by meteorologists over many years of using the attendant cloud distributions to infer the condition of large-scale circulation features such as extratropical cyclones, tropical cyclones (hurricanes and typhoons), pressure ridges and troughs, frontal systems, jet streams, air masses and, to a lesser extent, the tropopause and stratosphere. Acceptance of cirrus as a diagnostic tool has persisted in spite of the difficulty of observing it reliably from the ground, from aircraft, or from satellites. A satellite lidar could conceivably provide continuous quantitative measurement of cirrus extent and distribution for use both by human analysts and in numerical models.

A fully operational lidar should be capable of achieving complete coverage by scanning over the full width of each subsatellite swath with a sampling density on the order of one sounding per degree of latitude and longitude. The utility of the concepts involved could be demonstrated, however, with an appreciably simpler system viewing at the nadir, making

soundings approximately once every 60 nautical miles, and carefully correlated with concurrent data from other sensors.

A pulsed ruby lidar capable of radiating one joule per pulse and having an effective receiving aperture of at least one square meter would be required to yield meteorologically useful soundings of simple back-scatter as a function of range from a 1000 km orbit. The minimum pulse rate which should be considered for a full-coverage (scanning) system is approximately two per second and for a bare-minimum, downward-looking system approximately one every 18 seconds. The equipment requirements for all other applications considered--including principally the measurement of gaseous temperature, density, or composition by spectroscopic means--call for orders of magnitude more power and/or receiving area, and for much more stability and calibration. While there is no denying that the desire for remote measurement of temperature and density remains at or near the top of the meteorological "wish" list, competitive employment of satellite lidar for such applications must be considered only as an extremely remote possibility, at least until the practicability of the simpler cloud-monitoring system has been demonstrated.

B. Recommendations

Current lidar technology appears capable of equipping a meteorological satellite with the ability to make at least a few soundings per orbit of cloud densities and altitudes. Such soundings are useful for both operations and research and are very difficult to obtain by any other means. The prospects are good that improved laser efficiencies, output powers, and reliabilities will permit better coverage and more sophisticated measurements to be made in the future. It therefore seems desirable to begin serious planning toward a meteorological satellite lidar, having a minimum capability of ranging on cirrus clouds.

The project seems well adapted to a stepwise development sequence involving, first, the obtaining of additional design data via measurements from ground-based lidars; second, selective sounding of high cloud from above by a relatively simple lidar carried in a high-altitude

aircraft; third, operation of basically similar equipment from a manned satellite; and fourth, incorporation of scanning and nonscanning systems into unmanned satellites.

To realize such a program, the following problems need early attention:

- (1) Refined data are required on the volume backscatter coefficients of real cirrus clouds and how they correlate with weather, with radiometric data, and with the traditional means of observing clouds, i.e. physical measurements and optical visibility. Particularly important is a specification of the allowable measurement errors for various potential applications.
- (2) Means should be sought for achieving a minimum of something like two soundings per second from orbit. Unless one is willing to tolerate staggering problems of primary power supply and removal of excess heat, this will call for significant improvements in laser efficiency.

One possibility here is to investigate the use of high-PRF, Doppler, or even CW systems, since these systems in general tend toward higher transmitter efficiency than is obtained with present Q-switched ruby systems.

- (3) Methods should be investigated for constructing satellite-borne optical receivers having exceptionally large collecting apertures ($>10\text{m}^2$) but with only very modest angular resolution. These receivers should be capable of being scanned over relatively wide angles (approximately $\pm 50^\circ$).

One approach would be to track together an array of many smaller mirrors.

- (4) Techniques need to be developed for on-board processing and temporary storage of the return-signal characteristic of pulsed lidars, which has a very large amplitude range. Photoelectron-counting methods are applicable at the low end of the range and very fast analog-to-digital converters with logarithmic input response might be used at the upper end. In the middle or transition region no satisfactory method of data recording is known to the authors. A single unified approach, useful over the whole range, would of course be preferable and should be sought.

Appendix

NATURE AND DISTRIBUTION OF CIRRUS CLOUD

Appendix

NATURE AND DISTRIBUTION OF CIRRUS CLOUD

A. Introduction

This section provides a brief account of the nature and distribution of cirrus cloud with special reference to its potential detection by satellite-borne lidar. The material has been condensed from a much more comprehensive but as yet unpublished study prepared under this contract.

Of the numerous references used in compiling the data herein, attention is drawn particularly to Stone (1957) and Borovikov (1961). These publications, in themselves, represent surveys of the literature on cirrus clouds and provide a convenient and comprehensive background to the study of the physical aspects of cirrus cloud.

B. Structure and Distribution of Cirriform Clouds

All of the rationales and models of cirriform cloud distribution to date recognize three genera: cirrus (thin, irregular, and wispy); cirrocumulus (thin or thick, of marked configuration such as scaly ripples or flakes); cirrostratus (thin or thick, rather uniform and sheet-like). These three genera may appear simultaneously or individually. Cirrus is often present in layers and in various configurations such as long parallel bands, stripes, streaks, or cross-bandings. Certain meteorological significance is attached to these conditions, primarily in the realm of formative processes and/or wind effects. For example, layering signifies the presence of stratified "stable" zones in the free atmosphere in which moisture is trapped; parallel bands are ascribed to certain wave motions and wind shear conditions; and cross-bandings reveal areas of changing winds and "unstable" atmospheric conditions.

The physical constituents of these clouds vary from super-cooled water droplets to ice, with various mixtures in between (however, many

cloud physicists define cirrus as a pure ice-crystal cloud). In addition, the microstructure of cirrus clouds varies markedly in the type of crystals that compose them and there is some evidence of a relationship between the form of the cirriform clouds, their microphysics, and the synoptic condition involved.

The water content in cirriform clouds is small but opinions on its magnitude differ. Stone states that:

"The concentration of cirrus particles is very much smaller than for droplets in water clouds--Weickmann estimates 170,000 to 500,000 crystals per cubic meter. The equivalent water content is correspondingly low (0.1 g/m^3) for 'pure cirrus,' 0.4 for cirrostratus."

Borovikov indicates somewhat lower values of water content:

"Auf'm Kampe attempted to calculate the water content of cirrus clouds from Trabert's formula assuming a visibility of 2000m and crystal size of 200μ in length and 20μ in diameter (which should, in his view, correspond to droplets with $r = 20\mu$). The calculation yielded a water content of 0.03 g/m^3 , a figure which is probably closer to reality...

"According to the measurements of V. E. Minervin, in crystal alto-stratus clouds the water content was often as low as $0.002\text{--}0.003 \text{ g/m}^3$. It is hardly likely that in the optically far less dense cirrus clouds the water content could be higher than this figure."

To date, data of this nature are not ordinarily available to the meteorologist and, consequently this type of information is generally not considered in practice.

Numerous studies have shown that the altitude of cirrus varies with latitude. In the polar regions, the bases are usually found near the 6 to 8 km level and the tops near 9 km; in the tropics the bases lie at about 11 km and the tops near 15 km. On some occasions the bases may lie as high as 17 to 20 km.

A summation of the data on cirrus cloud altitudes is given in Table A-1:

Table A-1
CIRRUS CLOUD ALTITUDES AT CERTAIN GEOGRAPHICAL LOCATIONS
(After Borovikov)

Point	Latitude	Altitude of Ci-Cs (km)	
		average	maximum
Bossekop (Northern Norway)	70°N	7.3	
Pavlovsk (USSR)-Uppsala (Sweden)	60	7.6	
Potsdam (West Germany)-Trappe (France)	51	8.7	12.67
Blue Hill-Washington (USA)	40	10.15	15.01
Mera (Japan)	35	11.02	16.79
Manila (Philippines)	14	12.05	20.45
Jakarta (Indonesia)	6°S	11.04	18.60

Borovikov also presents data on the seasonal change of altitude of cirrus clouds, shown in Fig. A-1. Although cirrus altitude increases in summer, the seasonal variation is small. The higher altitudes of the cirrus-cloud bases are just slightly lower than the mean altitude of the tropopause. Some cirriform cloudiness has been found in the lower stratosphere but it can be considered rare.

In thickness, the majority of cirriform cloudiness varies from a few meters to 6 km. This is demonstrated in the various graphs of Fig. A-2. The majority of the cirrus, however, is less than 2 km thick and much is quite thin.

Of interest is the fact that vertical visibility through cirrus is in general not uniquely related to vertical dimension. Some

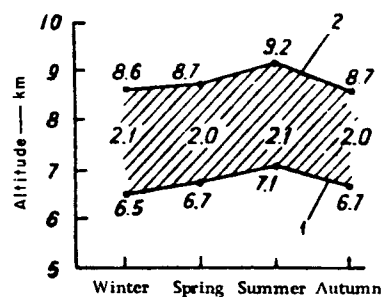
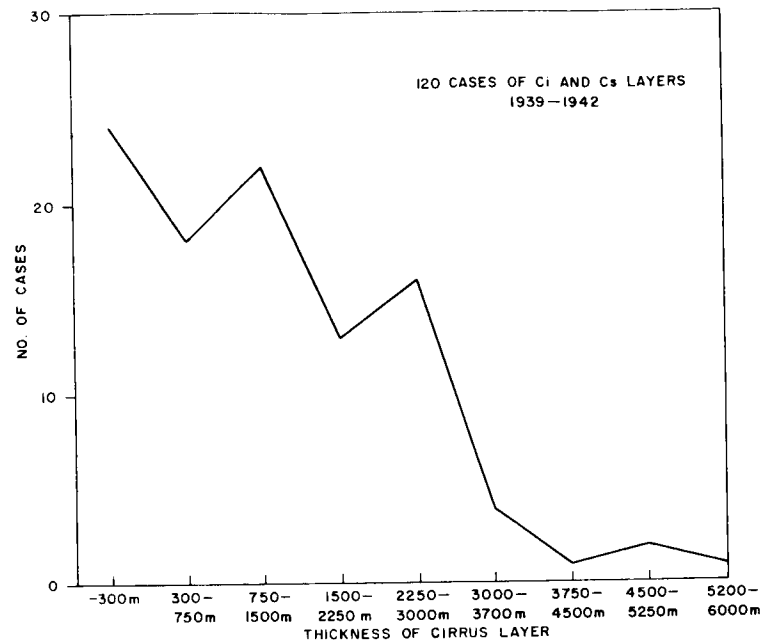
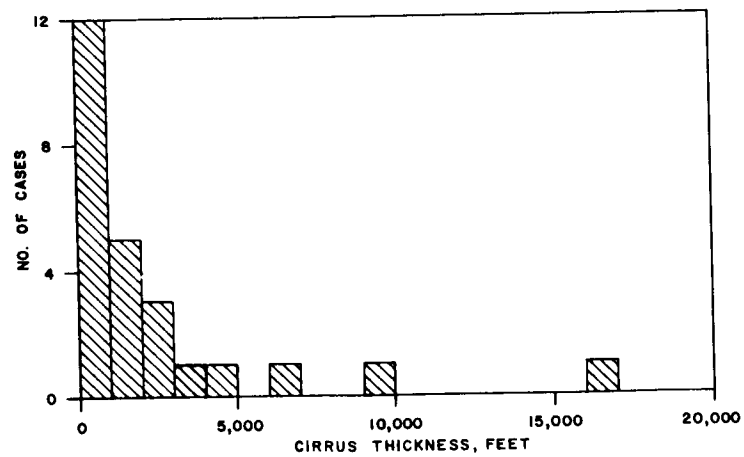


FIG. A-1 AVERAGE ALTITUDES
OF BASE AND SUMMIT



(a) Frequency Distribution of Thicknesses of Individual Cirrus Layers Observed on Research Flights from Ainring, Bavaria, 1939-42



(b) Frequency of Cirrus Thicknesses Observed on Project Wiback B-47 Flights over the United States, Winter-Spring 1951; Tabulated by 1000 ft Intervals

FIG. A-2 GRAPHS OF CIRRUS THICKNESS

dimensionally thick clouds may be more transparent than dimensionally thin but denser cloud. Kadlec reports:

"This overcast cirrus usually occurs in a layer from 4,000 to 6,000 feet thick but occasionally as much as 15,000 feet thick. It is called 'thin' because it allows vertical visibility through the layer."

It has been noted that the vertical visibility through cirrus is often quite good (ground visible) at the same time that horizontal visibility in cloud is less than a mile, even in cases when the cirrus is of considerable vertical extent.

In area, cirriform cloudiness is extremely varied. Figure A-3 gives an estimate of the length of the east-west (L_x) and north-south (L_y) components of the areas within which upper-level cloudiness can occur in the case of moderately to fully developed cyclones (tropical and extratropical) and jet streams. With respect to cyclone-generated cirrus the components were obtained from an examination of a large number of gridded TIROS photographs of cloud vortex patterns (Wiegman, et al), and define approximately the latitude-longitude boxes that enclose the major upper cloudiness. Data on jet-stream-generated cirrus were

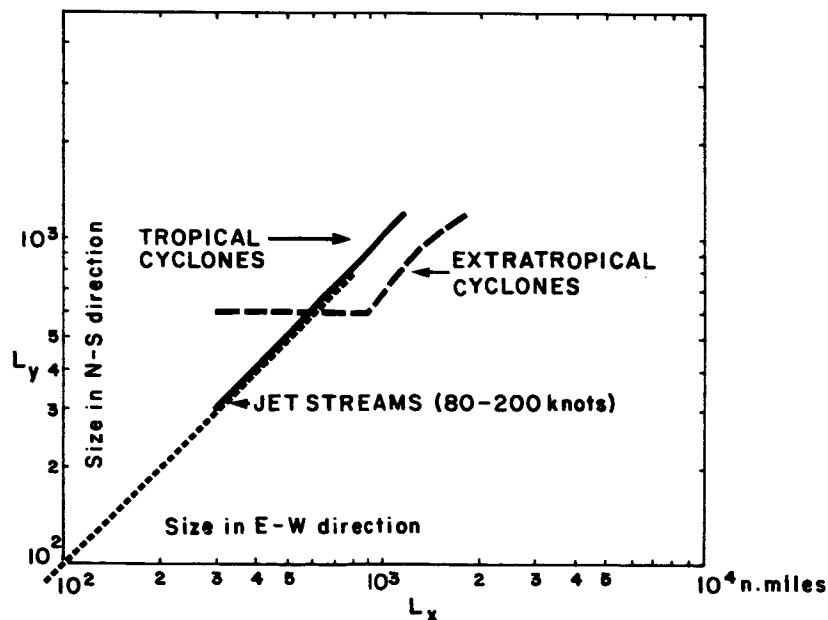


FIG. A-3 SIZE ESTIMATE OF AREAS OF UPPER CLOUDINESS

estimated by using a relationship between maximum wind speed and jet-stream width to define an area over which cirrus can be anticipated.

Figure A-3 shows that in the region of tropical cyclones (0° to 30°N), major cirrus can be expected to cover areas ranging in size from 300×300 nmi ($5^{\circ} \times 5^{\circ}$ latitude) to about 1200×1200 nmi ($20^{\circ} \times 20^{\circ}$ latitude). In the region of extratropical cyclones (30°N to 70°N) where large-scale cirrus can be expected most frequently, the areas covered by upper cloudiness can be elongated in either the north-south or the east-west direction. The more fully developed systems, however, appear to cover areas that are larger in the east-west than in the north-south direction. In general, dimensions range from $L_y = 600$ nmi and $L_x = 300$ nmi to $L_y = 1200$ nmi and $L_x = 1800$ nmi for moderately and fully developed extratropical cyclones, respectively.

The spatial components of areas connected with jet-stream cirrus where the jet stream is oriented southwest-northeast range mostly from 80×80 nmi to 850×850 nmi or more. These values, on the average, are smaller than those connected with cyclone-generated cirrus. Where the jet stream is oriented zonally (west-east) the cirrus areas may range from 120 to 1200 nmi in the north-south direction and may extend for several thousand miles in the east-west direction. These higher values are not common, however.

In the case of cirrus streaming from the top of a cumulonimbus cloud, the area is often about 10 miles wide and 50 to 80 miles long.

Borovikov presents data to show that frontal cirrus encompasses an area in excess of 60×600 nmi (see Table A-2). Along the front these clouds may extend for its entire length.

These dimensions are important since they specify the size of the areas over which detailed observations of cirrus from a satellite platform may be of interest.

Since high clouds have not been studied in situ until comparatively recent years, information on physical characteristics, conditions of formation, and climatology is somewhat incomplete, particularly the

Table A-2
PERCENT FREQUENCY OF DIFFERENT HORIZONTAL SPREADS
OF MASSES OF FRONTAL Ci-Cs
(After Borovikov)

Frontal type	Spread of Cloud Along Normal to Front (km)						Number of cases
	<200	201-400	401-600	601-800	801-1000	>1000	
Warm		15	49	31	5		98
Cold	26	59	15				118
Occluded	16	31	38	16			32

climatology. By and large, the most significant amounts of cirrus are associated with cyclones, fronts, squall lines, ridges, and jet streams. A reasonable, though approximate, climatology of cirrus can be inferred from the climatology of these systems. An example is shown in Table A-3.

Table A-3
PERCENT FREQUENCY OF Ci-Cs AS A FUNCTION OF SYNOPTIC SITUATION
(After Borovikov)

	Synoptic Situation						
	Uniform Air Mass		Front				Central Region of Cyclone
	Warm	Cold	Warm	Cold	Occluded	quasista- tionary	
Frequency	43.0	25.7	85.9	79.8	82.4	100	100
Number of cases	97	97	78	84	34	17	14
Average frequency	34.4		89.6				

Since cirrus is formed by both advective and convective processes,* it probably has the highest frequency of occurrence in the areas of the world most favorable to cyclonic circulations, such as the Central United States, Icelandic low regions, Aleutian low regions, and Central Russia.

* Cirrus may also form by nonadiabatic processes, but when and where this occurs is indeterminate.

The subtropical latitudes, particularly in the areas of the subtropical jet stream, are favored regions for the production of cirrus. Cirrus formations are plentiful within the equatorial convergence zone.

It is believed that a realistic picture of the frequency of occurrence of extensive cirrus can also be obtained by charting the frequency of occurrence of the systems that produce most of the cirrus. Assuming that tropical and extratropical cyclone systems generate cirrus with a probability of 100 percent (Borovikov, 1961), the frequency of occurrence of these systems in space and time must closely portray the frequency of occurrence of cirrus. Jet-stream systems are also important cirrus-generating systems. However, there is evidence that less than 50 percent of observed jet streams are associated with significant cirrus (Sawyer and Ilett). Admittedly, such approximations tend to underestimate the real frequency distribution, especially in the tropics, since certainly more cyclones occur than are observed. Furthermore, no account is taken of the "drift" of cirrus away from its parent system and the generation of cirrus by isolated thunderstorms.

In Fig. A-4, percentage frequencies are given around the latitude belt 0° to 30°N and 50° to 70°N for extratropical cyclones and jet streams. ["Jet stream" is defined as approximately straight flow with a maximum wind speed (observed or geostrophic) greater than 30m/s at 300 mb.] The frequencies shown should be representative, since the jet-stream patterns for both summer and winter periods were similar to known climatological patterns.

Although these frequencies of occurrence for the three major cirrus-generating systems (tropical cyclones, extratropical cyclones and jet streams) were derived from data that differ in spatial and temporal detail, they are believed to be reasonable estimates of the average occurrence of extensive cirrus cloudiness in the northern hemisphere.

Table A-4, which summarizes Fig. A-4, presents averages around the latitude of belts of the frequency of occurrence of days with jet streams and cyclones for summer and winter.

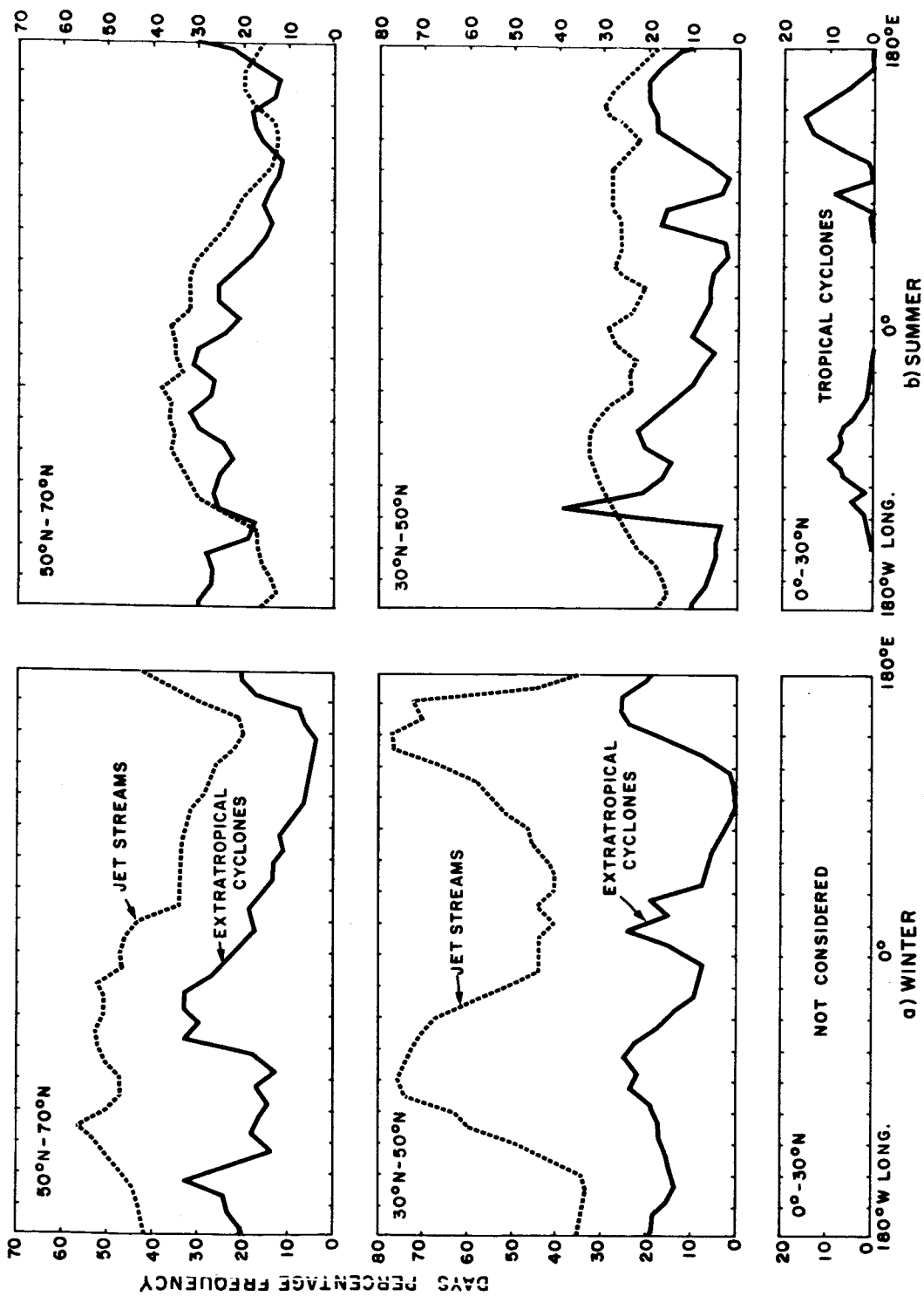


FIG. A-4 . ESTIMATE OF FREQUENCY OF DAYS WITH MAJOR CIRRUS-PRODUCING SYSTEMS

Table A-4
PERCENT FREQUENCY OF JET-STREAM AND CYCLONE DAYS
FOR ANY 10° INCREMENT OF LONGITUDE
IN THE NORTHERN HEMISPHERE

	Summer		Winter	
	30°-50°N	50°-70°N	30°-50°N	50°-70°N
Jet Streams	27	26	55	43
Cyclones	12	23	15	18

Except for the latitude belt 50° to 70°N in summer, there are more than twice as many days with 300 mb wind speed greater than 30m/s than there are days with cyclones.

Under the assumption that (1) 50 percent of the jet-stream cases and all of the extratropical and tropical cyclone cases generate major cirrus cloudiness, and that (2) some days with jet-stream-generated cirrus do not coincide with days of cyclone-generated cirrus, the longitudinal variations of the frequency of days that large-scale cirrus can be anticipated is shown in Fig. A-5.

The distribution of cirrus can be summarized by outlining on a northern hemispheric map various categories of the frequency of occurrence of days when large-scale cirrus can be anticipated in summer and winter. Figure A-6 presents such a summary.

Figure A-6 shows that during the winter, frequency variations with longitude are large. Between 50° and 70°N, a relative minimum in the frequency (less than 20 percent) is found over Siberia and a relative maximum (50 to 60 percent) over the northern Atlantic. A secondary maximum is present over the northern Pacific Ocean. In the latitude belt 30° to 50°N, a relative minimum (less than 30 percent) in the frequency of occurrence of days with large-scale cirrus can be anticipated over China, and relative maxima (60 percent) over eastern Japan and the eastern United States.

During summer the longitudinal gradient of the frequency is less than during winter. The general locations of relative maxima and

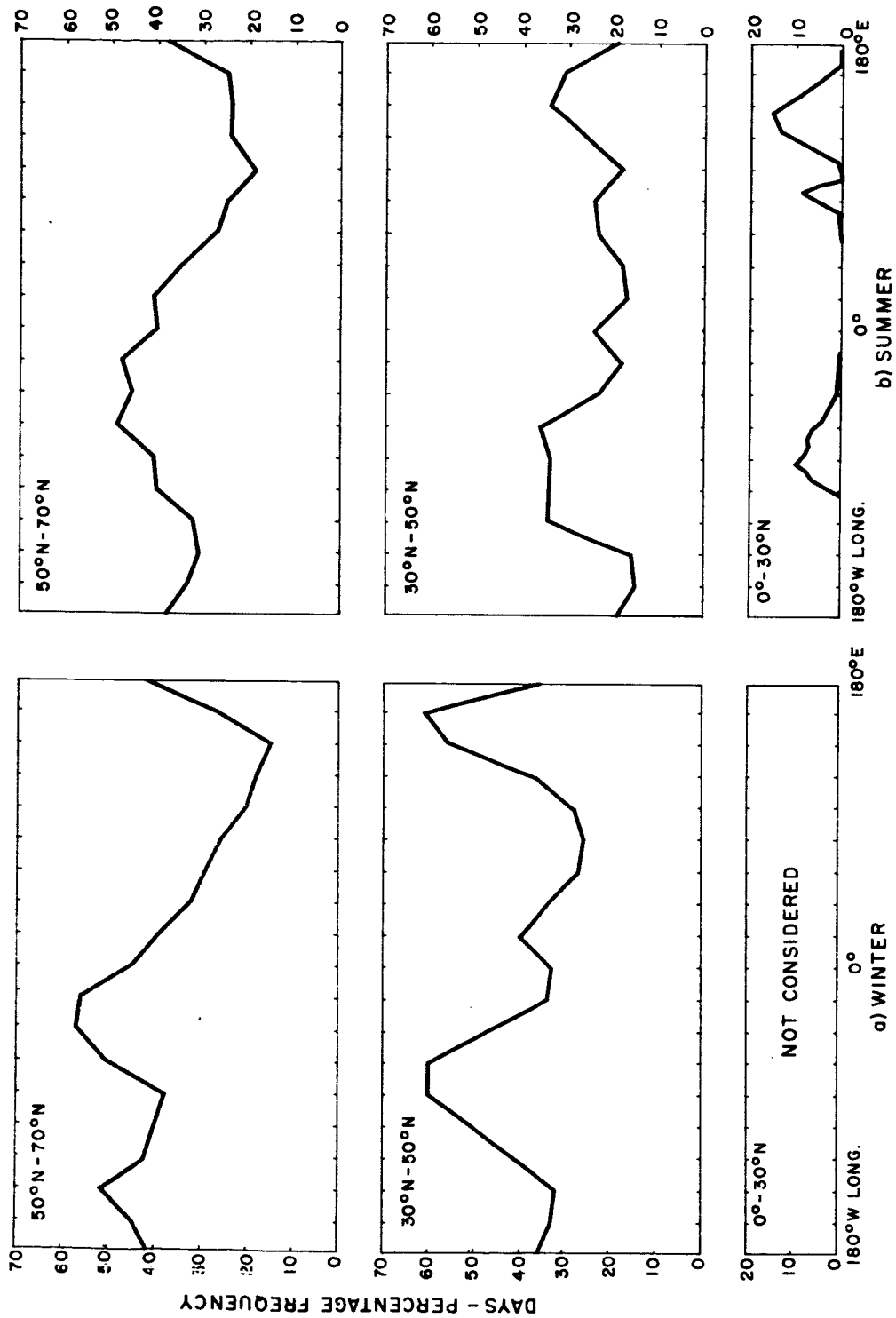


FIG. A-5 ESTIMATE OF FREQUENCY OF DAYS WHEN MAJOR CIRRUS CLOUDINESS CAN BE ANTICIPATED

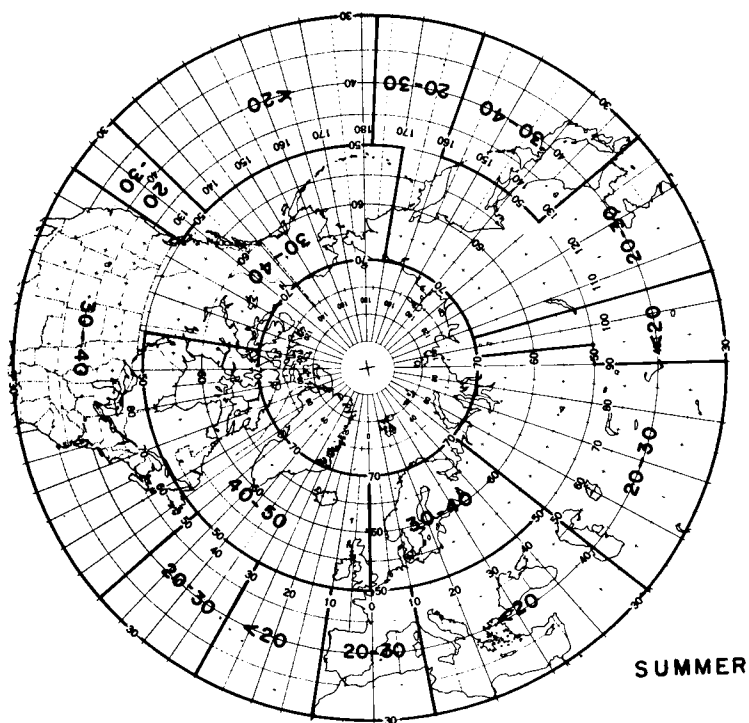
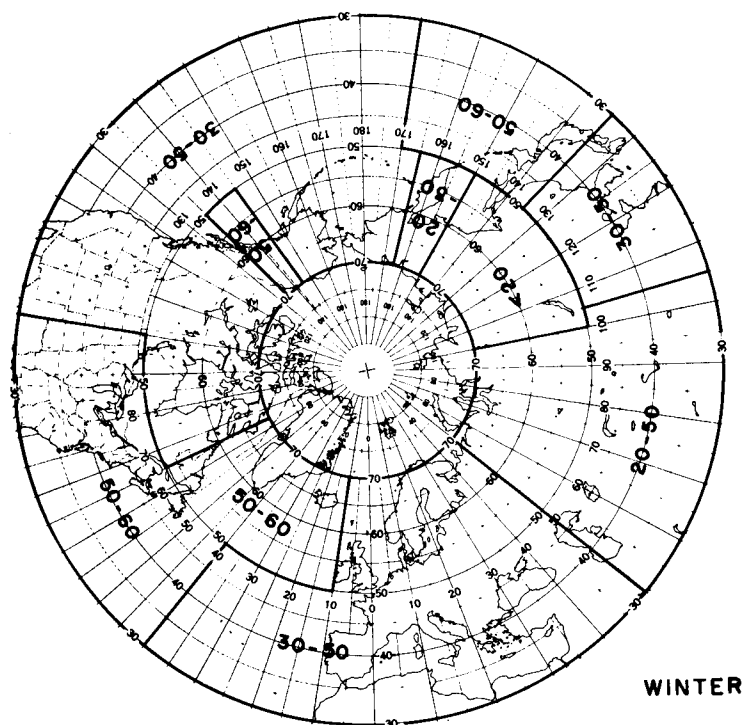


FIG. A-6 DISTRIBUTION OF PERCENTAGE FREQUENCY
OF LARGE-SCALE CIRRUS

minima, however, does not change much. Only in the northern Pacific Ocean, between 50° and 70°N , is the wintertime maximum replaced by a secondary minimum. Siberia still shows a pronounced minimum (20 percent) and the northern Atlantic still shows a pronounced maximum (50 percent). Between 30° and 50°N , relative maxima (30 to 40 percent) are found again over Japan and the United States. In the tropics, areas where large-scale cirrus can be anticipated coincide with the well-known areas of tropical storm and hurricane (typhoon) activity. The frequency of occurrence is well below 20 percent.

Because of the large variation in percentage frequency with season and with longitude for each season shown in Fig. A-6, a programmed operation of a satellite-borne lidar may be preferable to an automatic operation on a routine basis.

C. Cirrus Coverage Related to Synoptic Pattern

It is from the association of cirrus with synoptic patterns that the meteorologist derives his estimate of the significance of cirrus. With reference to circulation features, cirrus systems are associated with extratropical cyclones, frontal systems, and tropical cyclones (hurricanes). In regard to the latter, cirrus has been used as evidence of the development state, with absence of cirrus indicating decay of the storm. Cirrus occurrence is also intimately associated with the jet stream, both polar and subtropical, being found generally on the warm or high-pressure side of the jet stream and parallel to it; in pattern it may occur in sheets, bands or transverse waves. In the mid-latitudes cirrus is particularly prevalent on the east side of the low-pressure trough up to the center line of the downstream high-pressure ridge, but in the subtropics the cirrus will often extend throughout the ridge configuration.

The satellite gives the meteorologist the opportunity to view the broad-scale distribution of clouds with these synoptic patterns, but at the same time forces him to change his frame of reference with respect to cloud characteristics. Illustrations of this broad-scale

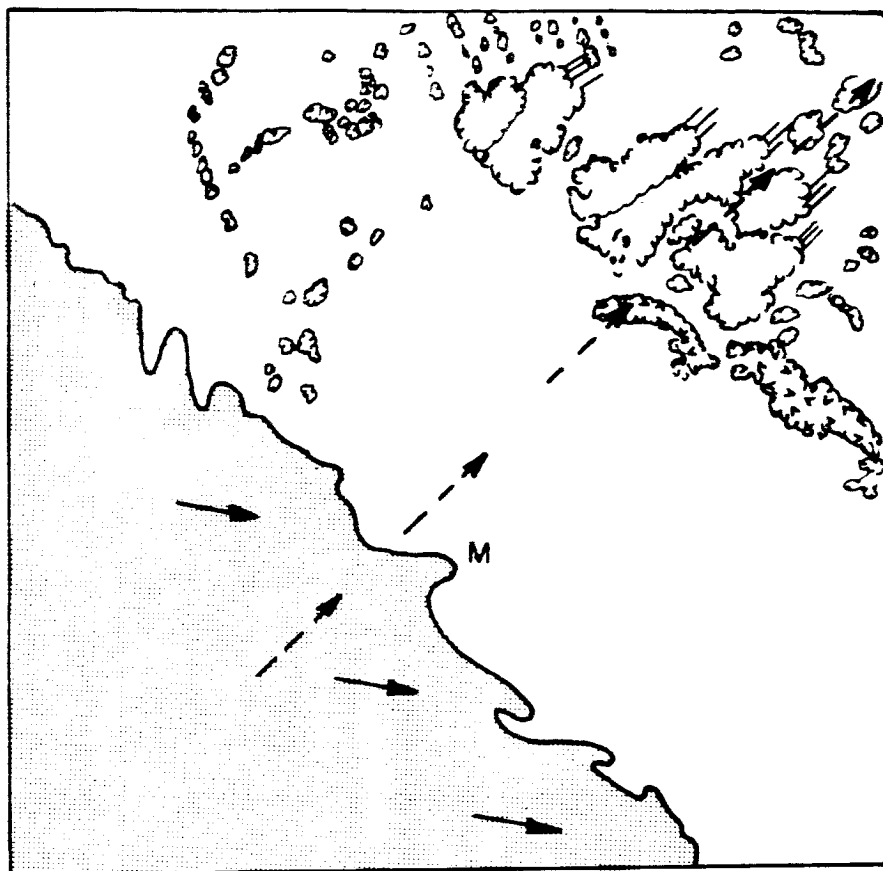
cirrus distribution with selected synoptic patterns are shown in the following examples.


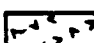




Figure A-7 is a view of a mature extratropical cyclone-cloud vortex, located approximately 200 nmi south of Adak, Aleutian Islands. The extent of the cirrus-cloud cover through the northwest and northeast sectors of the cyclone is approximately 400 nmi. This includes the cirrus cloud on the outer fringes of the storm, as well as that over the bright frontal-cloud spiral nearer the center of the frame.

Note the medium-grey, veil-like appearance of the cirrus. Low underlying clouds are visible through the thinner or more transparent cirrus clouds on the outer edge of the cyclone. Over the frontal arm of the cyclone, where the cloud spiral appears as grey-white, a positive identification of cirrus is more difficult. In this area of a cyclone, cirrus clouds usually overlies altostratus clouds.

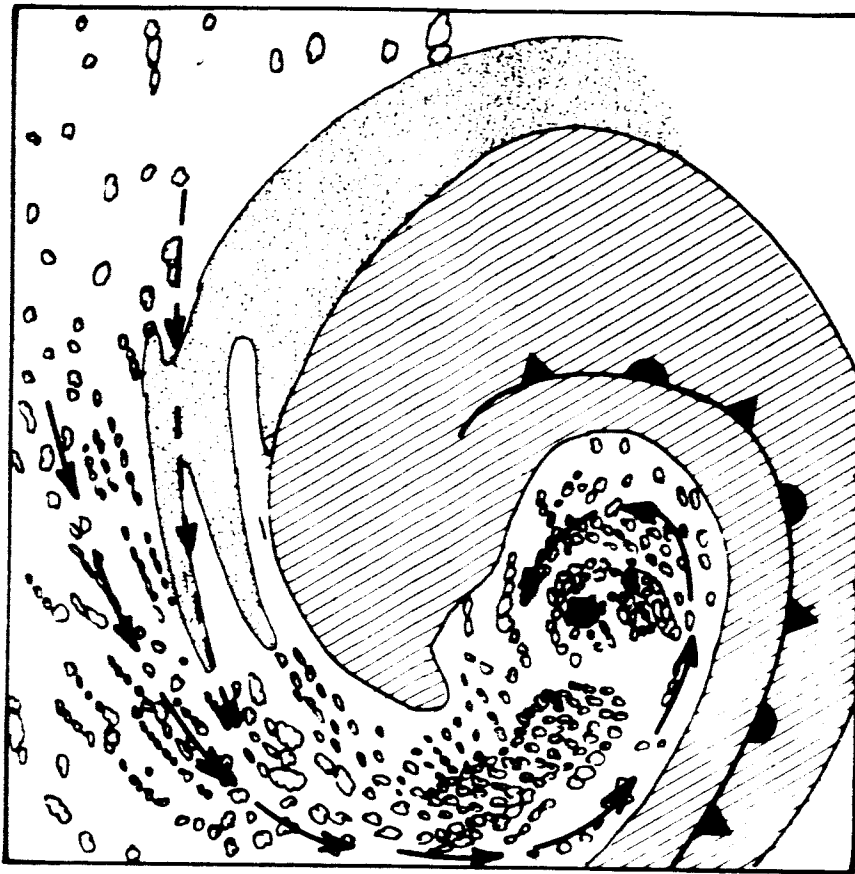
Figure A-8 is a mosaic of 4 frames showing a cirrus-cloud system accompanying a polar jet stream, located over the Sea of Okhotsk. Lower clouds are visible beneath the cirrus. The thin stripes in the cirrus are oriented parallel to the jet-stream flow, which is centered through the center of the frames. The width of the band is about 200 nmi (370 km) and the length is 1465 nmi (2700 km). Note that the cirrus is formed in very narrow stripes, parallel to the main flow, quite fibrous, with a well-marked leading edge of the system (center of frames).

Radiosonde plots for stations 32150, 47412, 47582, and 47646 indicate a double tropopause near the 200 mb level (40,000) and again near the 100 mb level (53,000 ft), characteristic of stations on the high-pressure side of the polar jet stream. The strong wind speeds on 47412 would suggest that this station is closest to the center of the jet stream. The sounding at 32150 shows strong stability, possibly the tropopause, beginning at the 300 mb level (30,000 ft). The configuration of this sounding is typical of those through the northern or low-pressure side of the jet stream. Unfortunately, there is only one low-level wind to substantiate this.



-  CUMULONIMBUS WITH CIRRUS STREAMERS
-  SNOW COVER ON SIERRA NEVADAS
-  COASTAL STRATUS
-  CUMULUS OVER TERRAIN
-  LOW LEVEL WIND FLOW
-  UPPER LEVEL WIND FLOW
- M** MONTEREY BAY

OVERLAY
ON
1518



VORTEX CENTER



FRONTAL BAND (Middle and High Clouds)



CUMULIFORM CLOUDS (Cells) IN COLD AIR MASS



CIRRUS SHIELD



UPPER LEVEL WIND FLOW



LOW LEVEL WIND FLOW

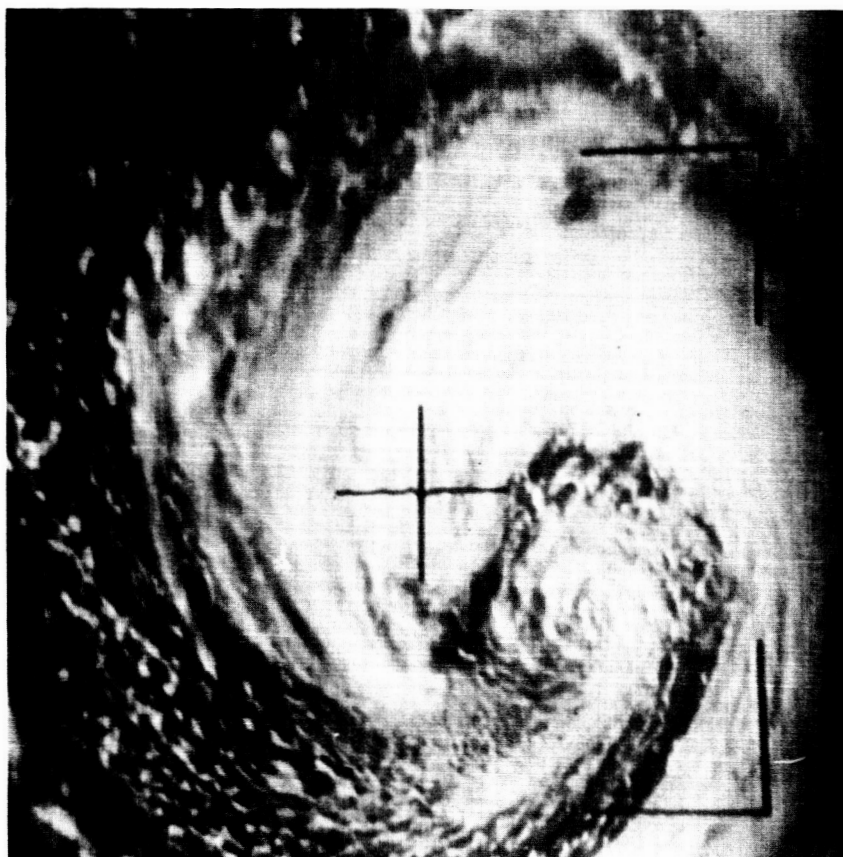


OCCCLUDED FRONT

OVERLAY
ON
153

TIROS VII ORBIT 3312/3306T, FRAME 28 0136GMT 29 JANUARY 1964

WIDE ANGLE LENS



SCALE: 1 in. \approx 190 nm near mid-frame

FIG. A-7 EXTRATROPICAL CYCLONE CLOUD SYSTEM

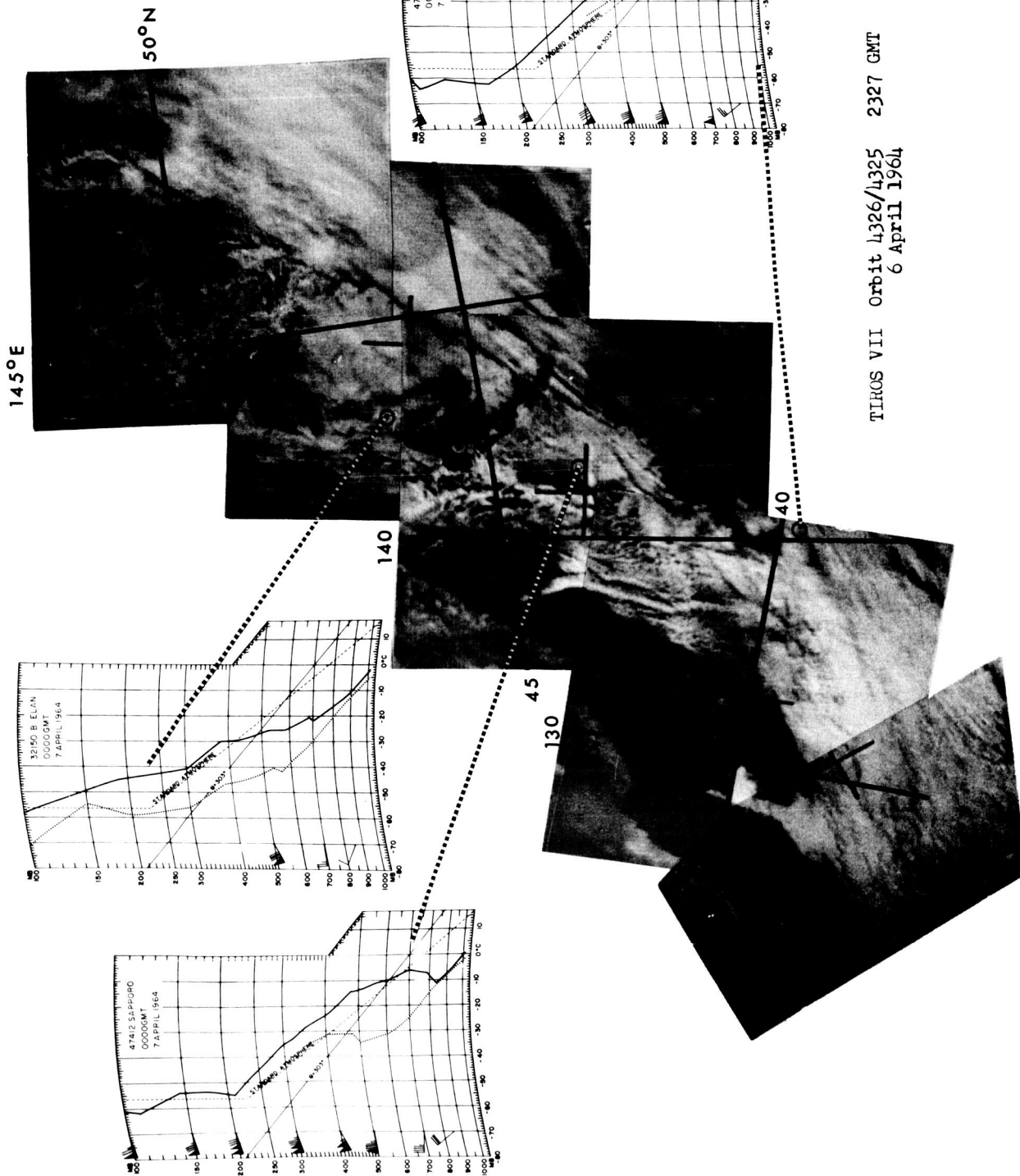


FIG. A-8 POLAR FRONT JET-STREAM CLOUD SYSTEM

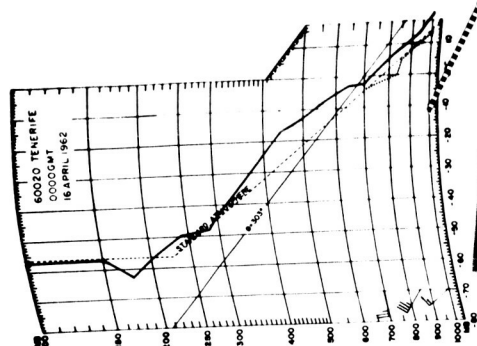
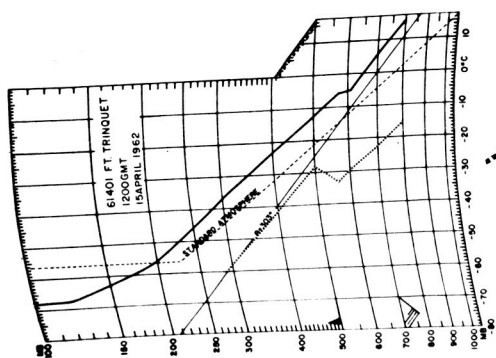
An example of subtropical jet-stream cirrus is shown in Fig. A-9, which presents two frames (24 hours apart) showing a cirrus-cloud system accompanying the subtropical jet stream off West Africa. In the left-hand frame the visible jet-stream cirrus is approximately 100 nmi wide. The length of this band cannot be measured due to the orbital limits; however, it is at least 600 nmi. It crosses the Atlantic coast of Africa at approximately 24°N and is oriented southwest-northeast. Note the small-scale transverse waves along the major axis.

In the right-hand frame the cirrus band in the intervening 24 hours has moved south, crossing the African coast near Cap Blanc. Its appearance has changed substantially. The transverse bands are obscured or obliterated, and seem to have concentrated in narrow stripes (less than 60 miles wide). The orientation has remained about the same with the extent of the cirrus exceeding 500 nmi.

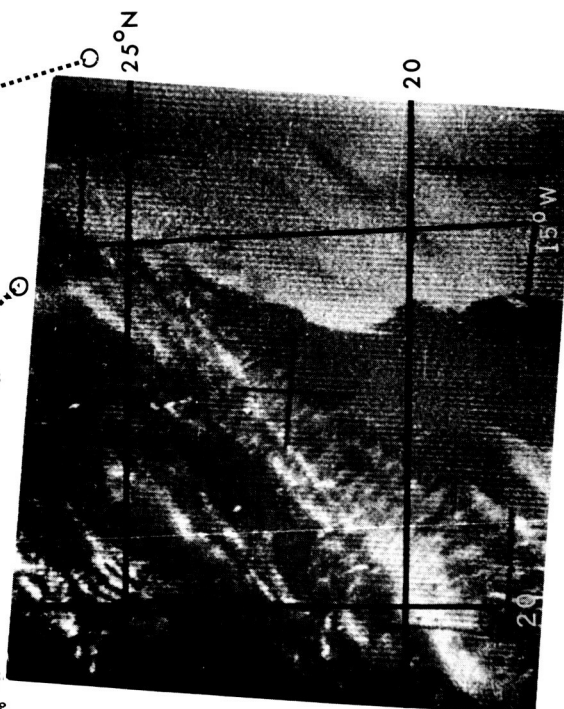
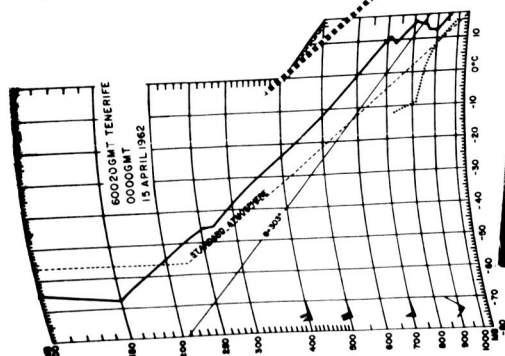
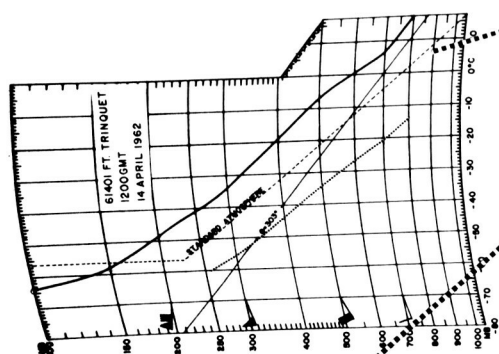
An example of tropical-cyclone cloud systems is shown in Fig. A-10 which presents photographic frames of tropical storms in pretyphoon and typhoon stages. In both storms the pretyphoon stage has the characteristic feature of a dense smooth cirrus shield over the center of the storm (upper frames). These cirrus shields may be quite extensive (more than 400 miles across) and rather thick, particularly towards the storm center.

The cirrus shield tends to band and/or break up after strong intensification has been reached (lower frames).

One of the prime progenitors of cirrus in air-mass situations is the thunderstorm, particularly when present as a squall line. The cirrus appearing from this latter phenomenon may cover an area equal to that of an extra-tropical cyclone. A view of air-mass cirrus due to thunderstorm activity is shown in Fig. A-11, which shows cirrus cloud at the tops of cumulonimbus cloud, streaming in the direction of the prevailing high level wind (see upper right of frame). The cirrus



TIROS IV Orbit 952/950 T
Frame 5 1715 GMT 15 April 1962

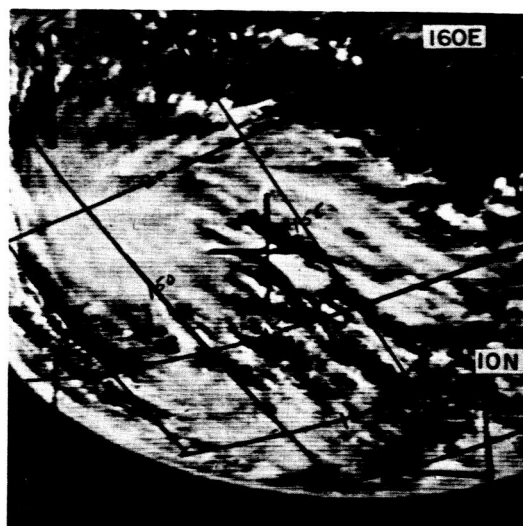


TIROS IV Orbit 938/936T
Frame 6 1750 GMT 14 April 1962

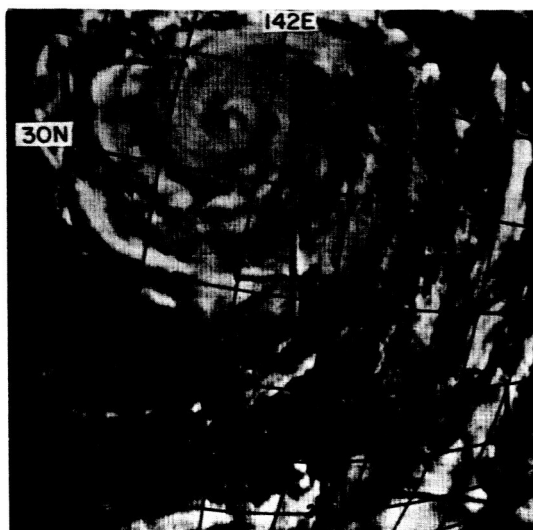
FIG. A-9 SUBTROPICAL JET-STREAM CLOUD SYSTEM



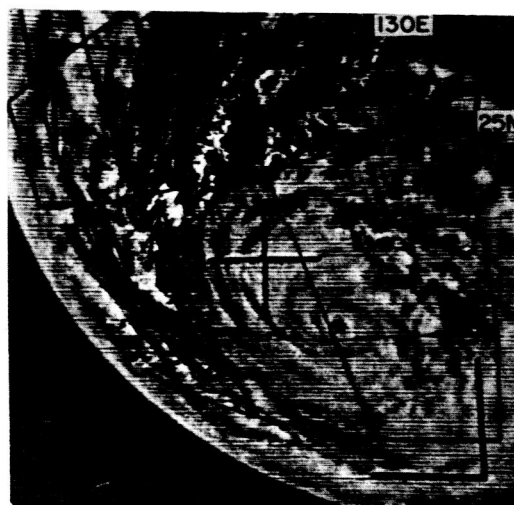
TROPICAL STORM RUTH
TIROS V ORBIT 798/797T, FRAME 16
0430GMT 14 AUGUST 1962
MAXIMUM WIND 60KTS



TROPICAL STORM AMY
TIROS V ORBIT 1024/1024T, FRAME 22
2250GMT 29 AUGUST 1962
MAXIMUM WIND 45KTS



TYPHOON RUTH
TIROS V ORBIT 855/855T, FRAME 13
0351GMT 18 AUGUST 1962
MAXIMUM WIND 95KTS



TYPHOON AMY
TIROS V ORBIT 1096/1096T, FRAME 27
2326GMT 3 SEPTEMBER 1962
MAXIMUM WIND 130KTS

FIG. A-10 TROPICAL CYCLONE CLOUD SYSTEMS

TIROS V ORBIT 049D, FRAME 20 2252GMT 22 JUNE 1962
MEDIUM ANGLE LENS



SCALE: 1 in. \approx 75 nm near mid-frame

FIG. A-11 AIR MASS CLOUD SYSTEM

cover, though patchy, covers an area of approximately 9500 square miles, located over the Sierra Nevada. This frame presents a good example of cumulonimbus clouds being formed by terrain in an air mass. The presence of cirrus implies glaciation of the cloud and a rather high vertical extent.

CONTRIBUTORS

Many members of the Aerophysics Laboratory contributed directly to this study, and in many respects the role of the first-listed author was one of coordination and editing. He must, however, take responsibility for most of the remarks in Sec. V on equipment design.

M. G. H. Ligda prepared the review of possible meteorological uses, Sec. II. S. M. Serebreny, E. J. Wiegman, and W. Viezee prepared Sec. IV and the Appendix. W. Viezee also did most of the analysis of infrared applications, and authored Sec. VII.

R. C. Honey of the Electromagnetic Techniques Laboratory wrote Sec. VIII on current laser technology.

Other major contributors were J. Oblanas, J. W. Davies (principally in Sec. X), and P. A. Davis. Formation of the overall project philosophy was greatly aided by many valuable discussions with R. T. Collis.

GLOSSARY*

Attenuation Coefficient: A measure of the space rate of diminution of any transmitted electromagnetic radiation. This quantity σ may be identified in a form of Beer's Law,

$$I = I_0 \exp - \sigma x,$$

where I is the flux density at the selected point in space, I_0 is the flux density at the source, x is the distance from the source, and σ is the attenuation coefficient. Often the attenuation coefficient is specified only when the attenuation is known to be due to both absorption and scattering or when it is impossible to determine which is the cause. "Extinction coefficient" is a term often used synonymously, but rigorously it applies only to diminution of visible radiation when measured in luminous units.

Brewster Angle: That angle of incidence for which a plane polarized monochromatic light wave, whose E vector lies entirely in the plane of incidence, is not reflected by a transparent dielectric-i.e., experiences total refractive transmission. At this angle of incidence, the corresponding reflection path is along the zero-reradiation direction of the wave induced electron oscillations in the dielectric. The Brewster angle for common glass is $\sim 57^\circ$.

Cavity, Laser: An optically resonant and hence mode-selecting low-loss structure in which laser action occurs through the buildup of electromagnetic field intensity upon multiple reflection.

Cyclone: A closed atmospheric circulation having a sense of rotation about the local vertical the same as that of the earth's rotation: that is, as viewed from above, counterclockwise in the Northern Hemisphere, clockwise in the Southern Hemisphere, undefined at the equator. A cyclone's direction of rotation is opposite to that of an anticyclone. Because cyclonic circulation and relative low atmospheric pressure usually coexist, in common practice the terms cyclone and low are used interchangeably. Also, because cyclones are nearly always accompanied by inclement (often destructive) weather, they are frequently referred to simply as storms.

*

The laser terminology is adapted from Seed (1965) and the meteorological terminology from Huschke (1959).

Cyclone, Extratropical: Any cyclonic-scale storm that is not a tropical cyclone, usually referring only to the migratory frontal cyclones of middle and high latitudes.

Cyclone, Frontal: Any cyclone associated with a front; often used synonymously with "wave cyclone" or with "extratropical cyclone" (as opposed to tropical cyclones, which are nonfrontal).

Cyclone, Tropical: The general term for a cyclone that originates over the tropical oceans. At maturity, the tropical cyclone is one of the most intense and feared storms of the world; winds exceeding 175 knots (200 mph) have been measured, and its rains are torrential.

Cyclone, Wave: A cyclone which forms and moves along a front. The circulation about the cyclone center tends to produce a wavelike deformation of the front.

Front: The interface or transition zone between two air masses of different density. Since the temperature distribution is the most important regulator of atmospheric density, a front almost invariably separates air masses of different temperature. Along with the basic criteria of differing densities and temperatures, many other features may distinguish a front, such as a pressure trough, a change in wind direction, a moisture discontinuity, and certain characteristic cloud and precipitation forms.

Front Occluded: (Also "occlusion," "frontal occlusion"): A composite of two fronts, as a cold front overtakes a warm front or quasistationary front. This is a common process in the late stages of wave-cyclone development, but is not limited to occurrence within a wave cyclone.

Inversion: The condition in which an upper energy level is more densely populated than a lower level. Since an inverted population is not in thermal equilibrium, a pump is required to create and sustain this necessary, though not sufficient, condition for laser action.

Lapse Rate: The decrease of an atmospheric variable with height, the variable being temperature unless otherwise specified.

Laser: Acronym for Light Amplification by Stimulated Emission of Radiation. A device capable of absorbing energy from an external source and reradiating an appropriate portion of it at essentially a single wavelength in an extremely intense beam of high spectral purity. See definitions of Two-Level, Three-Level, and Four-Level Systems at end of Glossary; also Storage Laser and Q-Switched Laser.

Noise, Quantum: A random variation or noise signal due to fluctuations in the average rate of incidence of quanta on a detector. The basic electromagnetic quantum of noise power is just one photon per electromagnetic mode.

Noise, Thermal (also "Johnson noise," "Nyquist noise"): Noise generated in resistive media due to the random motions of current carriers.

Optical Pumping: The use of visible light to raise the energy level of electrons in a laser material. Typically, short-duration, high-intensity output from an electronic flash lamp is used. This energy is mostly absorbed by the impurity atoms in an otherwise transparent host solid-e.g., ruby.

Pump: An external source used to increase the electron population of excited energy states. A laser requires a pump to produce inversion.

Q-Switched Laser: See Storage Laser

Raman Effect: The virtual absorption and prompt ($<10^{-8}$ s) re-emission of optical radiation at various higher and lower frequencies which are characteristic of the material. The emission at lower frequency is known as Stokes radiation. The somewhat surprising emission at higher frequencies (which leaves the material's electrons in a lower energy level than initially) is known as Anti-Stokes radiation. The Raman effect is appreciable in intense optical fields only. Under moderate irradiation, the Raman-active material is essentially transparent at the incident optical frequency, ν_0 , although the effect becomes strong when ν_0 is close to characteristic absorption lines.

Raman Laser: Produced when a Raman-active material is placed in the resonant cavity of an "initial laser" or is otherwise strongly illuminated with intense, coherent "drive power" to induce radiation of Raman frequencies.

Ridge: (Also "wedge".): An elongated area of relatively high atmospheric pressure, almost always associated with and most clearly identified as an area of maximum anticyclonic curvature of wind flow. The locus of this maximum curvature is called the ridge line.

Spiking: Short, multiple, irregular bursts of laser-output radiation. Spiking is characteristic of pulse lasers, especially flash-pumped solid-dielectric types (e.g., ruby, neodymium in glass). Spike duration is typically 0.2 to 2 μ s.

Spontaneous Emission: The loss of energy of an excited bound electron by the random emission of radiation (fluorescence).

Squall: 1) A strong wind characterized by a sudden onset, a duration on the order of minutes, and a rather sudden decrease in speed. 2) (Common nautical definition) A severe local storm considered as a whole, i.e., winds, cloud mass, thunder and lightning, and precipitation (if any).

Squall Line: Any nonfrontal line or narrow band of active thunderstorms (with or without squalls); a mature instability line.

Stimulated Emission: The emission of radiation by a system going from an excited electron energy level to a lower energy level under the influence of a radiation field. The emitted radiation is in phase with the stimulating radiation and produces a negative-absorption condition.

Storage Laser: Any laser which stores unusually high energy prior to discharge. For example, a "storage diode laser" is one in which some carriers are electrically excited for a time longer than the lasing period. This results in power gain--i.e., during some portion of the operating time more optical power is emitted than electrical power applied. Storage solid-state lasers are called giant-pulse lasers because of the immense peak powers obtainable (at some trade-off in efficiency). Most storage methods are based on Q-switching (controlling the Q of the laser cavity to delay the time development of a giant laser pulse), but other techniques, such as double pumping and line broadening, are also used. (Note that conditions for a storage laser are essentially opposite to those for a good, low-threshold laser.)

Threshold (also "threshold operation," "thresholding"): A characteristic operating feature of all lasers denoting the abrupt onset of coherent laser output at a specific pump power input. Below threshold there is no coherent emission; at threshold the coherent output rises from zero, usually linearly with pump power.

Tropopause: The boundary between the troposphere and the stratosphere, usually characterized by an abrupt change of lapse rate. The change is in the direction of increased atmospheric stability from regions below to regions above the tropopause. Its height varies from 15 to 20 km in the tropics to about 10 km in the polar regions. In polar regions in winter it is often difficult or impossible to determine just where the tropopause lies, since under some conditions there is no abrupt change in lapse rate at any height.

Trough: An elongated area of relatively low atmospheric pressure; the opposite of a ridge. This term is commonly used to distinguish the above from the closed circulation of a low, or cyclone.

Two-Level System: A laser which uses only two electron energy levels. Electrons in the ground state (Level 1) are pumped to the excited

state (Level 2). The electrons then surrender their energy by stimulated emission and return to the ground state.

Three-Level System: A laser involving three electronic energy levels. The ground state (Level 1) is pumped to Level 3. This is followed by a transition to the Upper Laser Level 2, which in turn is followed by stimulated emission back to the ground state.

Four-Level System: A laser involving four electronic energy levels. The ground state (Level 1) is pumped to Level 4, from which the excited electrons make a downward transition to the Upper Laser Level 3 (or Metastable Level 3). Then, stimulated transition to the Lower Laser Level 2 occurs followed by rapid decay to the ground state. The four-level system has the advantage that the pump level and ground state are isolated from the laser action. Therefore, inversion between Levels 2 and 3 requires a relatively small population of excited electrons. Here, the requirement for inversion is that $\tau_{32} \geq \tau_{21}$, where the τ 's represent transition decay times.

BIBLIOGRAPHY

Appleman, H. S., "Occurrence and Forecasting of Cirrostratus Clouds," WMO No. 109, 47--Technical Note 40 (1961).

Beckmann, P., "Signal Degeneration in Laser Beams Propagated Through a Turbulent Atmosphere," J. Res. Section D - Radio Science 69D, pp. 629-640 (April 1965).

Blackmer, R. H., Jr., and J. E. Alder, "Distributions and Characteristics of Various Broadscale and Special Cloud Systems," Final Report, Contract AF 19(628)-1681, Stanford Research Institute, Menlo Park, California (April 1965).

Blau, H. H., Jr., and R. P. Espinola, "Infrared Spectral Properties of High Altitude Clouds," Final Report for ARPA, Optics Branch (June 1965).

Borovikov, A. M., et al., "Cirrus Clouds," Ch. VIII of Cloud Physics, ed. A. Kh. Khygian, Leningrad. Pub. for U.S. Dept. Commerce and National Science Foundation, Washington, D.C., by the Israel Program for Scientific Translation, Jerusalem (orig. 1961; trans. 1963).

Borovikov, A. M., I. P. Mazin, and A. N. Nevzarov, "Some Properties of the Distribution of Large Particles in Various Clouds," Izv. Atmospheric and Oceanic Physics Series 1, No. 3, pp. 291-301 (1965).

Boeing Company, "Infrared Reflection Measurements on Cirrus Clouds," Final Report, Contract AF 04(695)-45 (Boeing Document D2-20981) for U.S. Air Force Systems Command, The Boeing Company, Aero-Space Division, Seattle, Washington (June 1962).

Breece, R. C., et al., "Remote Measurement of Differential Atmospheric Velocity," Proc. Conf. on Clear Air Turbulence, pub. Soc. Auto. Eng., Inc., pp. 135-162 (1966).

Burch, D. E., et al., "Infrared Absorption by Carbon Dioxide, Water Vapor, and Minor Atmospheric Constituents," Air Force Cambridge Research Laboratory Report AFCRL-62-698, Contract AF-19(604)-2633, Ohio State University, Columbus, Ohio (1962); AD-287406.

Clemesha, B. R., G. S. Kent, and R. W. H. Wright, "A Study of Measuring Atmospheric Densities by Using a Laser-Searchlight Technique," Scientific Report reproduced under Contract AF AFOSR 616 64, University of the West Indies, Mona, Kingston 7, Jamaica (May 1965).

Collis, R. T. H., "'Lidar' Looks at the Sky," New Scientist 27 (450) pp. 27-29 (July 1965).

Collis, R. T. H., and M. G. H. Ligda, "Laser Radar Echoes from the Clear Atmosphere," Nature 203, No. 4948, p. 508 (1964).

- Collis, R. T. H., and M. G. H. Ligda, "Note on Lidar Observations of Particulate Matter in the Stratosphere," J. Atmos. Sci. 23, pp. 255-257 (1966).
- Combs, A. C., et al., "Application of Infrared Radiometers to Meteorology," J. Appl. Meteorology 4, pp. 253-262 (April 1965).
- Conover, J. H., "Cirrus Patterns and Related Air Motions near the Jet Stream as Delivered by Photography," J. Appl. Met. 17, No. 5, pp. 532-546 (1960).
- Cooney, J., "Satellite Observations of the Atmosphere Using Raman Component of Laser Backscatter," Astro-Electronics Div. of Radio Corporation of America, Princeton, New Jersey (1965), presented at Int. Symposium on Electromagnetic Sensing, Miami, Florida (November 1965).
- Deirmendjian, D., "Scattering and Polarization Properties of Water Clouds and Hazes in the Visible and Infrared," Appl. Optics 3, No. 2, pp. 187-196 (1964).
- Deirmendjian, D., "Note on Laser Detection of Atmospheric Dust Layers," J. Geophysical Res. 70, No. 3, pp. 743-745 (February 1965).
- Duntley, S. Q., "Reduction of Apparent Contrast by the Atmosphere," J. Opt. Soc. Am. 38 (1948).
- Duntley, S. Q., "Visibility of Distant Objects," J. Opt. Soc. Am. 38 (1948).
- Elterman, L., "Atmospheric Attenuation Model, 1964, in the Ultraviolet, Visible, and Infrared Regions for Altitudes to 50 km," AFCRL Report No. 64-740; Environmental Research Papers, No. 46 (September 1964).
- Fiocco, G., "An Interpretation of Some Optical Radar Results," Quarterly Progress Report No. 72, Massachusetts Institute of Technology, Research Laboratory of Electronics, Cambridge, Massachusetts; also in J. Geophysical Res. 69, No. 9, pp. 1795-1803 (May 1964).
- Fiocco, G., "Optical Radar Results and Ionospheric Sporadic E," J. Geophysical Res. 70, No. 9, pp. 2213-2215 (May 1965).
- Fiocco, G., and G. Colombo, "Optical Radar Results and Meteoric Fragmentation," J. Geophysical Res. 69, No. 9, pp. 1795-1803 (May 1964).
- Fiocco, G., and G. Grams, "Observations of the Aerosol Layer at 20 km by Optical Radar," J. Atmos. Sci. 21, pp. 323-324 (May 1964).
- Fiocco, G., and L. D. Smullin, "Detection of Scattering Layers in the Upper Atmosphere (60-140 km) by Optical Radar," Nature 199, pp. 1275-1276 (1963).
- Fiocco, G., and E. Thompson, "Thomson Scattering of Optical Radiation from an Electron Beam," Phys. Rev. Letters 10, No. 3, pp. 89-91 (February 1963).
- Franken, P. A., J. A. Jenney, and D. M. Rank, "Airborne Investigations of Clear Air Turbulence with Optical Radar," Progress Report, Contract NONR 1224(51), University of Michigan, Ann Arbor, Michigan (1965).
- Gergen, J. L., "Atmospheric Infrared Radiation over Minneapolis to 30 mb," J. Meteorology 14, pp. 495-504 (December 1957).

Geeraets, W. J., et al., "Laser Versus Light Coagulator: A Funduscopy and Histologic Study of Chorioretinal Injury as a Function of Exposure Time," Federation Proceedings 24, p. S-60 (January-February 1965).

Gordon, J. I., "Optical Properties of Objects and Backgrounds," Appl. Opt. 3, No. 5, pp. 556-562 (May 1964).

Götz, F. W., "Das Nachthimmelslicht," Handbuch der Geophysik 8, pp. 415-427 (1942).

Gucker, F. T., and S. Basu, "Right-Angle Molecular Light Scattering from Gases," Scientific Report No. 1, Contract AF-19(122)-400, University of Indiana, Bloomington, Indiana (1953).

Handbook of Geophysics (Macmillan Company, New York, New York, 1965).

Harris, E. D., L. J. Nugent, and G. A. Cato, "Laser Meteorological Radar Study," Final Report, U.S. Government Research Report AD-615 444, Electro-Optical Systems Inc., Pasadena, California.

Henderson, S. T., and D. Hodgkiss, "The Spectral Energy Distribution of Daylight," Brit. J. Appl. Phys. 15, pp. 947-952 (1964).

Hirono, M., "On the Observation of the Upper Atmospheric Constituents by Laser Beams," J. Radio Res. Laboratories 11, No. 56, pp. 251-271 (July 1964).

Hoffmeister, C. von, "Die Strömungen der Atmosphäre in 120 km Höhe," Zeit. für Met. I, pp. 33-41 (1946).

Huschke, R. E. (editor), Glossary of Meteorology (American Meteorological Society, Boston, Massachusetts, 1959).

Kadler, P.W., "A Study of Flight Conditions Associated with Jet Stream Cirrus, Atmospheric Temperature Change, and Wind Shear Turbulence," Final Report, Contract Cwb-10674 for U.S. Weather Bureau, Eastern Air Lines Meteorological Department, Miami, Florida (1964).

Kaminskii, A. A., L. S. Kornienko, and A. M. Prokhorov, "Continuous Solar Laser Using Dy^{2+} in CaF_2 ," Soviet Phys.--Doklady 10, No. 4, pp. 334-335 (October 1965).

Kislovskii, L. D., "Optical Characteristics of Water and Ice in the Infrared and Radiowave Regions of the Spectrum," Opt. and Spect. VII, No. 3 (September 1959).

Knecht, W. L., "Life Performance of Prism Q-Switched Laser," Proc. IEEE 53, No. 11, pp. 1785-1786 (November 1965).

Kondrat'yev, K. Ya., "Practical Use of Radiation Data from Meteorological Satellites," Meteorol. i Gidrol. (Meteorol. and Hydrol.) No. 4, pp 28-39 (May 1965).

Kuiper, G. P., and B. M. Middlehurst (editors) Planets and Satellites (University of Chicago Press, 1961).

- La Marre, D. A., "Experimental Verification of Sun-Powered Laser Transmitter," Interim Engineering Report, Contract AF 33(657)-8619, American Optical Company, Southbridge, Massachusetts (April-August 1962).
- Langer, G., and J. Stockham, "High Altitude Tracking by Chemical Smokes," J. Geophys. Res. 65, No. 10, pp. 3331-3338 (1960).
- Latter, R., and R. E. Le Levier, "Detection of Ionization Effects from Nuclear Explosions in Space," J. Geophys. Res. 68, p. 1643 (1963).
- Ligda, M. G. H., "Meteorological Observations with Lidar," Proc. 11th Wea. Rad. Conf. NBS, Boulder, Colorado (1964).
- Ligda, M. G. H., "The Laser in Meteorology," Discovery (July 1965).
- Maiman, T., "Prediction of Things to Come," Federation Proceedings 24, No. 1, Part 3, Sup. 14, pp. S164-S166 (January-February 1965).
- Martin-Marietta Corporation, Laser Safety, Manual OR6672 (September 1965; rev. November 1965).
- May, A. D., E. G. Rawson, and H. L. Welsh, "Rayleigh Scattering from Low Density Gases," Paper E-2 pres. at Phys. of Quantum Electronics Conf., U.S. Office of Naval Research, San Juan, Puerto Rico (June 1965).
- Middleton, W. E. K., Vision Through the Atmosphere (University of Toronto Press, Toronto, Canada, 1958).
- Minneart, M., The Nature of Light and Color in the Open Air (Dover Publications, New York, New York, 1954).
- Moss, E. B., "Systems Problems in the Use of Lasers in Space Communication," Electronics in Transition: Winter Conf. on Military Electronics 4 (February 1965).
- Mossop, S. C., "Stratospheric Particles at 20 km Altitude," Nature (London) 199, pp. 325-326 (1963).
- Murgatroyd, R. J., and P. Goldsmith, "Cirrus Cloud over Southern England," Armed Services Technical Information Agency, MRP 833, S.C. II/158 (September 1953).
- Peppers, N. A., "Laser Safety Standards," J. Soc. Photo-Optical Instrumentation Eng. 4, No. 3, pp. 111-115 (February-March 1966).
- Porto, S. P. S., "The Use of Lasers in Raman Spectroscopy," Paper 7.1 pres. at International Electron Devices Meeting, Washington, D.C. (October 1965).
- Probert-Jones, J. R., "Surface Waves Associated with the Backscattering of Microwave Radiation by Large Ice Spheres," Proc. Interdisciplinary Conf. on Electromagnetic Scattering (MacMillan Company, New York, New York, 1964).
- Randall, J. L., and E. J. Reinholt, "Analytical Studies Defining Laser Experiments for Future Technology Satellites," IEEE Int. Conv. Rec. Part 4 (1965).

- Reiter, E. R., Jet Stream Meteorology (University of Chicago Press, 1963; trans. from German edition, 1961).
- Riehl, H., "Radiation Measurements over the Caribbean During the Autumn of 1960," J. Geophys. Res. 67, No. 10 (September 1962).
- Roberts, W. O., "Weather and Cosmic Influences," Bull. Am. Met. Soc. 46, No. 4 (1965).
- Robinson, F. R., "Transmission and Scattering of Infrared Radiation by Clouds, Part I, Cloud Data and Simple Extinction Laws," Report No. DMP 1665/1, EMI Electronics Limited, Hayes, Middlesex, England (December 1963).
- Ross, M., "Choosing Detectors for Laser Receivers," Microwaves, p. 49 (January 1966).
- Rozenberg, G. V., and Iu. A. R. Mullamaa, "Possible Determination of Wind Velocities Above an Ocean Surface Through Satellite Observations (O Nekotorykh Vozmozhnostiakh Opredeleniia Skorosti Vetra Nad Okeanicheskoi Poverkhnost'iu Po Nabliudeniiam S Iskusstvennykh Sputnikov Zemli)" Akademiia Nauk SSSR, Fizika Atmosfery i Okeana 1, pp. 282-290 (March 1965) in Russian.
- Saiedy, F., D. T. Hilleary, and W. A. Morgan, "Cloud-Top Altitude Measurements from Satellite," Appl. Opt. 4, pp. 495-500 (April 1965).
- Saiedy, F., W. A. Morgan, and D. Q. Wark, "Determination of Cloud Altitudes from Gemini-Titan-5," Nature 208, No. 5012, p. 775 (November 1965).
- Sandomirskii, A. B., N. P. Al'tovskaya, and G. I. Trifonova, "Seasonal Brightness Variations at Altitudes up to 17.5 km," U.D.C. 551.593.5, Izv. Geofyz. Ser. No. 7, pp. 1121-1127 (1964) in Russian; trans. C. M. Wade.
- Sawyer, J. S., and B. Ilett, "The Distribution of Medium and High Cloud near the Jet Streams," The Meteorological Magazine 80, No. 952 (1951).
- Seed, R. G., "Laser Formulas and Definitions," Microwaves, pp. 103-110 (October 1965).
- Schotland, R. M., "The Determination of the Vertical Profile of Atmospheric Gases by Means of a Ground Based Optical Radar," Proc. 3rd Symp. on Remote Sensing of Environment, Ann Arbor, Michigan pp. 215-224 (February 1965).
- Sherr, P. E., and R. Wexler, "Operational Use of Tiros Radiation Measurements," Final Report, Contract AF 19(628)-4074, Aracon Geophysics Co., Concord, Massachusetts (April 1965).
- Skolnik, M. I., Introduction to Radar Systems, (McGraw Hill, 1962).
- Soules, S. D., "Spectral Reflectance Photography of the Earth from Mercury Spacecraft MA-8," Meteorological Satellite Laboratory Report No. 22, U.S. Department of Commerce, Washington, D.C. (November 1963).
- Stampfl, R. A., "The Nimbus Satellite and its Communication System," invited lecture presented at University of California at Los Angeles (Goddard Space Flight Center, Greenbelt, Maryland, September 1961).

Stone, R. G., "A Compendium on Cirrus and Cirrus Forecasting," U.S. Air Force Technical Report AWS, TR105-130 (March 1957).

Twitchell, P. F., "Extra-Terrestrial Influences on Atmospheric Circulation," Bull. Am. Met. Soc. 46, No. 10 (1965).

U.S. Standard Atmosphere, 1962, Sponsored by NASA, U.S. Air Force, and U.S. Weather Bureau; U.S. Government Printing Office (December 1962).

Van de Hulst, H. T., Light Scattering by Small Particles (John Wiley and Sons, New York, New York, 1957).

Van Ornum, D. G., "Global Tropopause Maps by Satellite," J. Meteorology 18, pp. 234-241.

Vassiliadis, A., and R. B. Battelle, "A Study of the Applicability of Laser Radars to Probe Nuclear Weapon Effects and Natural Upper-Atmosphere Phenomena (U)," Final Report, Contract DA-49-146-XZ-324, Stanford Research Institute, Menlo Park, California (1965) SECRET.

Wark, D. Q., and D. M. Mercer, "Absorption in the Atmosphere by the Oxygen 'A' Band," Applied Optics 4, pp. 839-844 (1965).

White, G. R., L. J. Nugent, and L. W. Carrier, "Laser Atmospheric Probes," Electro-Optical Systems, Inc., Pasadena, California, presented at 20th Annual ISA Conference, Los Angeles, California (October, 1965).

Wiegman, E. J., R. G. Hadfield, and S. M. Serebreny, "Atlas of Cloud Vortex Patterns Observed in Satellite Photographs," Final Report, Contract Cwb-10627 for U.S. Weather Bureau, Stanford Research Institute, Menlo Park, California (1964).

Zirkle, R. E., Jr., "The Feasibility of Optical Radar to Detect Clear Air Turbulence," Proc. Conf. on Clear Air Turbulence, pub. Soc. Auto. Eng., Inc., pp. 55-68 (1966).

Zdunkowski, W., D. Henderson, and J. V. Hales, "The Influence of Haze on Infrared Radiation Measurements Detected by Space Vehicles," Tellus XVII 2, pp. 147-166 (1965).

UNCLASSIFIED

Security Classification

DOCUMENT CONTROL DATA - R&D

(Security classification of title, body of abstract and indexing annotation must be entered when the overall report is classified)

1. ORIGINATING ACTIVITY (Corporate author) Stanford Research Institute 333 Ravenswood Avenue Menlo Park, California		2a. REPORT SECURITY CLASSIFICATION UNCLASSIFIED	
		2b. GROUP	
3. REPORT TITLE PERFORMANCE SPECIFICATIONS FOR A METEOROLOGICAL SATELLITE LIDAR			
4. DESCRIPTIVE NOTES (Type of report and inclusive dates) Final Report			
5. AUTHOR(S) (Last name, first name, initial) Evans, W. E.; Wiegman, E. J.; Viezee, W.; Ligda, M. G. H.			
6. REPORT DATE June 1966		7a. TOTAL NO. OF PAGES 175	7b. NO. OF REFS 83
8a. CONTRACT OR GRANT NO. NASr-49(22)		9a. ORIGINATOR'S REPORT NUMBER(S) Final Report, SRI Project 5373	
b. PROJECT NO.		9b. OTHER REPORT NO(S) (Any other numbers that may be assigned this report)	
c.			
d.			
10. AVAILABILITY/LIMITATION NOTICES			
11. SUPPLEMENTARY NOTES		12. SPONSORING MILITARY ACTIVITY National Aeronautics and Space Administration Washington 25, D.C. Attn: Office of Research Grants & Contracts	
13. ABSTRACT <p>Numerous suggestions have been made regarding measurements of meteorological significance which might be made with a laser radar (lidar) carried in a satellite. In this study a wide variety of possibilities is examined, and it is concluded that the most important thing that can be done with reasonable amounts of power is to provide routine height and density data on cirrus cloud. Cloud-top elevations of lower cloud would also be determined.</p> <p>A review of the literature emphasizes the widespread acceptance of cirrus as an important diagnostic tool of meteorology in spite of the traditional difficulty of observing it reliably from the ground, from aircraft, or even via satellite television.</p> <p>In addition to its role as an indicator of large-scale circulation features, such as cyclones and jet streams, cirrus cover is currently of considerable interest in connection with infrared studies of the earth. It is shown that even extremely low-density cirrus shields are capable of introducing several degrees of error into radiometric determinations of temperature made from space.</p> <p>Calculations, supported by experimental backscatter measurements made at SRI with a ground-based pulsed ruby lidar, show that it should be barely possible to measure low-density cirrus cloud at night from a 1000 to 1500 km satellite using a radiated energy of one joule per sounding and a receiving aperture of one square meter.</p> <p>This is roughly equivalent to proposing that within the next decade we duplicate in space equipment performance which is currently being achieved on the ground under controlled laboratory conditions.</p> <p>Soundings frequent enough to provide complete map-like coverage are not presently feasible, but the unique ranging capability of the lidar, properly used in conjunction with television or HRIR, could provide very important supplementary information with a relatively small number of samples. A sounding rate of 1.8 per second is suggested as a goal, but lower rates might be considered.</p> <p>The equipment requirements for all methods currently envisioned for measuring gaseous temperature, density, and composition by lidar from satellite elevations are shown to call for several orders of magnitude more power, and thus must be considered to be only extremely remote possibilities from the standpoint of the present state of laser technology.</p> <p>It is recommended that planning toward a meteorological lidar satellite be continued with heavy emphasis on more precise definition of the optical and meteorological characteristics of potential atmospheric targets and improvement of lidar system efficiency.</p>			

DD FORM 1 JAN 64 1473

UNCLASSIFIED

Security Classification

Security Classification

14. KEY WORDS	LINK A		LINK B		LINK C	
	ROLE	WT	ROLE	WT	ROLE	WT
lidar laser radar satellite weather cirrus cloud large-scale circulation backscatter ranging low output power cloud-top altitude measurement						

INSTRUCTIONS

1. **ORIGINATING ACTIVITY:** Enter the name and address of the contractor, subcontractor, grantee, Department of Defense activity or other organization (*corporate author*) issuing the report.

2a. **REPORT SECURITY CLASSIFICATION:** Enter the overall security classification of the report. Indicate whether "Restricted Data" is included. Marking is to be in accordance with appropriate security regulations.

2b. **GROUP:** Automatic downgrading is specified in DoD Directive 5200.10 and Armed Forces Industrial Manual. Enter the group number. Also, when applicable, show that optional markings have been used for Group 3 and Group 4 as authorized.

3. **REPORT TITLE:** Enter the complete report title in all capital letters. Titles in all cases should be unclassified. If a meaningful title cannot be selected without classification, show title classification in all capitals in parenthesis immediately following the title.

4. **DESCRIPTIVE NOTES:** If appropriate, enter the type of report, e.g., interim, progress, summary, annual, or final. Give the inclusive dates when a specific reporting period is covered.

5. **AUTHOR(S):** Enter the name(s) of author(s) as shown on or in the report. Enter last name, first name, middle initial. If military, show rank and branch of service. The name of the principal author is an absolute minimum requirement.

6. **REPORT DATE:** Enter the date of the report as day, month, year, or month, year. If more than one date appears on the report, use date of publication.

7a. **TOTAL NUMBER OF PAGES:** The total page count should follow normal pagination procedures, i.e., enter the number of pages containing information.

7b. **NUMBER OF REFERENCES:** Enter the total number of references cited in the report.

8a. **CONTRACT OR GRANT NUMBER:** If appropriate, enter the applicable number of the contract or grant under which the report was written.

8b, 8c, & 8d. **PROJECT NUMBER:** Enter the appropriate military department identification, such as project number, subproject number, system numbers, task number, etc.

9a. **ORIGINATOR'S REPORT NUMBER(S):** Enter the official report number by which the document will be identified and controlled by the originating activity. This number must be unique to this report.

9b. **OTHER REPORT NUMBER(S):** If the report has been assigned any other report numbers (*either by the originator or by the sponsor*), also enter this number(s).

10. **AVAILABILITY/LIMITATION NOTICES:** Enter any limitations on further dissemination of the report, other than those

imposed by security classification, using standard statements such as:

- (1) "Qualified requesters may obtain copies of this report from DDC."
- (2) "Foreign announcement and dissemination of this report by DDC is not authorized."
- (3) "U. S. Government agencies may obtain copies of this report directly from DDC. Other qualified DDC users shall request through _____."
- (4) "U. S. military agencies may obtain copies of this report directly from DDC. Other qualified users shall request through _____."
- (5) "All distribution of this report is controlled. Qualified DDC users shall request through _____."

If the report has been furnished to the Office of Technical Services, Department of Commerce, for sale to the public, indicate this fact and enter the price, if known.

11. **SUPPLEMENTARY NOTES:** Use for additional explanatory notes.

12. **SPONSORING MILITARY ACTIVITY:** Enter the name of the departmental project office or laboratory sponsoring (*paying for*) the research and development. Include address.

13. **ABSTRACT:** Enter an abstract giving a brief and factual summary of the document indicative of the report, even though it may also appear elsewhere in the body of the technical report. If additional space is required, a continuation sheet shall be attached.

It is highly desirable that the abstract of classified reports be unclassified. Each paragraph of the abstract shall end with an indication of the military security classification of the information in the paragraph, represented as (TS), (S), (C), or (U).

There is no limitation on the length of the abstract. However, the suggested length is from 150 to 225 words.

14. **KEY WORDS:** Key words are technically meaningful terms or short phrases that characterize a report and may be used as index entries for cataloging the report. Key words must be selected so that no security classification is required. Identifiers, such as equipment model designation, trade name, military project code name, geographic location, may be used as key words but will be followed by an indication of technical context. The assignment of links, roles, and weights is optional.